LA-13579-PR
Progress Report

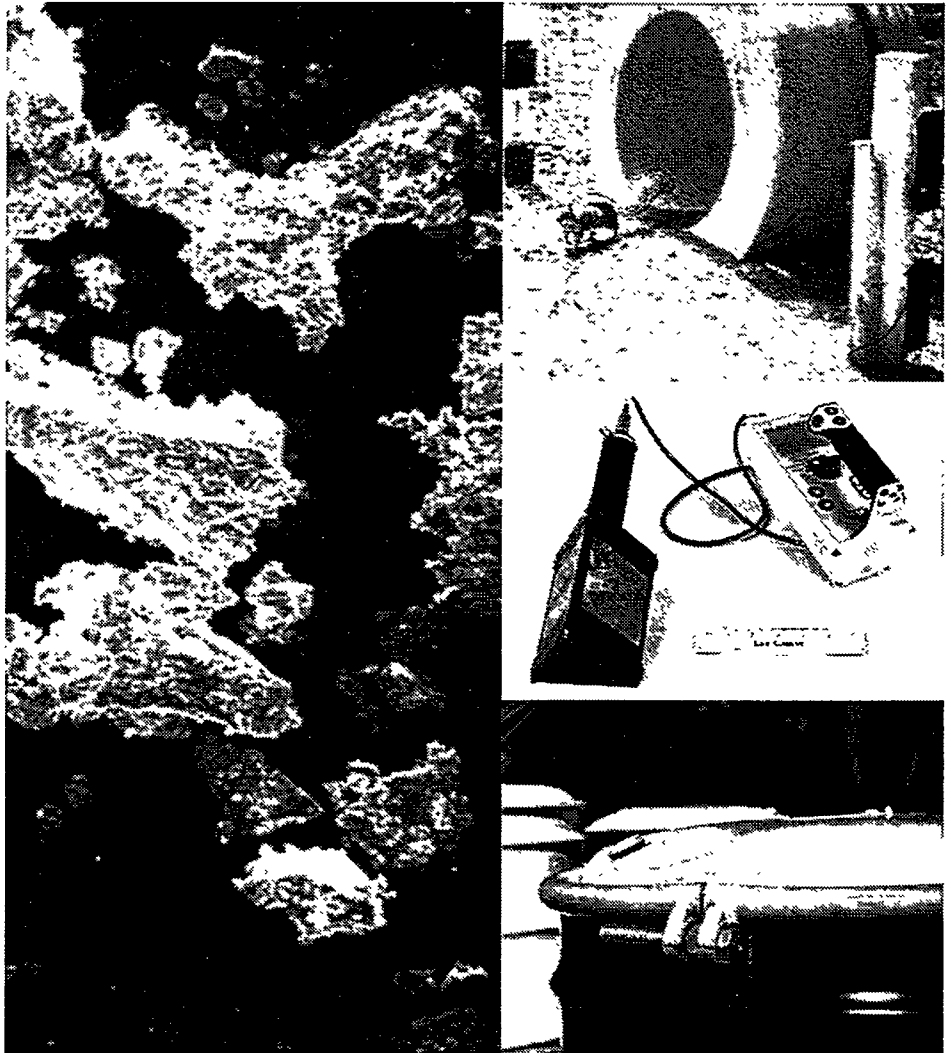# Technology Development, Evaluation, and Application (TDEA)

FY 1998 Progress Report

Environment, Safety, and Health (ESH) Division

Los Alamos
NATIONAL LABORATORY

Abstract

This progress report presents the results of 10 projects funded ($504K) in FY98 by the Technology Development, Evaluation, and Application (TDEA) Committee of the Environment, Safety, and Health Division. Nine projects are new for this year; two projects were completed in their third and final TDEA-funded year. As a result of their TDEA-funded projects, investigators have published 19 papers in professional journals, proceedings, or Los Alamos reports and presented their work at professional meetings. Supplemental funds and in-kind contributions, such as staff time, instrument use, and work space were also provided to the TDEA-funded projects by organizations external to ESH Division. Products generated from the projects funded in FY98 included a new extremity dosimeter that replaced the previously used finger-ring dosimeters, a light and easy-to-use detector to measure energy deposited by neutron interactions, and a device that will allow workers to determine the severity of a hazard.

Photographs without negative numbers are the property of the author.

DISCLAIMER

Portions of this document may be illegible
in electronic image products. Images are
produced from the best available original
document.

Technology Development, Evaluation,
and Application (TDEA) FY 1998 Progress Report

Environment, Safety, and Health (ESH) Division

Prepared by
Larry G. Hoffman (ESH-10)

TDEA Review Committee
Kenneth Alvar (ESH-4)
Thomas Buhl (ESH-4)
Bruce Erdal (EM/TD
Philip Fresquez (ESH-20)
Eslizabeth Foltyn (NMT-9)
Wayne Hansen (ESH-DO)
Larry Hoffman (ESH-10)
Bruce Reinert (ESH-5)

Los Alamos

N A T I O N A L   L A B O R A T O R Y

Los Alamos, New Mexico 87545

Contents

Introduction

The public expects that the Los Alamos National Laboratory (LANL, Laboratory) will operate in a manner that prevents negative impacts to the environment and protects the safety and health of its employees and the public. To achieve this goal within budget, the Department of Energy (DOE) and the Laboratory must develop new and improved environment, safety, and health (ES&H) technologies and implement innovative more cost-effective ES&H approaches to operations.

The Environment, Safety, and Health Division (ESH) is multifaceted and has activities and responsibilities that require technology development and application in addition to the technical and operational support of Laboratory activities. Protecting the health of LANL workers and the public is a major effort with expenditures of over $60 million dollars a year. In fiscal year (FY) 1995, ESH Division established a Technology Development, Evaluation, and Application (TDEA) program that emphasizes improving health and safety of the worker through improved efficiency and use of resources. The magnitude of the cost associated with the Laboratory's total ES&H effort resulted in the Division's initiating this program to find applied studies to address special needs and problems. Much of the technology developed is not only applied in the Laboratory, but throughout the DOE complex, other government organizations, industry, and international community.

The benefit of the TDEA program, now in its fourth year, is to address ES&H problems cost effectively. The program is at a point where we can evaluate its success as clearly defined against the TDEA Committee's initial priorities. This year, the reader will find a detailed progress report before each ES&H discipline represented in the body of this report.

In 1995, the first year of TDEA, funding for the program was $300K, which supported five projects for six months work. The FY96 allocation was $400K and the committee sponsored seven projects. The allocation was increased again in FY97 to $447K and provided funding for 10 projects. In FY98 the Division allocated $504K.

The TDEA Committee maintains the following program priorities. In addition, the committee has decided that funding for any given project should not exceed three years.

Improve ES&H protection to Laboratory workers and the public. Although all funded projects contribute to protecting workers and the public, two projects have the potential to reduce worker exposure to radioactive material in a plutonium facility where historically significant exposures to workers have occurred. Those projects, a ventilation study and characterization of photon fields, once implemented, will have a measurable reduction on workers internal and external exposures. A third project, a method for evaluating pressurized drums, will not only reduce the risk of injury to emergency workers at the Laboratory, but can be readily applied to emergency responses in industrial societies worldwide.

Support Laboratory mission objectives. The Laboratory's central mission is reducing the danger of nuclear weapons and nuclear materials worldwide. Whether it is stockpile stewardship and management, nonproliferation, or environmental stewardship, TDEA projects provide support by developing instruments, equipment, methods, and processes that improve the protection of Laboratory worker health and of the environment in support of this central mission.

Respond and build on the unique expertise of the Laboratory and Laboratory requirements. Investigators for TDEA-funded projects have accomplished the following:

• developed lightweight, more sensitive instruments to measure worker exposure to neutrons;

• applied sophisticated analytical chemistry techniques to bioassay sample measurement methods;

• determined the impacts to the environment with regard to wildlife interaction within the Laboratory;

• determined pressure-deformation correlation criteria to allow emergency responders to evaluate the hazards from pressurized drums;

• identified methods to reduce worker exposure to internal and external radioactive material in plutonium facility glove box lines; and

• evaluated the reusability of organic vapor air-purifying respirator cartridges.

Achieve success within three years. This annual report summarizes the progress for the fourth year of this program. The success of the program is demonstrated by the implementation of funded project products in the workplace. The success of the implementation process for TDEA-funded projects is discussed in detail in the body of the report.

Find potential to transfer technologies to other DOE sites. Information and methods generated by TDEA-funded projects are transferable to other DOE organizations with the same ES&H concerns. The developed technology has also been sought by other government organizations, universities, and private industry.

The TDEA program focuses on the following subjects:

- dosimetry,
- hazards protection,
- instrumentation,
- monitoring, and
- neutron measurements.

However, other topics with compelling justification or significant immediate impact are also considered. Several of the ten projects funded in FY 1998 fit into more than one of the five chosen subject categories. The committee has funded three dosimetry projects, four in hazards protection, one in instrumentation, five in monitoring, and one in neutron measurements.

The FY98 projects listed by discipline include

Environment

Development and Evaluation of a Radio-Frequency Identification System (RFID) to Measure Time Spent by Medium-Sized Mammals at Contaminated Sites at Los Alamos National Laboratory (LANL)

Seasonal Movements, Activity Patterns, and Radionuclide Concentrations of Rocky Mountain Elk (Cervus elaphus nelsoni) Inhabiting the Pajarito Plateau

Comparison of Two Permanent Plots within the 1977 La Mesa Fire and Observations from the Oso Fire

Health Physics

Detection and Internal Dosimetry of Insoluble Metal Tritides

Proton Recoil Scintillator Los Alamos Neutron Dose Meter (PRESCILA)

Determining and Monitoring the Inhalable Fraction of Plutonium Aerosols in an Accident

Characterization of Photon Radiation Fields in a LANL Plutonium Facility

Implications of Room Ventilation and Containment Design to minimize Worker Exposure to Plutonium Aerosols

Industrial Hygiene/ Safety

Pressure-Deformation Correlation in Waste Containers (PDCWC)

Reusability of Organic Vapor Air-Purifying Respirator Cartridges

Measures of success of the TDEA program include publication and presentations, cost savings, new technologies, and external support. Peer review is an important part of confirming the validity of the work. The interest from organizations external to ESH Division, especially financial support also is a measure. However, the primary factor illustrating success is the actual application of results to better protect workers and the environment. Measures of success including applications of TDEA-funded project results are briefly discussed at the beginning of each report section. In past annual TDEA reports, focus has been on the progress for projects performed in that year. Projects listed under FY95 are documented in LA-13191-PR, for FY96 in LA-13264-PR, and for FY97 in LA-13438-PR.

2

Environment

Development and Evaluation of a Radio-Frequency Identification (RFID) System to Measure Time Spent at Contaminated Sites by Medium-Sized Mammals at Los Alamos National Laboratory (LANL)

Seasonal Movements, Activity Patterns, and Radionuclide Concentrations of Rocky Mountain Elk (*Cervus elaphus nelsoni*) Inhabiting the Pajarito Plateau

Comparison of Two Permanent Plots within the 1977 La Mesa Fire and Observations from the Oso Fire

Since ESH Division initiated the TDEA program in 1995, it has supported three environmental projects.

Studies to date

FY96

Seasonal Movements, Activity Patterns, and Radionuclide Concentrations of Rocky Mountain Elk (Cervus elaphus nelsoni) *and Mule Deer* (Odocoileus heminous) *Inhabiting the Pajarito Plateau*

FY97

Development and Evaluation of a Radio-Frequency Identification (RFID) System to Measure Time Spent by Medium-Sized Mammals at Contaminated Sites at Los Alamos National Laboratory (LANL)

*Seasonal Movements, Activity Patterns, and Radionuclide Concentrations of Rocky Mountain Elk (*Cervus elaphus nelsoni*) and Mule Deer (*Odocoileus heminous*) Inhabiting the Pajarito Plateau*

Summary of progress

Investigators for FY98 environmental TDEA projects generated 39 papers and presentations. In addition to TDEA funds, an additional $23K of external funds derived from the Dual Axis Radiographic Hydrotest project.

FY96 was the first year TDEA supported a project that studied elk movement patterns on Laboratory lands. The study was completed in FY98. Principal investigators working on this study
• determined concentrations of radionu-clides in elk in and around the Laboratory,
• provided a model of elk migration patterns in and around the Laboratory, and
• evaluated a new technology, a global positioning system collar, for tracking elk movement patterns.

In FY97, the committee funded a two-year study of an RFID system for monitoring small mammal movements. The study was to evaluate the system's capability to collect data about the amount of time medium-sized mammals spend in a defined area. The information obtained from this study
• evaluated RFID as a viable system for monitoring small mammals and
• determined contaminant levels of radionuclides and toxic materials in medium-sized animals with access to a Laboratory waste site.

In 1998, TDEA provided minimal, short-term funding for a study that documents the process of natural environmental recovery in areas severely burned by wildfire.

Development and Evaluation of a Radio-Frequency Identification (RFID) System to Measure Time Spent at Contaminated Sites by Medium-Sized Mammals at Los Alamos National Laboratory (LANL)

Principle Investigators: Leslie A. Hansen, Rhonda Robinson, Phil Fresquez, Teralene Foxx, John Huchton, Ecology Group (ESH-20)

Introduction

Radioactive and nonradioactive contamination of soil, vegetation, invertebrates, and small mammals has been confirmed as occuring in areas on Laboratory land (Fresquez et al. 1996a, b; EAREG 1996; Biggs 1995; Fresquez et al. 1995a, b, c; Brooks 1989). Medium-sized mammals—raccoons (*Procyon lotor*), bobcats (*Felis rufus*), striped skunks (*Mephitis mephitis*), gray foxes (*Urocyon cinereoargenteus*), squirrels (*Spermophilus* spp., *Sciurus* spp.), and rabbits (*Sylvilagus* spp.)—may be exposed to heavy metals, organic compounds, and low-level radionuclides at the Laboratory (Brooks 1989).

Medium-sized mammals are important ecosystem components. Also, they are ceremonial animals for Native Americans, an economic resource for trappers, and a food source. Carnivores are particularly susceptible to detrimental effects from contaminants because their acidic digestive systems increase the bioavailability of some contaminants and because their food chains biomagnify some contaminants (Petron 1993, Kendall et al. 1990, Oehme 1978, Stickel 1975).

Although LANL annually conducts extensive monitoring of radioactive and nonradioactive contaminant levels in the atosmphere and in groundwater, surface water, soils, sediments, and foodstuffs (EAREG 1996), little information is available on the occurrence of contaminants in natural vegetation (Fresquez et al. 1996b, Fresquez 1995c, Wenzel et al. 1987) and herbivores (Biggs 1995, Fresquez et al. 1995a). To date, no data are available on contaminants in medium-sized mammals. Accumulation of

contaminants in individuals and contaminant transfer along food chains are among the more important processes that must be evaluated to predict contaminant effects on the environment (Petron 1993, Martin and Coughtrey 1982, Ketchum et al. 1975).

Medium-sized mammals are difficult to study because their population densities are low and because often they have nocturnal habits. Previously, the only technique to document movements of individual animals was radiotelemetry. We are evaluating a new application of RFID technology. This technology allows us to record remotely the amount of time individual animals spend at a potential release site (PRS) for contaminants. The RFID system consists of a monitor and automatic data recorder. A remote camera system continuously monitors an unlimited number of animals of different species at a specific site of interest. Once developed, this system can be used for studies of animal exposure to and uptake and transport of radioactive and nonradioactive contaminants anywhere animal exposure to point sources of contaminants is a concern, including LANL and other Department of Energy (DOE) facilities. Knowledge of contaminant levels and transport routes is used to evaluate risks of contaminants to the environment and provides data to examine cleanup options.

RFID technology allows the researcher to use a syringe and needle to subcutaniously implant a very small (23 mm x 3.2 mm) glass-encapsulated tag into an animal. Tags last for the lifetime of the animal. As a marked animal walks through a portal monitor (Figure 1), the monitor can record the identification
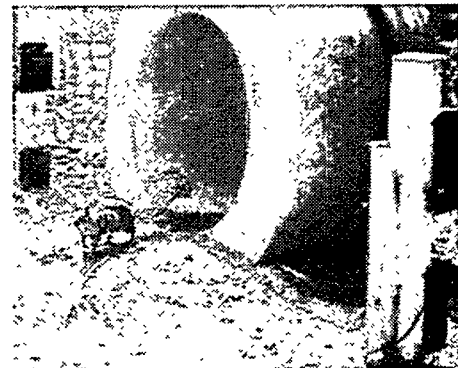
Figure 1. Picture of a squirrel just after it passed through the RFID portal monitor. The instruments mounted on posts in front of the monitor make and receive infrared beams. When a marked animal breaks a beam, it triggers a camera to take a picture.

number of the animal from the tag, along with the date and the time. The technology is similar to a barcode reader. In combination with a remotely activated camera, this system records time, date, and species as animals enter and leave a PRS and allows the investigator to determine the ratio of marked to unmarked animals of each species using a site.

The objectives of this project are

• To develop and evaluate a system that will allow LANL to efficiently document the amount of time spent at PRSs by individual animals.

• To determine whether medium-sized mammals on LANL property exhibit elevated levels of metals or radionuclides.

• To collect data during the evaluation process on the relationship between the amount of time spent at a PRS and levels of contamination.

Methods

We fenced in a PRS so that a RFID monitor setup provided the only easy access to the site, the radioactive liquid waste treatment lagoon for the Los Alamos Neutron Science Center (LANSCE) located at technical area 53 (TA-53), a piñon-juniper zone. LANSCE is a national user facility that provides intense sources of pulsed spallation neutrons for neutron research and applications. Operation of the linear accelerator and associated cooling systems produces radioactively contaminated liquid wastes. All potentially radioactive liquid wastes are collected and delivered to two sets of holding tanks. The waste is retained in the holding tanks until short half-life constituents decay completely. Tank contents are then pumped to the TA-53 radioactive liquid waste treatment lagoon.

During 1998, we improved the fence around the lagoon from its 1997 condition by burying chicken wire along the bottom to prevent animals from digging under it and by adding a solar-powered electrical "hot wire" along the top to discourage animals from climbing over it. The RFID monitor was set up as an opening in the fence through which animals could access the lagoon and the Trailmaster cameras photographed any animal passing through it. The monitor and cameras operated continuously during 1998 to document use of the lagoon area by marked and unmarked animals.

Through March and July, we captured medium-sized mammals (rock squirrels, raccoons, striped skunk, and bobcat) at two different TA-53 areas (see figure 2) using cage traps placed within 400 m of the lagoon (at the lagoon) and more than 400 m from the lagoon (away from the lagoon). Animals were also captured in Guaje and Rendija canyons on Santa Fe Forest Service lands. Captured animals were taken to an animal holding facility, where we anesthetized them, inserted RFID tags between their shoulder blades, took measurements, and collected 2–4 g of hair. We retained the animals in the holding facility overnight, collected their
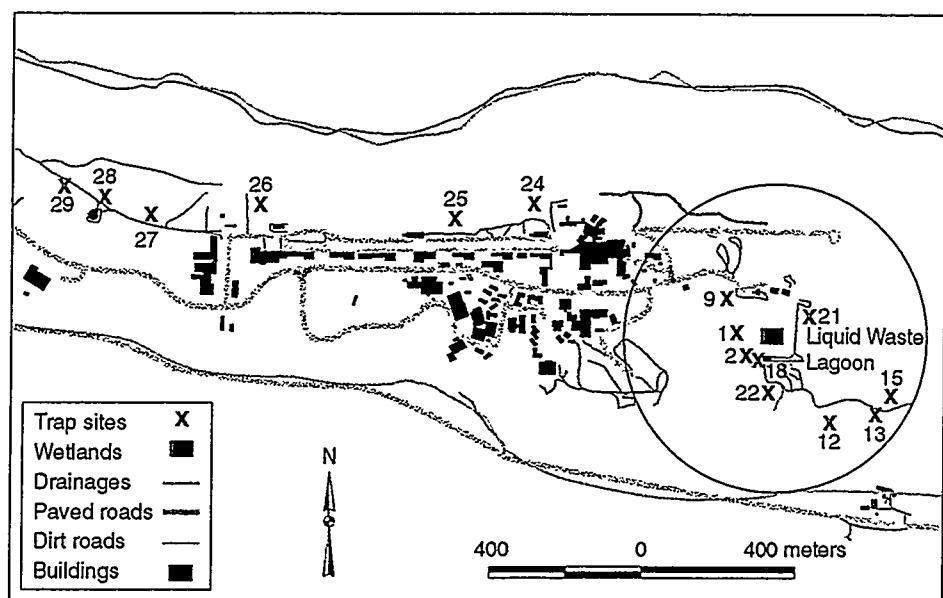
Figure 2. Locations of traps at TA–53. The circle is a 400-m buffer around the liquid waste lagoon. Animals captured inside the circle are considered to be at the lagoon. Animals captured outside the circle are considered to be away from the lagoon.

urine in trays beneath the cages, then released them the next day at their capture site. Urine samples collected in 1997 and 1998 were submitted to the LANL Chemical Science and Technology Division (CST) where they were analyzed for tritium concentrations. Hair samples submitted to CST were tested for concentrations of metals, including aluminum (Al), antimony (Sb), arsenic (As), barium (Ba), beryllium (Be), cadmium (Cd), chromium (Cr), copper (Cu), lead (Pb), mercury (Hg), nickel (Ni), selenium (Se), silver (Ag) and thallium (Tl). Results of contaminants samples were analyzed assuming that samples with nondetectable results had levels equal to one half of the detection limit.

Progress

Animal Capture

Between March 1, 1998, and July 31, 1998, we captured 35 animals a total of 56 times. Animals captured included 32 rock squirrels, 1 raccoon, 1 striped skunk, and 1 bobcat. At TA-53, 19 rock squirrels, 2 raccoons, 1 striped skunk, and 1 bobcat were implanted with RFID tags or retained RFID tags from 1997. Six rock squirrels and 1 striped skunk initially captured in 1997 were recaptured in

1998. One raccoon initially captured in 1997 was detected going through the RFID monitor in 1998. Thirteen rock squirrels were captured in Guaje and Rendija Canyons on Santa Fe National Forest land and sampled. Contaminant levels in these animals were used for comparison to levels in animals captured at TA-53. However, seven hair samples from the control area animals were not submitted for analysis in FY98 because funding ran out.

Effectiveness of the RFID Monitor

Of the 23 marked animals at TA-53, 4 animals (2 rock squirrels, 1 raccoon, and 1 bobcat) passed through the RFID monitor a total of 25 times between March 1, 1998 and September 1998. Eight pairs of readings appeared to represent 1 rock squirrel entering and leaving the lagoon area. The time the squirrel spent in the lagoon area ranged from 6 min. 3 sec. to 1 hr. 40 min. 40 sec. The bobcat also had 1 set of paired readings. It remained in the lagoon area 16 min. 23 sec. All other readings (7) were unpaired. The large increase in the proportion of paired readings in 1998 (72%) versus 1997 (44%) suggests our fence modification did improve our detection of animals using the lagoon. Despite the larger number of passages in

5

Table 1. Number of animals with detectable values[a] (n) and median values[b] with range (in parentheses) of metals (mg/g) and tritium (pCi/L) found in urine for animals captured in 1998 at Los Alamos National Laboratory[c].

	Rock squirrel (18)[d]		Raccoon (1)		Bobcat (1)		Striped skunk (1)	
	n	Median	n	Median	n	Median	n	Median
Al	18	310 (700)	1	340	1	170	1	370
Sb	2	0.05 (0.2)	1	0.34	1	0.05	1	0.04
As	0	0.2 (0)	1	0.2	0	0.2	0	0.2
Ba	18	11.0 (24.6)	1	14.0	1	15	1	9.5
Be	6	0.035 (0.051)	0	0.35	0	0.35	0	0.35
Cd	0	0.45 (0)	1	1.3	0	0.45	0	0.45
Cr	3	0.45 (1.15)	1	1.6	0	0.45	0	0.45
Cu	18	11.5 (52.9)	2	12.0	1	9.7	1	6.1
Pb	18	2.55 (8.1)	2	14.0	1	1.3	1	2.1
Hg	3	0.15 (0.45)	0	0.15	0	0.15	1	0.5
Ni	1	2.0 (2.2)	0	2.0	0	2.0	0	2.0
Se	18	1.05 (1.0)	1	2.0	1	1.0	1	1.0
Ag	2	1.0 (1.3)	0	1.0	0	1.0	0	1.0
Tl	18	0.021 (0.047)	1	0.066	0	0.01	0	0.017
Tritium	17	2890 (41980)	1	1081000	-		1	20

[a]Detection limits were: As, 0.4; Be, 0.07; Cd, 0.90; Cr, 0.9; Ni, 4.0; Se, 0.3; Ag, 2.0; Tl, 0.3: Hg, 0.3.

[b]Nondetectable values were reported as one-half the detection limit for the purposes of analyses.

[c]All animals were captured at TA-53.

1998 (25 in 1998, 16 in 1997), we detected the same number of animals (4) in each year. At the monitor between April 15, 1998, and July 11, 1998, we took 6 photographs of rock squirrels, 7 photographs of raccoons, 12 photographs of cottontail rabbits, 1 photograph of a mouse, and 2 photographs of birds. We are currently developing and analyzing the remaining FY98 photographs.

Contaminants Analyses

We used liquid scintillation analysis of urine to measure levels of tritium. Median values of tritium for animals captured on LANL in 1998 are presented in Table 1. The highest value recorded was for a raccoon captured on May 28, 1998. This animal had 1.1 million pCi/L of tritium in its urine. Levels of tritium in water samples taken once a month from the lagoon during April–July ranged from 3.2 million pCi/L to 14.7 million pCi/L. A raccoon was photographed entering the

lagoon early in the morning (01:12) of May 25, 1998, and leaving late that night (23:46). It is possible that we captured and sampled this same individual three days later.

An analysis of tritium levels in rock squirrel urine from three different areas (at the lagoon, away from the lagoon, and control) found significant differences among the groups in both 1997 (Kruskal-Wallis test, test statistic = 7.5, P = 0.024) and 1998 (Kruskal-Wallis test, test statistic = 19.96, P = 0.000). In both years, rock squirrels from the lagoon area had significantly higher concentrations of tritium in their urine than animals away from the lagoon or in the control area. Median values of tritium and ranges for 1997 and 1998 for rock squirrels from different areas are presented in Table 2. Plots of tritium values over time in rock squirrels from the lagoon area for 1997 and 1998 are presented in Figure 3.

During 1997, we submitted muscle and bone samples from rock squirrels that were captured at the lagoon area but died during the capture process. These individuals (1 male, 1 female) were pooled for radionuclide analyses. We found 0.0137 pCi/g ash of [241]americium, 0.0077 pCi/g ash of [238]plutonium, 0.0009 pCi/g ash of [239] plutonium,15500 pCi/L of tritium, 48.85 gCi/g ash of [90]strontium 90, 0.29 ug/g ash of total uranium, and 2.22 pCi/g ash of [137]cesium in muscle tissue. In bone tissue, we found 0.0029 pCi/g ash of [241]americium, 0.0014 pCi/g ash of [238]plutonium, 0.0009 pCi/g ash of [239] plutonium, and 16200 pCi/L of tritium.

No animals were submitted from this project in 1998. However, rock squirrels were collected from perimeter and regional locations by the Ecology Group's Contaminants Monitoring Team in 1998, and comparisons of rock

Table 2. Tritium concentrations (pCi/L) in rock squirrel urine from animals captured in 1997 and 1998 in three locations: at the lagoon, away from the lagoon, and at the control area.

Year	At Lagoon		Away from Lagoon		Control Area		Test Statistic and P[c]
	n	Median	n	Median	n	Median	
1997	8	4000 (9900)	3	1720 (8310)	4	585 (950)	7.5, P = 0.024
1998	15	4490 (41670)	2	250 (60)	13	-20 (2150)	19.964, P = 0.00
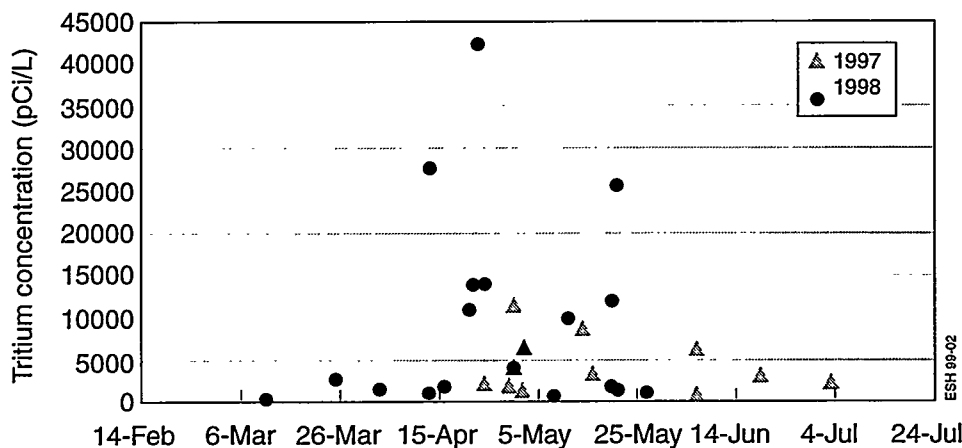
Figure 3. Graphic showing tritium concentration (pCi/L) in urine from rock squirrels captured in the lagoon area by date in 1996 and 1998.

squirrels from the different locations will be presented in the 1998 Environmental Surveillance Report.

Median values for metal concentrations in hair samples for each species captured on LANL in 1998 are presented in Table 1. Using Kruskal-Wallis tests (Table 3), we tested for significant differences in levels of metals in rock squirrel hair from animals captured in three areas: at the lagoon, away from the lagoon, and in the control area. There was no significant evidence of elevated levels of metals in animals from TA-53, although there was a slight trend toward higher levels of lead.

Conclusions and Deliverables

The RFID monitor and tags were very effective at documenting animal passages into the lagoon area. However, when we made comparisons with control animals, we were surprised at the low number of marked animals visiting the lagoon relative to the number of animals with elevated levels of tritium. Although only

2 rock squirrels were recorded entering the lagoon, 11 of the 15 rock squirrels tested from the lagoon area had tritium levels above 1550 pCi/L, the highest value recorded in the control area. These data strongly suggest that indirect routes of uptake are important in the transport of tritium from the TA-53 lagoon to wildlife.

Toxicity from metals occurs in critical organs, frequently the liver, kidney, or brain. For most metals, there is often not a close correlation between metals in hair and metals in critical organs. Therefore, the analysis of hair samples for metal concentrations is primarily useful as a screening tool. We have little information on the significance of our aluminum, arsenic, barium, beryllium, or chromium values. Both aluminum and barium occur naturally at relatively high concentrations in soils of Los Alamos County (Ferenbaugh et al. 1990). Ranges of selenium observed in our study were similar to those observed in a control population of raccoons (0.47-1.7 mg/g) that were used in a study in California

(Clark et al. 1989). This suggests that our animals were not exposed to excessive levels of selenium. For animals in which cadmium was detected, concentrations in hair were as high or higher than in beavers in an industrially cadmium-contaminated river in Germany. No population-level effects were observed in the German beaver population (Nolet et al. 1994).

Lead in hair has frequently been used as an indicator of exposure. A safety limit of 9 mg/g in hair has been proposed for children (Revich 1994). In our 1997 study 5 animals at TA-53 (4 rock squirrels, 1 raccoon) exceeded this level, with 1 rock squirrel having >25 mg/g. No animals exceeded this level in 1998. Beryllium was the only metal to be significantly different among areas in both 1997 and 1998. The reason for this pattern is not known.

Liquid wastes contaminated with high levels of metals are not released into the lagoon. Therefore, any excessive metal concentrations observed in animals around TA-53 are the result of contaminants from historical activities and not the result of current use of the lagoon waters.

We have proposed using the TA-53 population of rock squirrels as a sample population with known contamination to develop techniques for examining genetic damage in wildlife populations. We have received commitments for $25K from the Environmental Restoration Project and $10K from the Contaminants Monitoring Team to conduct this work during FY99. We are preparing a publication to be submitted to a peer-reviewed journal based on the 1997 and 1998 results of this project.

Table 3. *Number of animals with detectable values[a] (n) and median values[b] (mg/g) with range (in parentheses) of metals found in hair of rock squirrels captured in three locations: at the lagoon, away from the lagoon, and at the control area.*

Metals	At Lagoon (15)[c]		Away from Lagoon (3)		Control Area (6)		Test Statistic and P[d]
	n	Median	n	Median	n	Median	
Al	15	340 (700)	3	270 (100)	6	375 (400)	
Sb	15	0.05 (0.2)	3	0.05 (0.05)	6	0.045 (0.08)	
As	0	0.2 (0)	0	0.20 (0)	1	0.2 (0.7)	
Ba	11	11.0 (24.6)	3	19.0 (12.8)	6	17.5 (9.0)	4.92, P = 0.085
Be	3	0.035 (0.051)	2	0.77 (0.44)	3	0.056 (0.085)	6.03, P = 0.049
Cd	0	0.45 (0)	0	0.45 (0)	0	0.045 (0)	
Cr	3	0.45 (1.15)	0	0.45 (0)	0	0.045 (0)	
Cu	15	7.8 (8.3)	3	7.0 (4.2)	6	8.9 (4.1)	
Hg	3	0.15 (0.45)	1	0.15 (0.15)	0	0.015 (0)	
Pb	15	2.7 (8.1)	3	2.5 (1.2)	6	1.0 (0.9)	5.249, P = 0.072
Ni	1	2.0 (2.2)	0	2.0 (0)	0	2.0 (0)	
Se	15	1.1 (1.0)	3	1.0 (0.6)	6	0.65 (1.0)	
Ag	1	1.0 (1.3)	0	1.0 (0)	0	1.0 (0)	
Tl	15	0.020 (0.047)	3	0.026 (0.015)	6	0.025 (0.012)	

[a]Detection limits were: As, 0.4; Be, 0.07; Cd, 0.9; Cr, 0.9; Ni, 4.0; Se, 0.3; Ag, 2.0; Tl, 0.3: Hg, 0.3.

[b]Nondetectable values were reported as one-half the detection limit for the purposes of analyses.

[c]The number of animals tested (N) in each location follows the location name in the table.

[d]Kruskal-Wallis test statistics and probability levels are included for those metals which had significant differences among groups at the a = 0.10 level.

References

Biggs, J., K. Bennett, and P. R. Fresquez, "Radionuclide contaminant analysis of small mammals at Area G, TA-54, 1994," Los Alamos National Laboratory report LA-13015-MS (1995).

Brooks, G. H., Jr., "The comparative uptake and interaction of several radionuclides in the trophic levels surrounding the Los Alamos Meson Physics Facility (LAMPF) waste water ponds," Los Alamos National Laboratory report LA-11487-T (1989).

Clark, D. R., Jr., P. A. Ogasawara, G. J. Smith, and H. M. Ohlendorf, "Selenium accumulation by raccoons exposed to irrigation drainwater at Kesterson National Wildlife Refuge, California," *Arch. Envir. Contam. Tox.* **18**, 787–794 (1986).

"Environmental Assessments and Resource Evaluations Group (EAREG), Environmental surveillance at Los Alamos during 1994," Los Alamos National Laboratory report LA-13047-ENV (1996).

Ferenbaugh, R. W., E. S. Gladney, and G. H. Brooks, "Sigma Mesa: background elemental concentrations in soil and vegetation, 1979," Los Alamos National Laboratory report LA-11941-MS (1990).

Fresquez, P. R., M. A. Mullen, J. K. Ferenbaugh, and R. A. Perona, "Radionuclide and radioactivity in soils within and around Los Alamos National Laboratory, 1974 through 1994: Concentrations, Trends, and Dose Comparisons," Los Alamos National Laboratory report LA-13149-MS (1996a).

Fresquez, P. R., E. L. Vold, and L. Naranjo, Jr., "Radionuclide concentration in/on vegetation at Radioactive-Waste Disposal Area G during the 1995 growing season," Los Alamos National Laboratory progress report LA-13124-PR (1996b).

Fresquez, P. R., D. A. Armstrong, and J. G. Salazar, "Radionuclide concentrations in elk that winter on Los Alamos National Laboratory lands," Los Alamos National Laboratory report LA-12795-MS.

Fresquez, P. R., D. R. Armstrong, and J. G. Salazar, "Tritium concentrations in bees and honey at Los Alamos National Laboratory," Los Alamos National Laboratory report LA-12872-MS (1995b).

Fresquez, P. R., T. S. Foxx, and L. Naranjo, Jr., "Strontium concentration in chamisa (*Chrysothamnus nauseosus*) shrub plants growing in a former liquid waste disposal area in Bayo Canyon," Los Alamos National Laboratory report LA-13050-MS (1995c).

Kendall, R. J., J. M. Funsch, and C. M. Bens, "Use of wildlife for on-site evaluation of bioavailability and ecotoxicity of toxic substances found in hazardous waste sites," in *In Situ evaluation of biological hazards of environmental pollutants* (Plenum Press, New York. 1990) pp. 241-255.

Ketchum, B. H., R. G. V. Boelens, N. Fimreite, E. E. Kenaga, Q. Laham, H. Metzner, F. Moriarty, I. C. Munro, H. Remmer, and D. Saward, "Movements of heavy metals and organohalogens through food chains and their effects on populations and communities," in *Ecological Toxicological Research* (Plenum Press, New York, 1975) pp. 285-310.

Martin, M. H., and P. J. Coughtrey, *Biological Monitoring of Heavy Metal Pollution: Land and Air*, (Applied Science Publishers, New York,1982).

Nolet, B. A., V. A. A. Dijkstra, and D. Heidecke, "Cadmium in beavers translocated from the Elbe River to the Rhine/Meuse Estuary, and the possible effects on population growth rate," *Arch. Environ. Contam. Tox.* **27** 154-161 (1994).

Oehme, F. W., "Mechanisms of heavy metal inorganic toxicities," in *Toxicity of Heavy Metals in the Environment, Part 1* (Marcel Dekker, Inc., New York, 1978), pp. 69-85.

Petron, S. E., "Biological transfer of contaminants in terrestrial ecosystems," in *Ecological Assessment of Hazardous Waste Sites* (Van Nostrand Reinhold, New York, 1993) pp. 144-175.

Revich, B. A., "Lead in hair and urine of children and adults from industrialized areas," *Arch. Environ. Health* **49**:59-62 (1994).

Stickel, W. H., "Some effects of pollutants in terrestrial ecosystems," in *Ecological Toxicological Research* (Plenum Press, New York,1975) pp. 25-74.

Wenzel, W. J., T. S. Foxx, A. F. Gallegos, G. Tierney, and J. C. Rodgers, Cesium-137, Plutonium-239/240, "Total Uranium, and Scandium in trees and shrubs growing in transuranic waste at Area B," Los Alamos National Laboratory report LA-11126-MS (1987).

Seasonal Movements, Activity Patterns, and Radionuclide Concentrations of Rocky Mountain Elk (*Cervus elaphus nelsoni*) Inhabiting the Pajarito Plateau

Principal investigator: James Biggs, Kathryn Bennett, and Phil Fresquez, Ecology Group (ESH-20)

Introduction

The expansion of elk on Bandelier National Monument and Los Alamos National Laboratory (LANL) lands appears to be continually increasing, resulting in a variety of ecological and human-associated issues and concerns. In 1996, members of ESH-20 initiated a preliminary, multitasked study to evaluate the behavior and radioisotope concentrations of approximately 3%–5% of the elk inhabiting LANL property. This study is preliminary because the only previous study of elk at the Laboratory was conducted in the late 1970s (White et al. 1981) and elk use of Laboratory property has drastically changed during the interim. Consequently, we need to establish new base-line data and to test the efficiency of a new technology, global positioning system (GPS) radio collars, for this type of study.

We have identified behavioral patterns—movement and activity patterns, resource use—that will help us develop long-term management plans that include strategies to address issues of concern such as automobile accidents, radionuclide uptake and off-site transport, and overuse of sensitive habitats. To develop strategies to manage elk and other large herbivores, we must understand how the spatial distribution and availability of essential habitats and the landscape influence the animals' use of LANL property. One of several concerns is elk use of LANL technical areas (TAs) known to contain environmental contaminants that may ultimately constitute a pathway to transport radionuclides to people (Fresquez et al. 1994). However, to accomplish an accurate radiological study, we need to measure radionuclide concentrations in tissues of animals with a defined history of use on LANL technical areas. We must also identify movement patterns and resource use patterns in relation to contaminant sources to evaluate the potential exposure of contaminants to animals.

Before we initiated this study, the most common form for collecting activity data on wild animals was through the use of tracking via very high frequency (VHF) radio collars. Tracking requires locational fixes obtained by ground or aerial surveys. Although such surveys remain the most widespread technique, new methods are being tested. One method is the use of global positioning system (GPS) technology, which uses satellites to obtain locational fixes. We elected to try GPS collars because of inherent problems with conducting a study of this magnitude using VHF. Among these problems were inaccessibility of secured areas on a regular basis; inaccessibility of areas due to terrain, land ownership, and political boundaries; the high-cost requirement of human resources; and inaccuracies of data associated with triangulating positions— the act of obtaining a locational fix by taking a ground reading from at least two points.

As a result of issues of concern with elk at LANL and the need for more efficient and applicable technology, the objectives of this study were to

• evaluate GPS test collar data in various habitats around LANL,

• apply spatial and temporal analysis of data to evaluate activity patterns and resource use of elk,

• compare radionuclide content in collared elk from LANL to background locations,

• calculate the committed effective dose equivalent (CEDE) to people who consume meat from elk that use LANL lands,

• develop a habitat use predictive model for use in the LANL facility/project planning process,including meeting requirements of the National Environmental Policy Act, and

• collect data for initial development of long-term management strategies and to identify locations of concern for development of management strategies to aid local agency officials in minimizing human/animal conflicts.

This study supports the Laboratory's environmental compliance requirements by helping it meet DOE Orders 5400.1 and 5400.5, the Resource Conservation and Recovery Act, and the National Environmental Policy Act. The information collected in this study will be used as a foundation for further studies and biological opinions pertaining to large mammal ecology for use in a sitewide environmental impact statement (EIS), project-specific EISs, and environmental assessments. In addition, a series of interagency meetings between LANL, the State of New Mexico, local Native American pueblos, and Bandelier National Monument has identified the need for data on this species to develop a regional management plan.

Cost/Time Savings Analysis

Because these collars are self-activated and store and disseminate data from the collar, personnel are not needed in the field to collect data. The amount of time and saved costs has been significant (Table 1). Costs are based on the deployment of six GPS collars and do not include costs associated with data interpretation, special computer software

training, animal trapping, collar replacement, or other costs that will vary from project to project or researcher to researcher. Attempts to locate an animal are based on a rate of once per day. The success rate of obtaining a location on each animal is assumed to be similar for both methods. The figures provided for VHF collars are based on locating animals using ground rather than aerial surveys. If aerial surveys are used, labor hours will decrease, but one must account for costs associated with aircraft flight time, ground time due to adverse weather conditions, and increased risk to worker safety. The computer software and hardware requirements are not included in the table because they are a function of the researcher's needs and are not limited by the method used; both techniques result in the production of similar coordinate data.

Table 1 shows that within a two-year period, through the use of the GPS collars as compared to use of VHF systems, savings of approximately $25,000 would accrue, and thereafter an annual savings of $38,250. As the number of animals collared increases, so do the cost savings. Additionally, the calculation of savings is based on person-hourly-wages of $30, burdened rates including all benefits, etc. As the hourly wage increases, a significant increase in cost savings can occur. For example, if this rate increased to $40 per hour, the annual cost savings for using GPS over VHF would be approximately $43,400 during the first two years and $56,650 on an annual basis thereafter.

Prior to this study, we placed radio collars on five animals on LANL property with VHF units and attempted to obtain one to two locational fixes per week using triangulation techniques. The success rate of obtaining locations with GPS collars appears to be as high, if not higher, than rates associated with the use of the VHF units. When considering that only one to two fixes were being obtained weekly with VHF units, we expended approximately 10 hours per week to locate those animals when locations were relatively constant (nonmigratory periods) and in noncanyon or other steep

Table 1. Cost and labor requirements, GPS versus VHF telemetry

	GPS collar (n=6)		VHF collar (n=6)	
	Year 1	Additional years (per yr. cost/hrs)	Year 1	Additional years (per yr. cost/hrs)
Equipment/Services (dollars)				
Collar cost (6)	32,000		2,400	
GPS/VHF receiver cost	1,750		2,400	
Other telemetry equipment costs (antennae, batteries, etc.)			350	150
Collar refurbishment		6,000		900
Argos/Data management	6,000	6,000	250	
TOTAL EQUIP./SERVICE COST	$68,000	$12,000	$5,400	$1,050
Labor (person hours)				
Data collection (tracking, ground truthing of GPS)	50	50	1540[1]	1540
Data management (downloading, plotting)	150	150	300	300
TOTAL PERSON LABOR HOURS	200	200	1840	1840
Hypothetical labor cost (dollars) (based on $30 hourly wage; assumes overhead charges, benefits, etc.)	6,000	6,000	55,200 (plus OT charges for weekend, etc., tracking)	55,200
TOTAL ESTIMATED COSTS	$74,000	$18,000	$60,600	$56,250

[1]Based on previously conducted field work on and near LANL using VHF telemetry

mountainous terrain areas, i.e., mesa tops, foothills, open terrain. When animals were expected to be found in steeper canyons, tracking time increased by 50% to 100% due to the remoteness and inaccessibility of that terrain. Furthermore, approximately 30% to 40% of the first attempts to locate animals in canyons and other challenging terrain were unsuccessful and attempted again the following day or week. Additional limitations on obtaining fixes included inaccessibility to remote areas during adverse weather conditions, restricted access to private or federal property, and limited access to LANL-secured areas. Although the GPS reception rate in canyons may be lower relative to mesa tops and other terrain more visible to satellites, we estimate a greater reception

rate and more accurate locational fixes compared to those obtained using VHF units. The rate estimate is based in part on the number of revisits to obtain VHF triangulations in canyons and the large estimated triangulation errors frequently associated with those readings.

Method

This report includes updated summaries of previously published LANL reports, reports currently in preparation, manuscripts submitted to professional peer-reviewed journals, and new information not included as part of any other publication. Where applicable, references to these reports and other publications are given in the text. A more detailed description of field methods and

approaches to data analysis is provided in the references listed in this report.

Two methods are being used to obtain data to reach the objectives of this study:

• GPS radio collar locational data/ Geographical Information System (GIS) interfacing and

• the collection of tissue samples for radiological contamination studies.

A brief summary of methods for capturing and collaring elk are described here; a complete description is provided in the 1996 and 1997 TDEA Annual Report.

We captured six elk in 1996. All six animals were harvested or died as a result of collisions with automobiles. Collars from four of these animals were refurbished and, with the addition of two new collars, deployed on different animals in 1997 and 1998, resulting in a total of 12 collared animals. The two new collars malfunctioned within two weeks of deployment and two of the recently collared animals were killed by vehicle collisions within six weeks of deployment.

Progress and Results

GPS Collar Accuracy Testing

Before we deployed the Telonics GPS collar, we estimated its positional accuracy under various vegetation types and terrain conditions. We tested the positional accuracy of the collars by programming them to attempt to obtain a position location every 20 minutes with continuous uplink to ARGOS satellites to transfer position data files. We placed the collar on a stand equivalent to the neck height of an adult elk and then placed the stand within three different treatment categories: (1) topographical influence (canyon and mesa tops), (2) canopy influence (open and closed canopy), and (3) vegetation type influence (ponderosa pine and piñon pine-juniper).

We used a hand-held differentially corrected GPS to obtain the position of the test collar at the same time and location. We estimated a mean overall locational error of 106 ±6 m (354 ±53 ft). We found no statistical differences ($\alpha = 0.05$) in locational errors and

observation rates between vegetation, topography, and canopy types. For further details on the evaluation of locational error related to the GPS collars, refer to Bennett et al. (1997).

Elk Movement Predictive Model

As part of the objectives of this study, we developed a spatial model to predict travel corridors of elk in and around LANL. The model was developed using the Spatial Analyst extension of ArcView and GRID of ARC/INFO. The model is

based on weighted distance functions that modify the straight-line distance by other factors, which is the cost (impedance) to travel along a path. This type of analysis is commonly referred to as a least-cost path analysis. Model variables include land-cover type, slope, aspect, mean daily distance traveled, and human induced variables such as fences, roads, and permanent structures (Figure 1).

GPS radio-collared data from eight elk were used to define variable class weights (impedance values). We used a
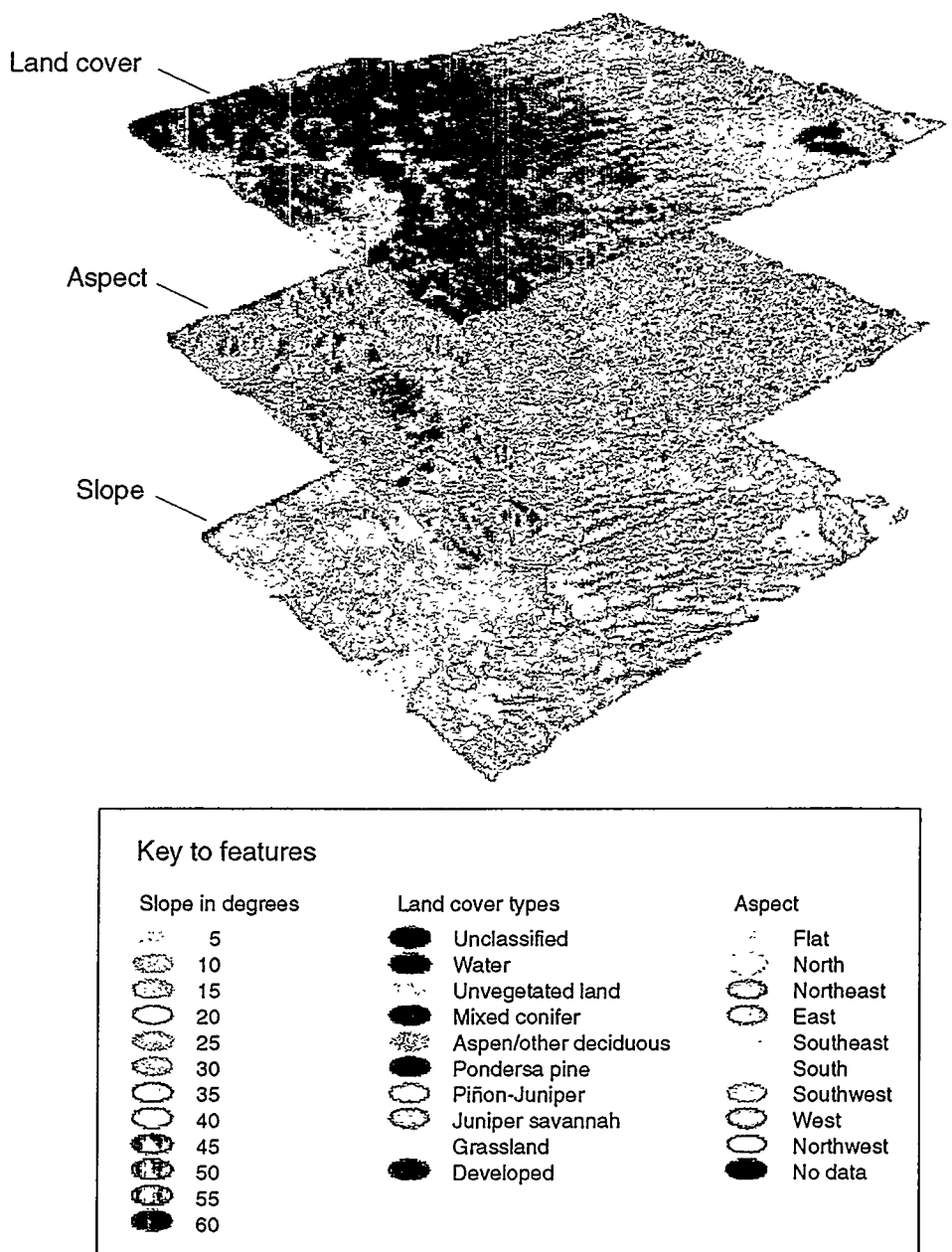
Figure 1. Three model variables used for the least-cost path analysis.

Key to features

Slope in degrees	Land cover types	Aspect
5	Unclassified	Flat
10	Water	North
15	Unvegetated land	Northeast
20	Mixed conifer	East
25	Aspen/other deciduous	Southeast
30	Pondersa pine	South
35	Piñon-Juniper	Southwest
40	Juniper savannah	West
45	Grassland	Northwest
50	Developed	No data
55		
60		

Chi Square Goodness-of-Fit analysis to evaluate elk locational data to each variable. The analysis compared the expected use of the variable classes (i.e., land cover type = ponderosa pine) to the actual observed data. If a variable class were used at a higher frequency than expected, we made the assumption that the variable class was favorable to elk movement and was given a low impedance score. However, if the variable was under utilized, the variable class was given a higher impedance score.

Impedance scores ranged from 0 to 999. Those variable classes that would always prevent travel (security fences) received a score of 999. Classes within natural variables such as cover types, slope, and aspect were given values between 0 and 100, zero representing no impedance and 100 being high impedance. The assignments of the impedance values were based on a ratio of the observed frequency to the expected frequency of variable use.

After impedance values were assigned to all variables, the variables were combined to yield a composite impedance surface. We used GRID to predict the movement path of elk from source locations to destination points. We specified a maximum distance to define the least-cost path. The maximum distance used was calculated from the average distance traveled by elk within its home range. The average would prevent the model from yielding a result that was incompatible with the elks' normal daily movement distance. For a more detailed description of the model, refer to Bennett et al. (1998).

Collar Observation Rates vs. Habitat Type/Cloud Cover

Following the conclusion of the study, we attempted to estimate observation rates for collars deployed on elk with respect to cloud cover and habitat characteristics within seasonal home ranges. Approximately 1800 fixes were obtained between March 1996 and June 1998 for all 10 elk combined. We calculated an approximately 69% observation rate (number of actual fixes/ total number of potential fixes) for all 10

animals combined (range of 54% to 96% for individual animals). The overall yearly observation rates ranged from 58% in 1996 to 82% in 1998.

The overall seasonal observation rates were lowest in fall (45%) and highest in spring (77%). The observation rates were significantly ($\alpha = 0.05$) higher in spring and winter compared with all other seasons and calving was significantly greater than fall. The observation rate was significantly higher during the period 1600-2000 compared to the period between 0000 and 1200 (p = 0.0005). The observation rate was generally higher from noon to midnight compared with midnight to noon. We did not observe any statistically significant differences in observation rates between cloud cover classes (p = 0.28) or between varying cloud base heights (p = 0.43). However, the observation rate was generally lower during overcast conditions.

Piñon pine and juniper made up the majority of most individual animal seasonal home ranges, followed by open (grassland) areas. Piñon pine and juniper were generally more prevalent in home ranges during spring and winter compared to other seasons. Ponderosa pine was more common in home ranges during calving, summer, and fall.

Approximately 60% of all seasonal individual animal home ranges consisted of 0%–10% slopes and composition of steeper slopes within home ranges tended to increase during warmer months. Multiple regression analysis showed that cover type was not a significant predictor of GPS observation rate (p = .0877, R^2 = 0.1923) nor was slope (p = 0.4758, R^2 = 0.2475).

Habitat Use

Overall and seasonal habitat use and availability was evaluated previously following the first year of data collection (Biggs et al. 1997). However, additional data collected through the calving season in 1998 and updates to the land cover map resulted in some changes to the habitat use and availability analysis. A more thorough discussion of habitat use is given in Biggs et al. (1998b).

We observed significant differences ($x^2 = 513$, DF = 7, n = 2009, p<0.001) between the amount of habitat available and the amount used throughout the year. Elk used grasslands much more than expected— >50% difference between observed and expected—and used aspen forests somewhat more than expected— between 25%–50% difference in observed and expected values. All other habitats were used relatively consistent with the amount available.

During summer and fall calving, elk use of aspen forests was much greater than expected and much less than expected in spring and winter. Elk tended to use forested habitats (ponderosa pine, aspen, mixed conifer) more than expected in summer and less than expected in winter. Our data showed that during all seasons, the elk had a a strong preference for LANL grasslands.

Movement Patterns

To better define travel corridors used by elk on and near LANL property and corridors used on a seasonal basis for elk moving off LANL property (figure 2), we examined the movement patterns of collared animals by plotting all locational fixes onto GIS coverages of topography and physical structures. A more detailed description of travel corridors is provided in Biggs et al. (1998b). The maps depict travel corridors based on collared animals only and should not be interpreted to indicate all travel corridors of elk on or near LANL. Based on the locational fixes of all collared animals, we have identified 6–8 primary travel corridors with several branches occurring on LANL property (figure 3).

Travel corridors in the east portion of LANL appear to be dictated by security fences and other structures. There are two areas within the east portion of LANL where corridors cross between LANL property and San Ildefonso property. Travel corridors in the west portion of LANL circulate around TA-16 with corridors extending into TA- 6, -8, -9, and -15. During some period of the study, three of the elk collared from 1996– 98 migrated or traveled west off LANL property toward or near the Valle Grande.
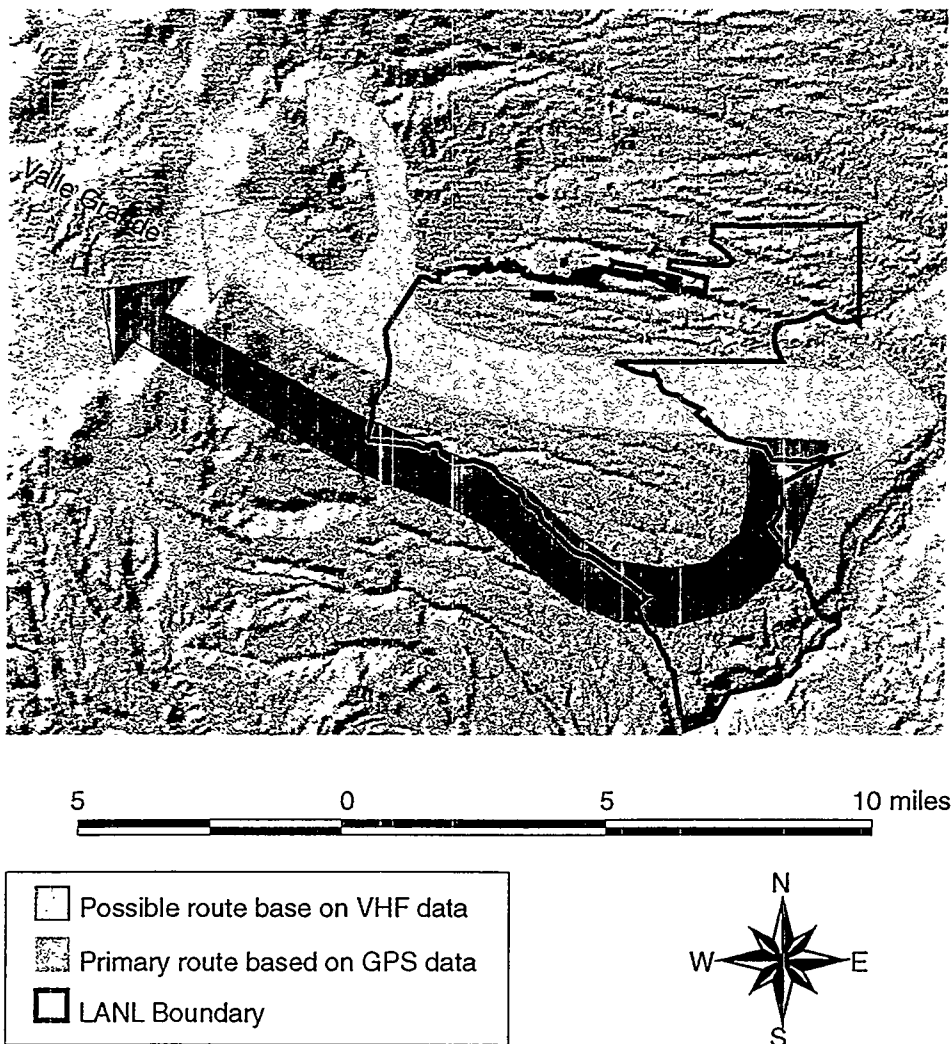
13

Figure 2. Migratory routes for collared elk, LANL-East Jemez Mountains.

The primary travel corridor for these animals occurred in the vicinity of Pajarito Mountain which extends off LANL property near TA-8 and -58.

We observed a different route of travel for the four elk collared in 1995 with VHF units. These animals moved along the southwest and southern border of LANL. Locations of VHF-collared animals were obtained less frequently than the GPS collared animals and therefore, the routes are only considered as "possible" travel routes.

Radioisotope Concentration/ Movement Analysis

Elk forage in many areas at LANL that may contain radioactivity above natural and/or worldwide fallout levels. We analyzed radionuclide concentrations

(^{3}H, ^{90}Sr, ^{137}Cs, ^{238}Pu, ^{239,240}Pu, ^{241}Am and total Uranium) in muscle and bone tissue of elk collected from LANL lands from 1991 to 1998, including those animals collared as part of this study (Fresquez et al. 1998). Most radionuclide concentrations in muscle and bone from individual elk collected from LANL lands were either at less than detectable quantities (where the analytical result was smaller than two counting uncertainties) or within upper (95%) level background (BG) concentrations.

As a group, most radionuclides in muscle and bone of elk collected from LANL lands were not significantly higher ($p<0.05$) than in similar tissues from elk collected from background locations. Also, GPS-collared elk that spent an average of about 50% of their time on

LANL lands were not significantly different in most radionuclides than road-killed elk collected as part of the environmental surveillance program. Overall, the upper-level net (95%) CEDE, i.e., the CEDE plus two sigma for each radioisotope minus background, at the most conservative ingestion rate of 50 lbs. of muscle and 13 lbs. of bone, was 0.117 mrem/yr. and 1.67 mrem/yr. for elk muscle and bone, respectively. The combined dose was less than 2% of the International Commission on Radiological Protection (all pathways) permissible dose limit for protecting members of the public.

Conclusions and Deliverables

In addition to providing data on the radioisotope concentrations in elk as related to their movement patterns on LANL, this study provides data that is a foundation for the initial development of long-term management strategies for elk. Our data also identify locations of concern on LANL property where specific management strategies may be necessary to aid local agency officials in minimizing human/animal conflicts. The general and specific results from this study provide data on radioisotope concentrations in elk tissues, seasonal habitat use, movement and activity patterns, and travel corridors of elk, which can be used to address contaminant concerns, human-elk interface issues, and LANL project management. Each of the primary objectives of this study are listed below with a discussion of results, including the completion of deliverables where applicable.

Evaluation of global positioning system (GPS) collar in habitats at LANL

The estimated error rates and observation rates we calculated in the evaluation of the GPS collars appear to be as high as rates calculated with the use of VHF collars and within acceptable ranges for applying elk resource use and movement analysis. The results of data analysis for this objective are presented in this and previous annual progress reports and are further detailed in Bennett et al. (1997) and Biggs et al. (1998a). If additional
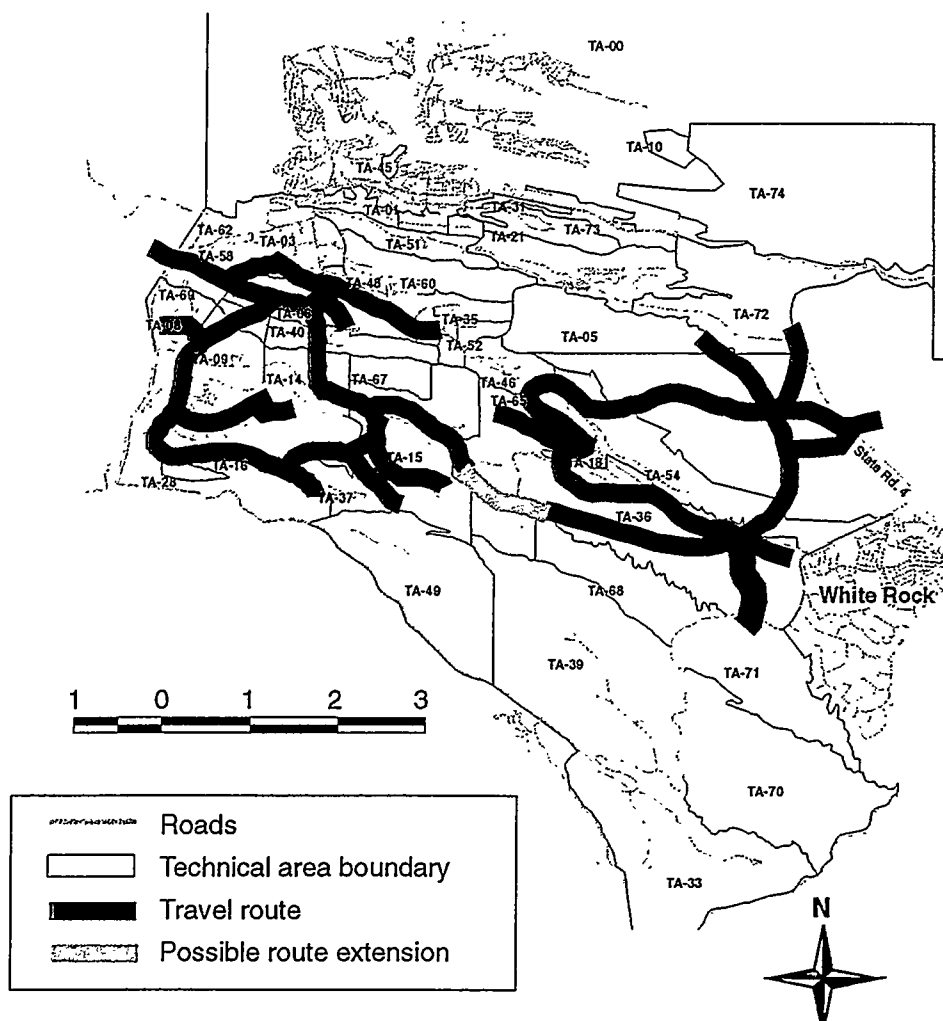
Figure 3. *Primary travel corridors of collared elk at LANL, 1996-98.*

higher than tissues from elk collected from background locations.

Calculation of CEDEs and risk of cancer fatalities to people who consume meat from elk that use LANL lands

We found that based on the elk tissue and bone analysis, the highest dose received from consuming elk found on LANL property is less than 2% of the International Commission on Radiological Protection permissible dose limit for protecting members of the public (Fresquez et al. 1998). The radio-tracking of elk on LANL property and subsequent tissue sampling have allowed us to determine the animals' potential exposure to contaminants by defining the elks' history of habitat use around contaminated sites.

Predictive models for use in the LANL facility/project planning process

By interfacing the GPS locational data and GIS coverage, we developed a model to predict the routes an elk would probably take to move from one point to another should its current route of travel be interrupted. Through application of the model, we can identify expected alterations in current habitat use resulting from the implementation of management recommendations and strategies. The model can also identify possible impacts to elk movement patterns from proposed LANL projects. The model is currently being applied to DARHT facility as part of the mitigation action plan developed as part of the EIS for that facility. We compared the model result to locational data collected from GPS-collared elk. Our GPS locational data suggest that the predicted route was being used heavily by elk. Further testing, evaluation, and verification of the model are ongoing. A detailed description of the model is given in Bennett et al. (1998).

Development of long-term management strategies/identification of locations of concern

Based on the collected data and analysis, we have identified several areas on LANL property that should be more closely assessed for their contribution or

work related to tracking animals with GPS collars is performed on LANL property, a correction factor will be developed and applied to all data based on these analyses.

Evaluation of activity patterns and resource use of elk via spatial and temporal analysis

A summary of results on activity patterns, resource use, and travel corridors of elk on LANL property is provided in various sections of this report. Detailed descriptions of these analyses are given in Biggs et al. (1998b).

We have identified seasonal differences in elk use of terrain and cover types that should be used as a basis in the future assessment of the impact of LANL operations and proposed projects on elk inhabiting LANL and adjacent areas.

Long-term management recommendations and strategies are needed to account for and identify the role that all habitats play in the use of LANL property by elk.

Comparison of radionuclide content in collared elk at LANL to background locations

Based on the analysis of movement and locational data, we conclude that elk move freely between areas of contamination and are likely to forage in and around these areas. Between 1996 and 1997, we collected and analyzed tissue and/or bone samples from five out of the six originally collared elk for concentration levels of various radioisotopes (Fresquez et al. 1998). Based on the analysis, most radioisotope concentrations in tissues of collared elk that have a defined history of use around these contaminated sites were not signifcantly

potential contribution to human/elk conflicts. Based on the identity of movement patterns and areas of concentrated use, we have concluded or strongly suspect the following:

• There is a minimum of two migratory routes from the Jemez Mountains to LANL property, as described previously in this report. These routes may act as "pinch points" for animals moving onto and off of LANL property and should be adequately considered and evaluated prior to permitting any development to occur at these locations.

• There are at least two primary travel corridors by which elk move back and forth on to San Ildefonso Pueblo property. These corridors must also be adequately evaluated as to their role in allowing elk to move onto Pueblo property prior to the implementation of management strategies in these areas.

• There are six areas of concentrated use on LANL property and of these, four occur along heavily traveled roadways. In addition, we have identified four travel routes that pass back and forth over major roadways. If any management strategies, i.e., fences, habitat alteration, are applied to these areas of concern, we recommend that the resulting impact to movement patterns be evaluated by initially applying the elk predictive model derived from the collaring and monitoring of animals in those areas.

Based on our study results, we recommend that several strategies be considered, either individually or in combination, in the development of management techniques for elk that inhabit Laboratory property:

• Evaluate the development of constructed water sources to draw elk away from current water sources (primary water sources occur in close proximity to major roadways and may act as an important factor in the distribution and movement patterns of elk).

• Evaluate use of habitat alteration/ manipulation to redistribute animals to more desirable locations.

• Evaluate construction of impenetrable fences (i.e., security fences) along roadways where highest elk concentrations occur, while assessing potential impact to alterations in movement patterns.

References

Bennett, K., J. Biggs, and P. R. Fresquez, "Determination of locational error associated with global positioning system (GPS) radio collars in relation to vegetation and topography of north-central New Mexico," Los Alamos National Laboratory report LA-13252-MS (1997).

Bennett, K., J. Biggs, and P.R. Fresquez, "Development and application of a movement predictive model for elk," Los Alamos National Laboratory report LA-UR-97-4009 (1997).

Biggs, J., K. Bennett, and P. R. Fresquez, "Evaluation of habitat use by Rocky Mountain elk in north-central New Mexico using global positioning system (GPS) radio collars," Los Alamos National Laboratory report LA-13279-MS (1997).

Biggs, J., K. Bennett, and P. R. Fresquez, "Estimation of observation rates of global positioning collars (GPS) deployed on elk," Los Alamos National Laboratory Report LA-UR-98-1080 (1998a).

Biggs, J., K. Bennett, and P. R. Fresquez, "Resource use, activity patterns, and disease analysis of Rocky Mountain elk (*Cervus elaphus nelsoni*) at the Los Alamos National Laboratory," Los Alamos National Laboratory report LA-13536-MS (1998b).

Fresquez, P. R., D. R. Armstrong, and J. G. Salazar, "Radionuclide concentrations in elk that winter on Los Alamos National Laboratory Lands," Los Alamos National Laboratory report LA-12795-MS (1994).

Fresquez, P. R., J. Biggs, K. Bennett, D. Kraig, M. Mullens, and J. Ferenbaugh, "Radionuclide concentrations in deer and elk at Los Alamos National Laboratory: 1991–1998," Los Alamos National Laboratory report LA-13553-MS (1998).

White, G. C., "Biotelemetry studies on elk," Los Alamos Scientific Laboratory report LA-8529-NERP (1981).

Comparison of Two Permanent Plots within the 1977 La Mesa Fire and Observations from the Oso Fire

Introduction

As a progress report for funding received, this paper is reporting on information from one plot on Bandelier National Monument and one plot on Los Alamos National Laboratory (LANL), both severely burned in a 1977 fire. The reason for this comparison is to look at the pattern of succession influenced by seeding and prescribed burning. In this paper, we are presenting some of the photographic comparisons from the various years. We are comparing species diversity on two plots: Bandelier, Burnt Mesa, a severely burned plot that was reburned by the prescribed fire in 1998 and LANL, a severely burned plot that was not reburned by prescribed fire and was influenced by the Bandelier seeding. No attempt is made to do an in-depth analysis of the data for this report.

History of the La Mesa Fire study

In June 1977, the La Mesa fire burned 15,270 acres of US Forest Service (USFS), Bandelier National Monument. Smoke was dense, and the fire became a threat to LANL and the community of Los Alamos. This fire was the first extensive wildfire in the area since the late 1890s. Since that time we have had two major fires—the Dome fire in 1996 and the Oso fire in 1998. Similarly, these fires have been a threat to LANL and the community.

After the La Mesa fire, the entire burned area on BNM was seeded with six grass species, a small area (180 acres) within Technical Area (TA) 49 was not seeded. Areas within BNM or TA-49 were not replanted with pines, but natural succession has taken place. By 1985,

most of the snags were lying on the ground where they had fallen, and now constitute down woody fuels. As a result of these fuel loads, BNM carried out a prescribed fire on Burnt Mesa and Escobas Mesa in April and June of 1998. Plots within LANL were not burned in 1998.

Before the La Mesa fire, Loren Potter from the University of New Mexico and I began a study to provide data on previous fire frequencies and plant succession after the fire at BNM (Foxx and Potter 1978). Figure 1 shows the fire history of BNM at that time. The La Mesa fire burned over most of the areas we had begun to study in 1975. Analysis of the pre- and post-fire data at four different times (1977, 1978, 1985, and 1993) was recorded in the 1994 symposium paper entitled Vegetation Succession after the La Mesa Fire at Bandelier National Monument (Foxx 1996).

Figure 1. Fire history of Bandelier National Monument before 1977.

In addition to the information gleaned from the pre- and post-fire transects, Dr. Potter and I established some permanent plots (a total of 15) within two months of the fire along transects on Frijoles (in a piñon-juniper woodland), Burnt, and Escobas Mesas (in a ponderosa pine
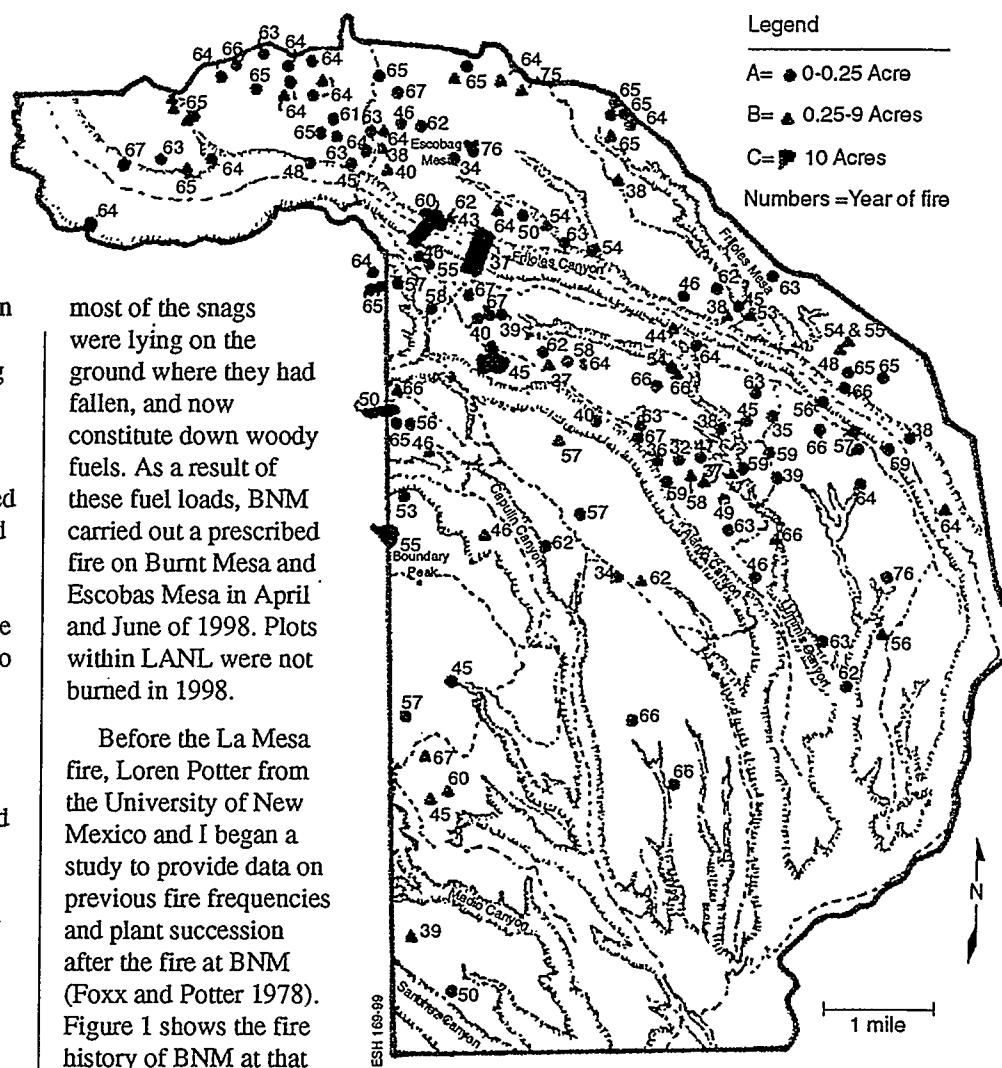
forest) and at Apache Springs (in mixed conifer forest). Plots located on Escobas Mesa, Burnt Mesa, and TA-49 were visited in 1978, 1985, 1992, and 1998. During each visit, we photographed the sites, recorded phytosociological data, and mapped tree locations. In addition to these plots, we set up a photo station on Burnt Mesa after a small fire in 1975 and on Escobas Mesa after the fire in 1976.

In 1998, we relocated these photo stations and took pictures. Although our primary goal in 1998 was to relocate each plot and identify the location with geographic information system (GIS) technology, the burning of the plots provided a unique opportunity to compare the site from 1992 (post-La Mesa but pre-prescribed burn) to 1998 (post-prescribed burn). Additionally, we decided to collect data on the LANL plots because they had not been burned by the Bandelier prescribed fire. This interim report is not comprehensive but is a start at the analysis of over 20 years of data on the BNM plots and those on LANL.

Description of the La Mesa Fire

Information reported by Foxx and Potter (1978) summarized the specifics of the La Mesa fire from Forest Service notes on fire behavior and weather prediction. Here is our summary.

The La Mesa fire was first reported at 1556 hours, June 16, 1977, by the St. Peter's Dome Lookout, and within 20 minutes of the original sighting, flames and heavy smoke were noted. The fire burned out of control for seven days, when weather patterns shifted and scattered thunderstorms produced heavy rains and reduced temperatures. The fire was declared controlled at 1600 hours June 23, 1977. The location and spread of the fire are given in Figure 2.

The fire began in a pile of slash on Mesa del Rito approximately two miles from the western boundary of BNM. Investigations by Forest Service personnel deemed it to be human-caused, either deliberate or accidental. The area consisted of dense ponderosa pine that had been logged 20 years previously. The slope of the mesa top was 10% to 15%

but steeper in the draws and precipitous at the edge of the mesa into Alamo Canyon.

At 1730 hours, an aerial reconnaissance flight revealed the fire to be approximately 50 acres in size. Six days later it was over 15,000 acres.

After the fire, BNM participated in a joint project with the USFS to seed grasses by helicopter. Since only minimal portions of the area were lightly burned, most of the 15,270 on Bandelier acres were seeded. Although native grasses were suggested for reseeding, seeds for native species were not available, and similar species were used. Grasses used were sand dropseed (*Sporobolus cryptandrus*); blue grama (*Bouteloua gracilis*); sheep fescue (*Festuca ovina*)— labels on sacks indicated "hard fescue" (according to Hitchcock [1950], this is *Festuca ovina* var. *duriuscula*, which is an exotic introduced from Europe; spike muhly (*Muhlenbergia wrightii*); western wheatgrass (*Pascopyrum smithii*); and slender wheatgrass (*Elymus trachycaulum*). These species were chosen because of (1) natural occurrence,

(2) soil-holding properties, (3) availability of seeds, and (4) ease of seeding. The canyon bottoms were to be hand-seeded with species such as *Poa interior* and *Oryzopsis asperifolia*, native to the canyon bottoms. Fire lanes were seeded by hand.

The helicopter seeding began July 12, 1977. An attempt was made to spread 60 seeds per sq. ft. In badly burned areas, the spread of 70 to 75 seeds per sq. ft. was desirable. In less severely burned areas, 50 to 55 seeds per sq. ft. was acceptable. Escobas Mesa was seeded on July 13 and Burnt Mesa on July 14. By the third week in August, after approximately 4.5 weeks, germination was first observed.

The Oso Fire

During the summer of 1998, the Oso fire burned out of control the last week of June. In August, I also visited areas of the Oso fire at Santa Clara Canyon with the Santa Clara Environmental Department. I provide a photographic record of areas within the Oso fire approximately two months post-fire. These photographs were compared with La Mesa fire
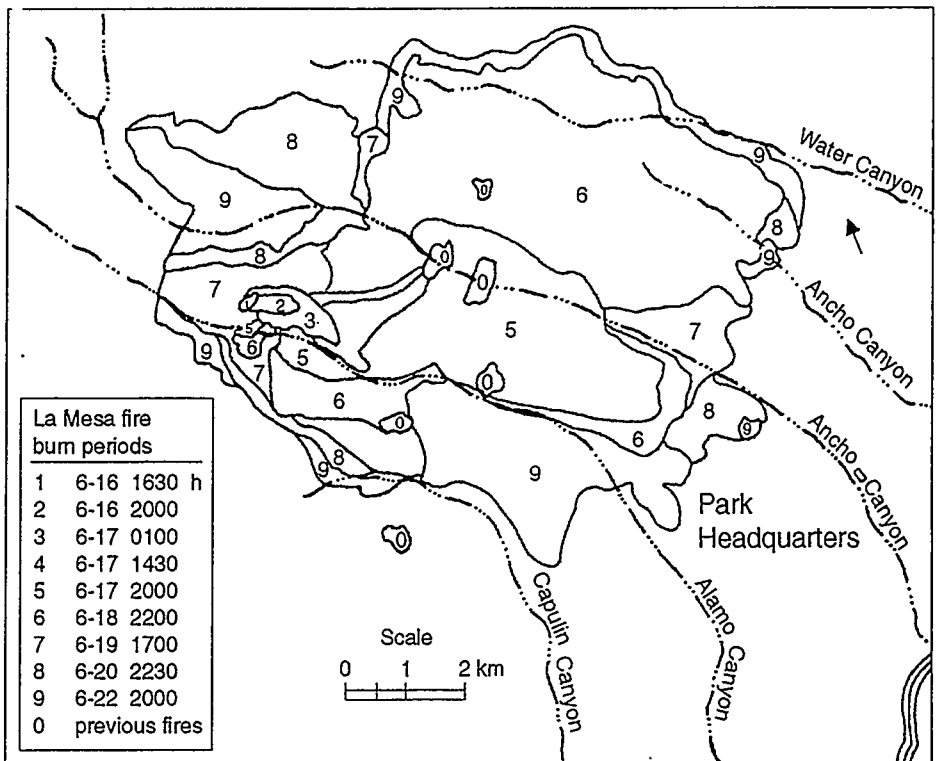

La Mesa fire burn periods		
1	6-16	1630 h
2	6-16	2000
3	6-17	0100
4	6-17	1430
5	6-17	2000
6	6-18	2200
7	6-19	1700
8	6-20	2230
9	6-22	2000
0	previous fires	

Figure 2. Rate spread of the June 1977 La Mesa fire

photographs taken two months after the La Mesa fire.

The data collected over the past 21 years provide long-term information that can help us understand the process of succession that will take place on the more recent fires such as the Dome and the Oso fires and provide some information for rehabilitation of these burned areas.

Methods

Selection of plots for post-La Mesa fire study

On July 6, 1977, representatives of BNM and LANL and investigators of the fire ecology study met to coordinate post-fire studies. At that meeting, a verbal agreement was made concerning the establishment of plots for future succession studies. LANL set aside an area that was not to be seeded. Permanently staked 20- by 50-meter plots would be used for measuring areas of varying degrees of fire damage. Previous to the La Mesa fire, Roland Wauer of the National Park Service had established transects for ornithological studies. At his request, the vegetation study plots were placed along these transects in areas of varying degree of burn damage, i.e., severe, moderate, and light. Areas were considered severely damaged when tree crowns were completely consumed and the litter and duff were burned to mineral soil. Moderate damage included areas where the tree crowns were only partly consumed and some trees were still green, although most of the understory vegetation was consumed, and in some areas, litter and duff were burned to mineral soil. Areas lightly damaged had a majority of trees remaining alive and litter and duff were only lightly scorched.

The plots were aligned either east-west or north-south and remaining entirely within the category of damage. Each plot was established by compass and lines were 50 m and 20 m in length. The 50-m side was divided into four equal parts. The 20-m side was marked off into 2-m increments. Photo stations were established at opposite corners, and photos were taken with a 35-mm camera

and a 28-mm wide-angle lens to obtain the widest coverage. The plots were marked using rebar and a t-pole. On LANL property, the plots were marked with angle iron and t-poles. The t-pole was placed were it would be the most visible from a road or trail.

Visits to the Plots

In 1998, we visited plots on Escobas Mesa, Burnt Mesa, and LANL. We photographed each plot, located comparative pictures from photo files, used a geographic positioning system (GPS) to locate the plots for future reference, took data along the five lines, and mapped each site for tree and shrub location. For this analysis we choose only to compare one Burnt Mesa Plot and the LANL Plot.

Plot Characteristics

Characteristics of the two plots we choose to analyze are seen in Table 1. The Burnt Mesa plot is approximately one mile from the gate to Burnt Mesa to the south side of State Route 4. The plot is located on the northwest side of an old fire road along a gently sloping northwest-facing slope. The LANL plot was established in TA-49. TA-49 is found in the southern portion of the Laboratory across from Burnt Mesa and on the north side of State Route 4, and on the south rim of Water Canyon. The plots are located both east and west of a utility line that traverses Water Canyon. Both of these plots were burned July 18, 1977 when the fire spread was estimated to be 38 chains/hr. The fire was a crown fire in both locations. All the trees were severely burned as evidenced by complete loss of crown and intense charring of trees. In 1998, the Burnt Mesa plot was burned as part of the Bandelier prescribed fire program, but the LANL plots were not.

Results

Comparative Photographs

We classified plots as severely burned based on the foliar damage (Foxx and Potter 98). The fire consumed the crowns of all of the trees. Additionally, the duff layer and some of the downed woody fuels were burned, and a significant amount of soil heating was evidenced by the condition of the soils. After the fire erosion rills were forming in the denuded soil and sprouting of deep-rooted species such as oak (*Quercus* spp.) and New Mexico locust (*Robinia neomexicana*) were evident.

Photographs were taken at various corners of both plots and along the lines. Figures 3 through 6 show views of Burnt Mesa from immediately after the fire to 21 years after the fire (1998). In Figure 3, all the trees are devoid of needles and are considered dead. Figure 4 shows a striking contrast with Figure 3 in that the seeded grass, slender wheatgrass, dominates the understory. Figure 5 illustrates the snag fall eight years after the La Mesa fire. Figure 6 illustrates the contrast after 21 years and post-prescribed fire.

Comparisons were made between 1985, 1992, and 1998. In Figure 7, the extensive snag-fall can be seen. Pictures taken in 1992 indicate extensive down woody fuels and a number of standing snags (Figure 8). After the prescribed burn in April 1998, the fuels have been reduced, and a number of the snags have either fallen in the last six years or were consumed by the prescribed burn (Figure 9).

When we visited the area in August 1998, we were impressed by the density and variety of species growing within the plot. The reduction of litter by the April

Table 1. Characteristics of the Plots

Plot	Date Burned (1977)	Burn Intensity (1977)	Seeded	Replanted with trees	Prescribed fire (1998)	Down woody fuels (1998)
Burnt Mesa	July 18, 1977	Severe	Yes	No	Yes	Few
LANL	July 18, 1977	Severe	No	No	No	Many

prescribed fire had produced a flush of growth. The bases of the grasses were devoid of litter and the grasses were luxuriant. Little bluestem and big bluestem were taller than usual, and plants were robust. In addition, species
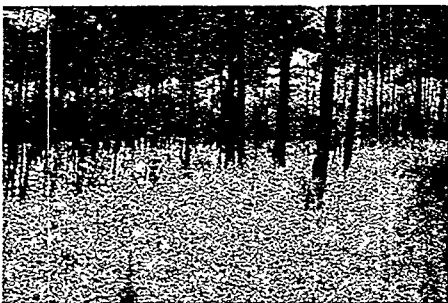

Figure 3. Burnt Mesa, 1977.

Figure 4. Burnt Mesa, 1978, one year after the La Mesa fire.

Figure 5. Burnt Mesa 1985, 8 years after the La Mesa fire.

Figure 6. Burnt Mesa, 1998, 21 years post-La Mesa Fire, a few months post-prescribe burn.

such as the dayflower (*Commelina dianthifolia*)—which had been seen immediately after the 1977 fire but then had disappeared from the floral element after a year or two—were abundant four months after the recent prescribed burn.

We also photographically compared the plots at LANL. The LANL plots were also considered to be of high-severity fire. The fire crowned in the area, and all trees, based on the foliar damage, were judged to be severely burned (Foxx and Potter 1984). In this plot, all trees were consumed by the fire. Additionally, the duff layer and some of the downed woody fuels were burned, and a signifi-

Figure 7. Burnt Mesa, 1985, 8 years after the La Mesa fire.

Figure 8. Burnt Mesa, 1992, 15 years after the La Mesa fire.

Figure 9. Burnt Mesa, 1998, 21 years after the La Mesa fire and after a prescribed burn in April 1998.

cant amount of soil heating was evident. The LANL plots were not seeded, but some sites got seed blow-over from the Bandelier overflights. We have chosen to compare one of these plots with the Burnt Mesa plot. Only one of the three plots was positioned in the landscape in an area that did not get seed blow-over. The dominant plant in 1978 within LANL was fetid goosefoot (*Chenopodium graveolans*) as seen in Figure 10. Similar to Burnt Mesa most of the snags had fallen by 1985 (Figure11). Much of the area in 1998 has large clumps of oak, and the dominant grass is mountain muhly (Figure 12). Some large snags remain. Not evident in these pictures is the extent of downed fules.

One of the most striking visual and measured differences between the areas on Burnt Mesa and Escobas Mesa burned by prescribed fire and those within LANL was the reduction of the large diameter fuels. Figure 13 shows the extent of the large diameter fuels. Recent pictures taken on Escobas Mesa illustrate the reduction of the large diameter fuels by the prescribed fire (Figures 14 and 15). The bases of the grasses had large mats of litter and dead material not seen in the Burnt Mesa plot burned by the April prescribed burn. Cover estimates indicated that there was a 40% reduction in the litter in the Burnt Mesa plot from the prescribed fire.

Photographic Comparison of the La Mesa Fire with the Oso Fire

The Oso fire began late in June 21 years after the La Mesa fire. Photographs taken in the La Mesa fire area and data analysis can be used to begin to understand the process of succession on the area of the Oso fire. One example is given here. In the severely burned area above Santa Clara Canyon, aspen was sprouting from the previously buried roots. The height of the aspen was similar to that for the same time period after the La Mesa fire (Figure 16 and 17). Figure 18 shows the aspen succession in the La Mesa fire. One can predict the height of the aspens in the burn area of the Oso fire after a certain number of years by studying the corresponding photograph of

the burn area of the La Mesa fire. This example illustrates the usefulness of long-term data for the rehabilitation of recently burned sites in the Jemez Mountains.

Figure 10. LANL plot, 1978, 1 year post La Mesa fire

Figure 11. LANL plot, 1985, 8 years post La Mesa fire. Not the downed fuels.

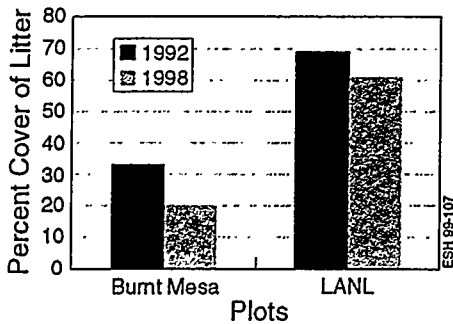*Figure 12.* LANL plot, 1998, 21 years post La Mesa fire.

Figure 13. Comparison of litter cover.

Figure 14. LANL plot, 1998, note the downed logs still evident 21 years post fire

Figure 15. Escobas Mesa at intersection of the Escobas Mesa road with upper crossing trail. This photo illustrates the reduction of downed logs from the La Mesa Fire by the June prescribed fire.

Figure 16 (a, b). Aspensprouts in OSO fire area, Santa Clara Canyon, August 1988, approximately 2 months post fire.
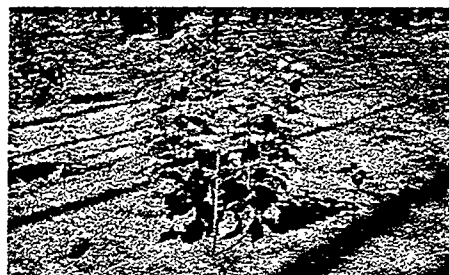

Figure 17. Aspensprouts in La Mesa fire area, 2 months post fire.

Figure 18. (a) Aspen sprouts in 1978 in La Mesa fire area 2 months post-fire. (b) Aspen sprouts in 1985 in La Mesa fire area 2 months post-fire.

Data Analysis

For this progress report we have primarily used comparative photographs to illustrate the succession in two severely burned plots over the past 21 years.

We have prepared data tables that present the total cover of each species for each of the two plots collected in 1978, 1985, 1992, and 1998 (Tables 2 and 3). Various analyses are being conducted on these and the other 15 plots established in Bandelier and LANL after the La Mesa fire and will be presented in a Los Alamos publication.

At this time, some general observations can be noted from the data collected on these two plots. First using the

Table 2. Comparison of Percent Cover of Species through Time in Burnt Mesa 3 Plot

Species Name	1977	1978	1985	1992	1998
Grass and Graminoides					
Pascopyrum smithii		< 1	< 1		1
Elymus trachycauly spp. trachycaulus		5	13.7	2	
Andropogon gerardii					< 1
Schizachyrium scoparium spp.scoparium				5	2
Aristida purpurea var. longiseb				< 1	
Bouteloua gracilis		< 1	< 1	< 1	< 1
Blepharoneuron tricholepis					< 1
Bromus spp.					
Bromus rubens		< 1			
Bromus tectorum				< 1	
Carex spp.		< 1			< 1
Festuca ovina		1	5.3	8	< 1
Koeleria macrantha			< 1		
Muhlenbergia montana		< 1	1.7	5	1
Muhlenbergia wrightii		< 1	1.3	3	1
Poa spp.				< 1	
Vulpia octoflora var octoflora			< 1		< 1
Total Grass Cover %	0	6.6	22.7	23.4	5.6
Forbs					
Achillea millefolium var. occidentalis			< 1		
Allium cernuum var. obtusum	< 1		< 1		
Antennaria parvifolia				< 1	< 1
Artemisia carruthii					< 1
Artemisia dracunculus			< 1		
Bahia dissecta	< 1	< 1	< 1	< 1	2
Ceanothus fendleri			< 1		< 1
Chenopodium album			< 1		
Chenopodium fremontii					
Chenopdium graveolens					
Cirsium undulatum				< 1	1
Commelina dianthifolia		1			
Conyza canadensis				< 1	
Convolvulus arvensis		< 1			
Cryptantha cinerea var jamesii				< 1	< 1
Cystopteris fragilis					< 1
Erocameria spp. nauseosus					
Erigeron spp.			< 1		
Erigeron divergens		< 1		< 1	
Erigeron flagellaris					< 1
Erysimun capitatum			< 1		
Euphorbia spp.	< 1				
Chamaesyce serpyllifolia spp.serpyllifolia	< 1				< 1
Geranium caespitosum			< 1	< 1	< 1
Helianthus petiolaris			< 1		
Heterotheca var. villosa				< 1	< 1
Hymenoxys richardsonii var. floribunda					< 1
Forbs (cont.)					
Liatris punctata					< 1
Linanthus nuttallii spp.tenuilobus			< 1	< 1	
Lithospermun multiflorum					< 1
Lotus wrightii	< 1			< 1	< 1
Lupinus spp.			< 1		
Lupinus caudatus spp argophyllus					2
Mentzelia multiflora var. multiflora			< 1		
Mirabilis multiflora				< 1	
Oenothera spp.			< 1		
Mirabilis lineraris					< 1
Physalis subulata var. neomexicana	< 1				
Rosa woodsii					< 1
Thelesperma filifolium var. filifolium					< 1
Tragopogon spp.			< 1		
Tragopogon dubius				< 1	
Verbascum thapsum			< 1	< 1	< 1
Total Forb Cover %	.4	1.5	1.5	1.4	6.7
Shrubs					
Quercus spp.			< 1	8	10
Robinia neomexicana					13
Total Foliar Cover %	.4	8.1	24.3	32.8	35.3
Bare Soil				32.87	45.70
Rock				1.35	
Litter				32.98	19.6
TOTAL COVER				100	100

photographic record and data analysis, we have observed that the prescribed burn done in Bandelier succeeded in reducing the fuel loads caused by the numbers of down trees. This, however, is not the case in LANL. The down fuels are still extensive and may represent a fire hazard. Only one species, wild chrysanthemum (*Bahia dissecta*), is consistently found within both plots for all years sampled. The seeded species were not found within the LANL plot but did exist in the Burnt Mesa plot. Sheep fescue, a seeded species, was found four years out of four years with the peak cover being in 1992 before the prescribed burn. A dominant early successional species appears to be the fetid goosefoot (*Chenopodium graveolans*) in these severely burned sites. This goosefoot disappears as a component in the understory within one to two years post-fire.

Conclusions

Considerable information has been gathered over the past 21 years in a total of 15 permanent plots established in 1977 after the La Mesa fire. Progress has been made in the photo interpretation of two of the 15 plots, and some analysis of quantitative data has begun for each of the plots.

Table 3. *Comparison of Percent Cover of Species through Time in the LANL plot*

Species Name	1978	1985	1993	1999
Grass and Graminoides				
Agropyron desertorum	< 1			
Aristida divaricata		< 1		
Blepharoneuron tricholepis				<1
Bouteloua gracilis	< 1	< 1		
Bromus tectorum		< 1		
Elymus elymoidas spp. elymoidas	< 1	< 1		
Elymus trachycaulum spp. trachycaulum	3	16		
Festuca ovina	< 1			
Muhlenbergia montana		< 1	4	7
Muhlenbergia wrightii	< 1			
Pascoppyrum smithii	< 1		4	
Poa spp.				
Sporobolus cryptandrus	< 1			
Total Grass Cover %	**3.7**	**16.5**	**8**	**7.1**
Forbs				
Artemisia spp.	< 1			
Artemisia carruthii		< 1	1	2
Artemisia dracunculus		< 1	3	5
Aster		< 1		
Bahia dissecta	< 1	< 1	< 1	< 1
Chenopodium album	< 1			
Chenopdium graveolens	< 1			< 1
Chrsopsis fovoisa	< 1		1	3
Cirsium undulatum		< 1	2	3
Conyza canadensis		< 1		
Cryptantha cinerca var. jamesii	< 1			
Ericameria nauseosus spp. nauseosus	< 1			
Erigeron divergens	< 1	< 1		
Erigeron flagellaris	< 1			
Gutierrezia sarothrae	< 1	< 1		
Hymenoxys richardsonii var. floribunda		< 1	< 1	< 1
Kochia scoparia	< 1			
Koeleria cristata	< 1		1	< 1
Linum spp.	< 1			
Lotus wrightii			< 1	< 1
Lupinus caudatus spp. argophyllus		< 1		
Lupinus kingii		< 1		
Lycurus phleoides		< 1		
Melilotus officinalis				< 1
Plantago patagonica	< 1			
Polygonum aviculare		< 1		
Salsola kali	1			
Senecio bigelovi var bigelovi		< 1		
Senecio multibatus	< 1			
Sonchus asper		< 1		
Taraxacum officinale		< 1		
Thelesperma filifolium var. filifolium	< 1			

Species Name	1978	1985	1993	1999
Forbs cont.				
Townsendia exscapa Tragopogon dubius		< 1	< 1	< 1
Vicia americana spp. americana	< 1			
Verbascum thapsum		< 1	< 1	< 1
Total Forb Cover %	**2.5**	**1.3**	**8.9**	**16**
Shrubs				
Juniperus monosperma				< 1
Quercus spp.				2
Ribes cereum	< 1			
Robinia neomexicana			< 1	< 1
Total Foliar Cover %	**6.2**	**17.9**	**17**	**25.3**
Bare soil			14.0	13.7
Litter			69.0	61.0
TOTAL COVER			**100**	**100**

References

Foxx, Teralene S. and L. D. Potter, "Fire Ecology at Bandelier National Monument," PX 7029-6-0769, PX 7029-7-0692 (1978).

Foxx, Teralene S., "Vegetation Succession after the La Mesa Fire at Bandelier National Monument. Fire Effects in Southwestern Forests," Proceeding of La Mesa Fire Symposium, General Technical Report RM-6TR-286.

Hitchcock, A. S., *Manual of Grasses of the United States* (Dover Publication, N.Y. 2 vol., 1950).

Foxx, T. S. and L. D Potter, "Fire Ecology at Bandelier National Monument," La Mesa Fire Symposium, Los Alamos, NM, October 6 and 7, 1981.

Health Physics

Detection and Internal Dosimetry of Insoluble Metal Tritides

Proton Recoil Scintillator Los Alamos Neutron Dose Meter (PRESCILA)

Determining and Monitoring the Inhalable Fraction of Plutonium Aerosols in an Accident

Characterization of Photon Radiation Fields in a Los Alamos National Laboratory (LANL) Plutonium Facility

Implications of Room Ventilation and Containment Design to Minimize Worker Exposure to Plutonium Aerosols

Since ESH Division initiated the TDEA program in 1995, it has supported ten health physics projects.

Studies to date

FY95

Optimization of Placement of Workplace Continuous Air Monitoring (CAM) Instrumentation

High-Energy Neutron Dosimetry

FY96

Applications of Thermal Ionization Mass Spectrometry (TIMS) to the Detection of ^{239}Pu and ^{240}Pu Intakes

High-Energy Neutron Dosimetry and Spectroscopy

Development and Implementation of the Los Alamos National Laboratory (LANL) Neutron Extremity Dosimeter

Optimization of Continuous Air Monitoring (CAM) Instrument Placement

FY97

Applications of Thermal Ionization Mass Spectrometry (TIMS) to the Detection of Pu-239 and Pu-240 Intakes

High-Energy Neutron Dosimetry and Spectroscopy

Development and Implementation of the Los Alamos National Laboratory (LANL) Neutron Extremity Dosimeter

Optimization of Continuous Air Monitoring (CAM) Instrument Placement

Resuspension of ^{238}Pu from Surfaces

Summary of progress

The investigators for 10 health physics projects funded by TDEA have generated *55* papers and presentations since the program began in FY95. Many of the longer term projects were completed in FY97 and a new set of projects were funded in FY98, some based on results from previous TDEA-funded studies. For example, the room ventilation study was based on the CAM placement model development, and the neutron extremity dosimeter work was based on the earlier high-energy neutron projects.

Based on the information obtained from the CAM project, principal investigators have

• recommended that facility managers implement upgrades to the current CAM placement configurations;

• provided study results to project management;

• provided a design model for a study on minimizing worker exposure to plutonium aerosols. (This project addresses ventilation configurations in glove-box facilities and methods for changing ventilation patterns to reduce the potential for exposure to internal radioactivity.);

• produced information that could be applied directly to glove-box rooms in TA-55, PF-4;

• completed a study of photon fields in a LANL plutonium glove-box setting.

As a result of the project that characterized plutonium facility photon radiation by *documenting exposure rates at various locations in the workplace*, investigators recommended methods that would allow a reduction of external exposure to plutonium glove-box workers.

Information from the high-energy neutron dosimetry and spectroscopy project resulted in the following:

• development of the LANL neutron extremity dosimeter, which was initiated in FY96 and completed in FY97

• use of the new dosimeter in FY99.

The new extremity dosimeter has replaced the previously used finger-ring dosimeters for all workers requiring extremity monitoring at LANL. The new design, in addition to upgrading the neutron monitoring capability, provided a dosimeter that was more comfortable to use in the workplace.)

The methods and procedures developed by a study to apply TIMS to detection of plutonium intakes has been implemented by the LANL internal dosimetry program making possible regulatory compliance for plutonium detection. (Federal regulations require

detection of internal dos
100 mrem—impossible
detection in urine sampl
tional analytical method
started in FY98 have pr
that will help in the proc
radiation worker exposu
radioactivity: one detern
monitors the inhalable fi
aerosols that result from
second detects insoluble

Principle investigator
information from previo
neutron dosimetry studi
*Recoil Scintillator Los A
Dose Meter (PRESCILA*
developed a light and ea
detector with better sens
of previously used instru
measure energy deposite
interactions. The comme
detection instrument ind
interest in this device.

Detection and Internal Dosimetry of Insoluble Metal Tritides

Investigators: W. C. T. Inkret, M. E. Schillaci, G. Miller, Radiation Protection Services Group (ESH-12); D. W. Efurd, Nuclear and Radiochemistry Group (CST-11); J. A. Musgrave, Environmental Systems and Waste Characterization Group (CST-7); Y. S. Cheng, Lovelace Respiratory Research Institute, Albuquerque; and J. R. Wermer, Tritium Science and Engineering Group (ESA-TSE)

Introduction

When tritium in the oxide form (HTO) is taken into the lungs, it is quickly distributed throughout the water-bearing cells of the body. The biological distribution of HTO in body water is nearly uniform within several hours of inhalation, ingestion, or skin absorption (Pinson and Langham 1957, Osborne 1966). In addition to the physical decay by β-emission with a half-life of 12.35 years, tritium leaves the body as HTO via transpiration, exhalation, and urination with a biological half-life of about ten days. The committed effective dose equivalent (CEDE) is determined by integrating the total number of decays over 50 years, multiplying by the energy absorbed per decay (~6–keV average), and dividing by the total body soft-tissue mass (~63–kg average). The biokinetic behavior of tritium retention in body water is adequately described by a single exponential function:

$$C_t = C_0 e^{-\lambda t}$$

where,

C_t = the concentration of tritium in body water at time t,

C_0 = the concentration of tritium in body water at time zero,

λ = the elimination rate constant ($ln\ 2\ /\ T_B$), and

T_B = the effective retention half-time in the body.

When an individual is exposed to elemental tritium gas, the lung is directly irradiated by beta particles originating from the decay of the tritium gas in the lungs. Radiation dose to the rest of the body is from absorption of tritiated water generated by oxidation of tritium gas in the lungs and skin absorption of tritium

that has been oxidized in the environment. The tritium gas dose component is delivered concurrently or within an hour after exposure.

When metal tritide particles are inhaled, they may be deposited in the pulmonary regions of the lungs. The tritium will dissolve at the particle surface and distribute throughout the body as HTO at a rate proportional to the solubility and mechanical clearance of the metal tritide particles. For metal tritides that are poorly soluble, the residence time in the lungs can be considerably longer than the biological half-time normally associated with HTO. In these cases, the effective dose increases due to the increased dose component from the long-term irradiation of the lungs by low-energy β-particles and bremsstrahlung x-rays. In cases where insoluble metal tritides are inhaled, values of effective dose equivalent and lung dose equivalent will be underestimated if urine bioassay data are interpreted assuming the intake is in the oxide form. This underestimate is due to the delay in release of tritium from the lungs.

Los Alamos National Laboratory (LANL) has initiated several programs that will require the handling of significant quantities of metal tritides. These materials will include the hydrides of hafnium, titanium, zirconium, and other metals associated with accelerator targets and weapons components. We initiated this project to measure the biological dissolution rate and particle-size distribution of hafnium tritide samples and apply those results to tritium dosimetry models. The dissolution rate is a major parameter determining a particle's retention, distribution, and clearance from the lung and therefore, is essential for dosimetric modeling of the inhaled particle.

Methods

We analyzed samples of hafnium tritide to provide a biologically based particle dissolution rate parameter to be used in dose assessment models. The particle sample was sandwiched in filters and placed in a flask with a lung simulant fluid. The system was maintained at 37° C. At predetermined sampling times, the fluid and air in the flask were sampled and counted for the presence of tritiated water and tritium, which is assumed to account for all tritium dissolved in the lung simulant fluid (Cheng et al. 1977).

Hafnium hydride (HfH) and hafnium dihydride (HfH$_2$) samples were analyzed for particle-size distribution. The HfH samples were mounted on carbon-coated, double-sided tape. The tape adheres the particles to a substrate and provides a conductive surface to dissipate the specimen current. For this particular experiment, the particles were not carbon coated. The uncoated samples were introduced into a Tracor-Northern ADEM scanning electron microscope. An initial x-ray emission analysis was performed on each sample to confirm that the material was primarily composed of hafnium. The samples were then scanned at an average working distance of 19 mm and an acceleration voltage of 15 kV.

We evaluated current internal dosimetry models (International Commission on Radiation Protection [ICRP] Publication 30 and ICRP Publication 66) for suitability of application to insoluble forms of tritium. Current lung model algorithms (ICRP Publication 30 and ICRP Publication 66) were evaluated for use with a long-term lung component. Estimates of urine excretion rates as a function of pulmonary half-times were made.

Results

Particle Solubility Studies

Figure 1 contains a plot of the measured fraction of tritium retained in hafnium tritide complex in a simulated lung fluid. The data indicate a dissolution rate of 1.3×10^{-5} day^{-1} and a corresponding biological half-time in the lungs of 1.1×10^{5} days. The results showed a remarkable break at about 40 days, after which the dissolution rate appears to have returned to the same slope.

Scanning Electron Microscopy of HfH Particles

We used scanning electron microscopy to study HfH and HFH$_2$ particles. The purpose of this study was to determine the morphology and size distribution of the particles. Parameters used to determine particle-size distribution were aspect ratio, maximum projection, and minimum projection.

Figure 2 is a histogram of the number of observed particles as a function of aspect ratio. Aspect ratio is the maximum projection divided by the minimum projection, where maximum projection is determined by finding the vertices of the convex perimeter and then searching these vertices for the pair farthest apart. An aspect ratio of 1 indicates a particle that is tending towards a spherical geometry, whereas particles with aspect ratios greater than 1 approach a rectangular form. Particles with aspect ratios between 3 and 6 are prismatic to acicular (needle-like) in crystal habit.

Six-hundred to seven-hundred particles were counted in each of the samples to determine size distribution in each sample. Examination of the histograms for the aspect ratio of both samples indicates the majority of the particles have an equant to slightly elongate crystal form, i.e., aspect ratio of 1 to 2. Both samples have smaller populations of prismatic crystal habits.

Figure 3 contains a histogram of the number of observed particles as a function of maximum projection length. Results for both the hydride and dihydride samples with maximum and
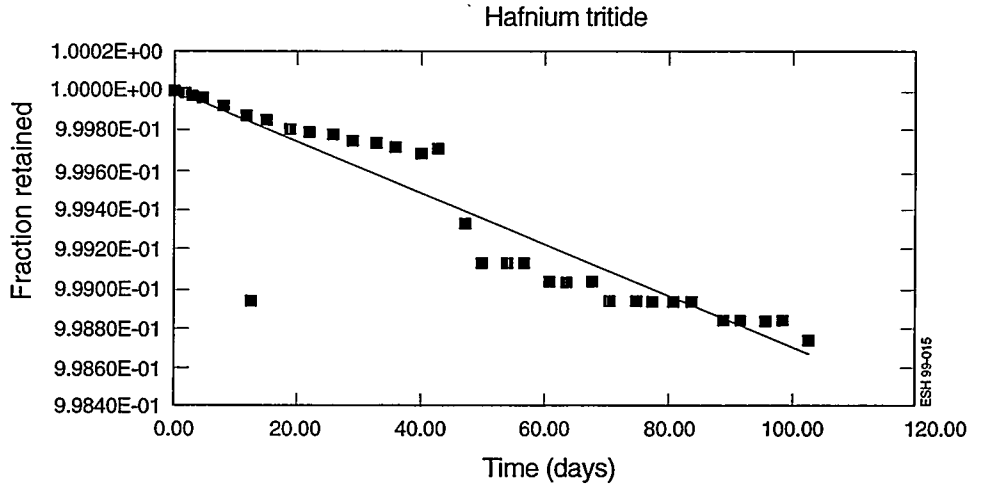
Figure 1. *Measured fractional retention data for ~1μm, AMAD, hafnium tritide particles in simulated lung fluid. The fitted line is a simple exponential function with a dissolution rate of 1.3 x 10⁻⁵ day⁻¹, and an associated biological half-time in the lungs of 1.1 x 10⁵ days.*
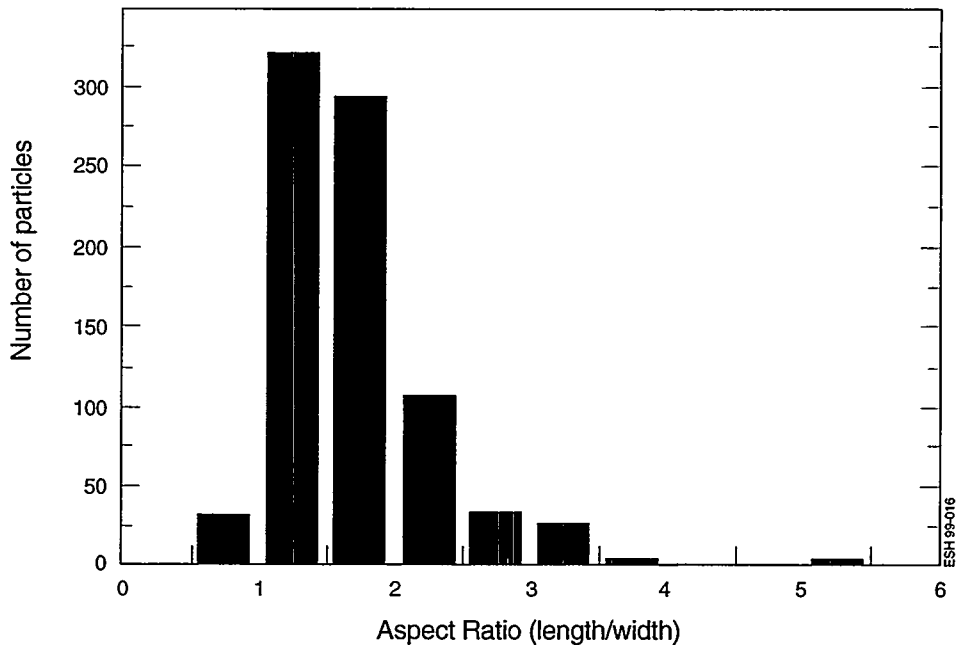

Figure 2. *Frequency histogram of aspect ratio for the HfH particles pictured in Figure 4. The histogram illustrates the majority of HfH particles have an aspect ratio between 1 and 2. An aspect ratio of 1 is indicative of a spherical or cubic particle.*

minimum projections plotted indicated the majority of particles are less than 15 μm with the greatest number of particles between 2 μm and 10 μm.

Figures 4 and 5 contain scanning electron photomicrographs of the two materials. These photomicrographs show that the particles are covered by a "dust" of smaller particles. It was impossible to

determine a size distribution for these particles because they lie on the surface of the larger particles, and the particle-sizing program cannot distinguish these small particles. A possible solution to this problem might be to sonicate the samples to try to dislodge and disperse these smaller particles.
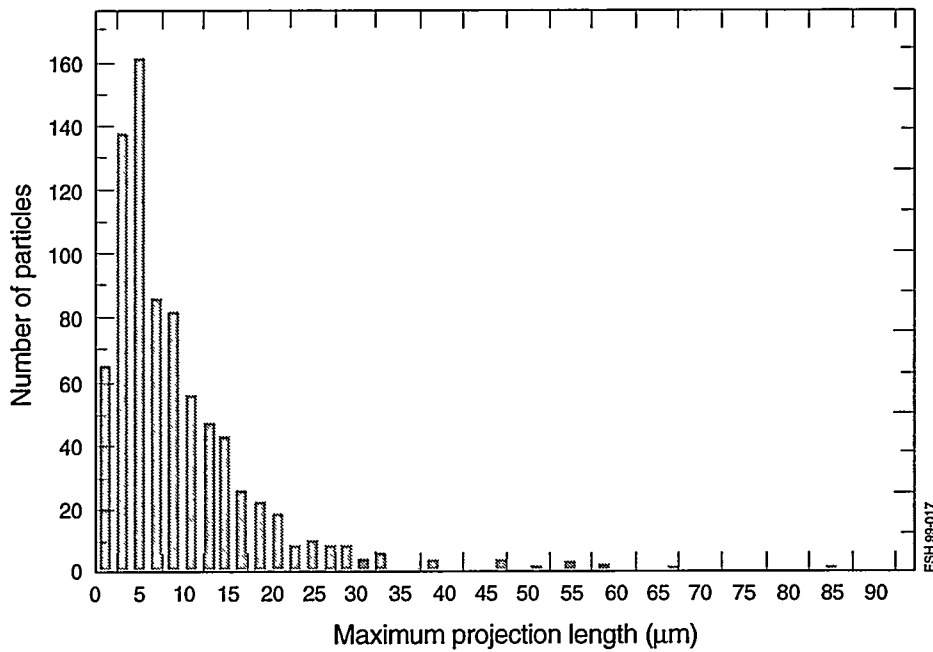
Figure 3. *Frequency histogram of the maximum projection length for the HfH particles pictures in Figure 4. The histogram indicates that the most probable particle size is in the range of 2 μm to 5 μm.*
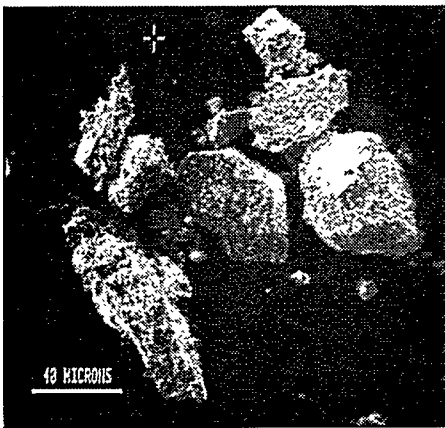
Figure 4. *Backscattered electron photomicrograph of HfH$_2$ particles at a magnification of 456X, working distance of 19.3 mm, electron acceleration voltages of 15 kV, and a specimen current of 47.2 pA. The apparent aspect ratio of the smaller particles, <5 μm, is on the order of 1 to 2. The larger particles display a large variation in aspect ratio.*
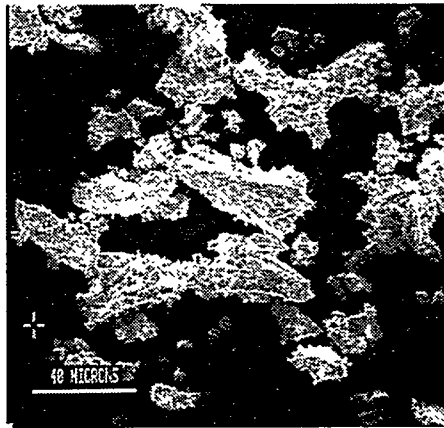
Figure 5. *Backscattered electron photomicrograph of HfH$_2$ particles at a magnification of 523X, working distance of 19.4 mm, electron acceleration voltage of 15 kV, and a specimen current of 29.4 pA. Note the apparent coating of smaller particles on the larger particles and the remarkable angularity in particle geometries. The apparent aspect ratio of the smaller particles, 5 μm, is on the order of 1 to 2. The larger particles display a large variation in aspect ratio.*

Application of Measured Particle Size and Solubility to Biokinetic and Dosimetry Models

Mathematical description of the problem

If the tritum were in the oxide form only, the effective dose would be given by the expression

$$D = (N_0 E/M)(\lambda_p/\lambda)[1- exp(-\lambda T)],$$

where N_0 is the initial number of tritium atoms taken into the body, E is the energy emitted per decay (~6 keV = 9.61×10^{-9} ergs), M is the total body soft-tissue mass (~6.3×10^4 g), $T = 50$y = 1.83×10^4 d. The effective rate constant, λ, is given by the sum of physical and biological rate constants

$$\lambda = \lambda_p + \lambda_b,$$

where the physical rate constant is

$$\lambda_p = ln2/t_{1/2}$$
$$= ln2/(12.35 \text{ y} \times 365.25 \text{ d/y})$$
$$= 1.54 \times 10^{-4} d^{-1}$$

and the biological rate constant is

$$\lambda_b = ln2/10d = 6.93 \times 10^{-2} d^{-1}.$$

Inserting these values, converting to rads (1 rad = 100 ergs/g), and using a quality factor, $Q = 1$, to convert to rems, we obtain the CEDE dose

$$D_{HTO} = 3.38 \times 10^{-18} N_0 \text{ rem.}$$

For the metal tritide, we assume that the particles are lodged in the lungs, and tritium dissolves from the surface of these particles with some rate constant, r, and is distributed quickly throughout the body as HTO. For the component remaining within the lungs, we assume that tritium decays irradiate the lungs uniformly (which is not strictly true). For the component distributed throughout the body as HTO, we must apply the biological rate constant, λ_b.

The CEDE dose has two components: (a) the dose to the lungs resulting from the decay of tritium in the metal tritide form; and (b) the whole-body dose resulting from the decay of dissolved tritium in the oxide form, HTO, which is distributed throughout the body.

29

(a) The lung dose over 50 years is given by

$$D_{lung} = (N_0 E/m)(\lambda_p/(\lambda_p+r))[1 - exp(-(\lambda+r)T)],$$

where m is the mass of the lungs (10^3g), and we assume that the entire energy of decay is deposited uniformly in the lung tissue. The contribution of this lung dose to the whole-body dose (CEDE) is given by

$$D_{MT} = 0.12 \, D_{lung},$$

where 0.12 is the organ weighting factor for converting lung dose to whole-body effective dose.

If the limit of r equals zero (i.e., zero dissolution rate), all of the dose is due to the metal tritide form and is deposited in the lungs. In this limit, the whole-body dose (CEDE) is given by

$$D_{MT}(r \rightarrow 0) = 1.8 \times 10^{-14} N_0 \text{ rem.}$$

(b) The number of tritium atoms, $N(t)$, distributed throughout the body as HTO is given as a solution to the equation:

$$-dN/dt = \lambda N(t) - rN_{lung}(t),$$

where $N_{lung}(t) = N_0 exp(-(\lambda_p+r)t)$.

The number of decays from HTO occurring throughout the body in a time T is given by

$$N_{decays}(T) = N_0(r\lambda_p/(\lambda_b-r))$$
$$\{[1 - exp(-(\lambda_p+r)T]/(\lambda_p+r) - [1 - exp(-\lambda T)]/\lambda\}.$$

The CEDE from HTO distributed throughout the body is then given by

$$D_{HTO} = (N_0 E/M)(r\lambda_p/(\lambda_b-r))$$
$$\{[1 - exp(-(\lambda_p+r)T]/\lambda_p+r) - [1 - exp(-\lambda T)]/\lambda\}.$$

For a small dissolution rate constant, r, on the order of 10^{-5}d^{-1} or less, practically all of the CEDE results from tritium decays from the metal tritide particles within the lungs. This dose is about 3000 times that expected if all of the tritium were distributed throughout the body as HTO. On the other hand, for large dissolution rate constant, r, on the order of 10 d^{-1}, practically all of the CEDE results from tritium decays from HTO distributed throughout the body, i.e., the dose is essentially that expected assuming the tritium is taken into the body as HTO.

Realistically, the factor of 3000 given in the preceding paragraph must be considered an upper limit because of the following considerations:

• mechanical clearance by mucociliary action of metal tritide particles from the lungs reduces the lung dose;

• not all of the decay energy is deposited in the lungs, as assumed, because some is self-absorbed within the metal tritide particles themselves;

• if the metal tritide particles are not completely insoluble, any solubility will decrease the effective dose.

Both of these mitigating considerations are strongly dependent on particle size.

Application of results to secondary limits.

Tables 1 and 2 contain estimated annual limits on intake, derived air concentrations, and surface contamination bioassay action levels for inhalation of 1-μm AMAD and 5-μm AMAD, polydispersed aerosols of hafnium tritide
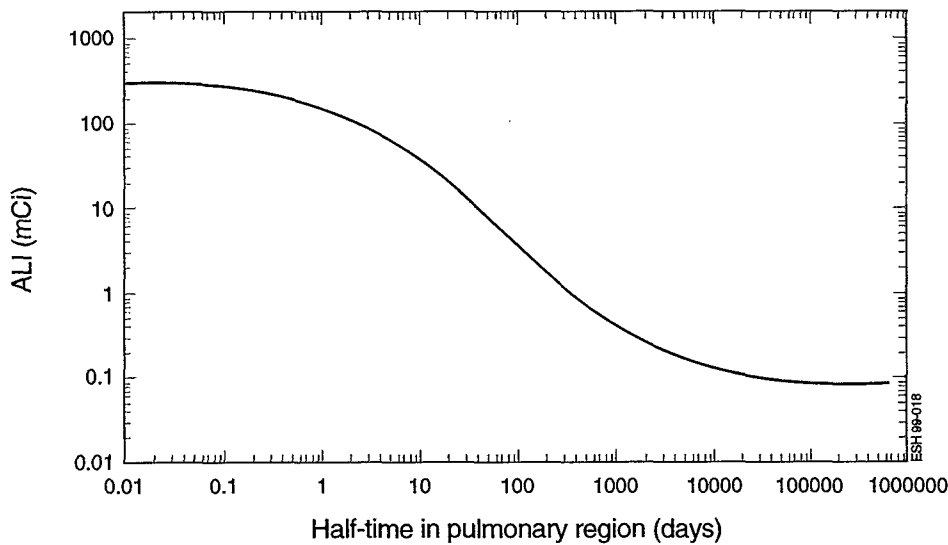
for several pulmonary retention half-times. For comparison, the annual limit on intake (ALI) for HTO is 81 mCi and the derived air concentration (DAC) is 22 Ci/μ^3. It is important to note that the pulmonary deposition fraction is 0.25 for a 1-μm AMAD particle and 0.05 for a 5-μm AMAD particle. The values in Tables 1 and 2 are based on the assumption that all beta energy and converted bremsstrahlung energy generated by the decay of tritium in the hafnium tritide particle matrix are deposited in 1000 g of lung tissue. The effective ALI is the sum of the dose delivered to soft tissue in the body from HTO with a 10-day half-time after transfer from the pulmonary compartment and the weighted lung dose (0.12) from the deposited metal tritide at the indicated pulmonary half time. The surface contamination action level is based on an 8-hour exposure period of light activity, 1-μm AMAD material, a hafnium self-absorption factor of 5, and a resuspension factor of 10^{-4} m^{-1} (Brunskill

Table 1. Estimated ALIs, DACs, and initial estimates of surface contamination bioassay action levels for inhalation for a 1-μm AMAD, polydispersed aerosol of hafnium tritide for several pulmonary retention half times.

Biological half time in pulmonary region (days)	ALI (mCi)	DAC (μCi/m³)	Surface contamination bioassay action level, 8-h exposure (10⁶ dpm/100 cm²)
50	7.4	2.9	600
100	3.8	1.5	300
500	0.8	0.3	70
1000	0.5	0.2	40
5000	0.2	0.1	10
10000	0.1	0.05	10

Table 2. Estimated ALIs, DACs, and initial estimates of surface contamination bioassay action levels for inhalation for a 5-μm AMAD, polydispersed aerosol of hafnium tritide for several pulmonary retention half times.

Biological half time in pulmonary region (days)	ALI (mCi)	DAC (μCi/m³)	Surface contamination bioassay action level, 8-h exposure (10⁶ dpm/100 cm²)
50	46	19	4000
100	24	9.5	2000
500	5.2	2.1	400
1000	2.9	1.1	200
5000	0.99	0.39	80
10000	0.76	0.31	60

Figure 6. *Estimated annual limit on intake for a 1-μm AMAD polydispersed aerosol of hafnium tritide as a function of biological half time in the lungs.*

1964). Figure 6 contains a plot of the estimated annual limit on intake for effective dose equivalent as a function of pulmonary half time.

Figure 7, shows the expected tritium concentration in urine 2 hours (top) and 7 days (bottom) after an intake of a 1-μm AMAD, polydispersed aerosol of hafnium tritide, corresponding to 100-mrem CEDE and 5-rem committed lung dose equivalent, as a function of the biological half time in the lungs. Note the line indicating the detection capability of intakes by urine bioassay.

Applications to dose assessment.

Evaluation of ICRP Publication 30 (1979) and ICRP Publication 66 (1994) lung models were performed. The ICRP Publication 30 lung model is simpler, both conceptually and mathematically. A LANL computer algorithm (Miller et al. 1993, 1995, 1996, 1997, 1998) and a commercial code CINDY (Strenge et al. 1992), both based on ICRP Publication 30 lung model concepts, were used to establish urine excretion rates as a function of particle solubility in the pulmonary region of the lung. The ICRP

Publication 66 model was evaluated via the commercial computer code LUDEP (Jarvis 1997).

The ICRP Publication 66 model was initially evaluated for inhalation, deposition, and excretion of HTO. This exercise was done to compare results with the established results of the ICRP Publication 30 model. In the case of HTO inhalation, which is rapidly distributed throughout the body from the lungs, it was expected that the results would be model independent. The LUDEP application defaults resulted in a very "stiff" compartment set. Changes in the ICRP Publication 66 model default parameters (e.g., changing the blood to urine half time from 10^{-8} d to 0.2 d) provided a more realistic response. Given the complexity of the ICRP Publication 66 model and the LUDEP application, there were some concerns about other default parameters and associated computational artifacts. A second problem with the LUDEP code is its inability to handle more than one acute intake. These results were reported to the authors of the LUDEP code and corrections are underway. All results discussed in this report are based on the simpler ICRP Publication 30 lung model.

The LANL-developed internal dosimetry code was used to evaluate urine excretion data from exposures to
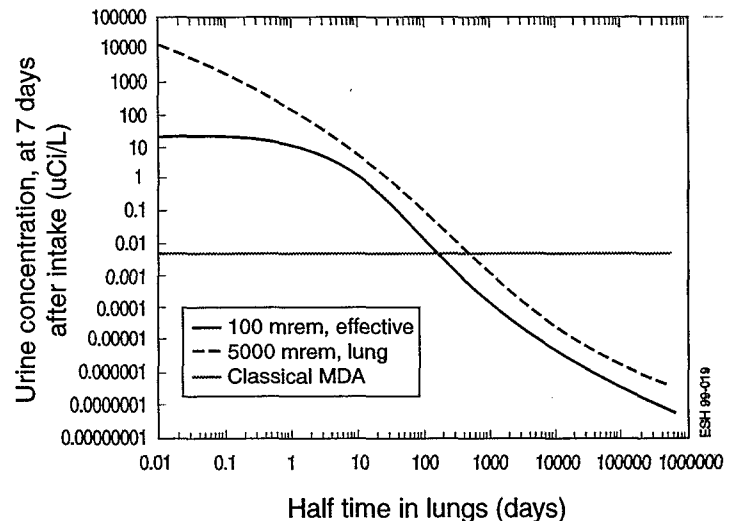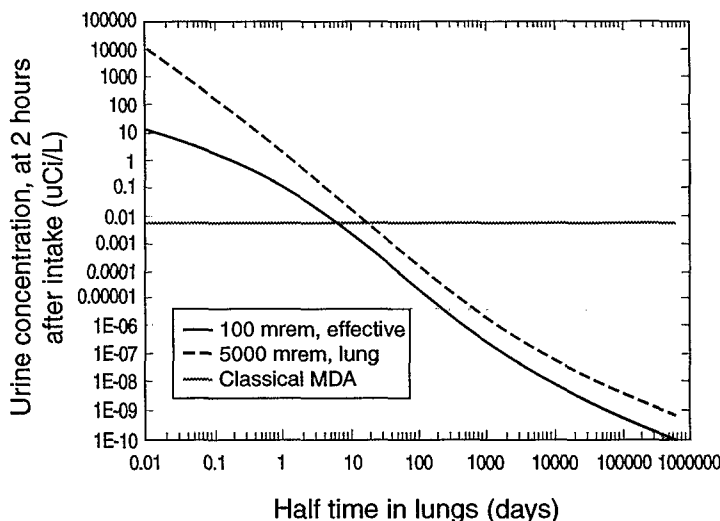
Figure 7. *Expected tritium concentration in urine two hours (left) and seven days (right) after an intake of a 1-μm AMAD monodisperse aerosol of hafnium tritide. Note the horizontal line indicating the detection capability of intakes by urine bioassay.*
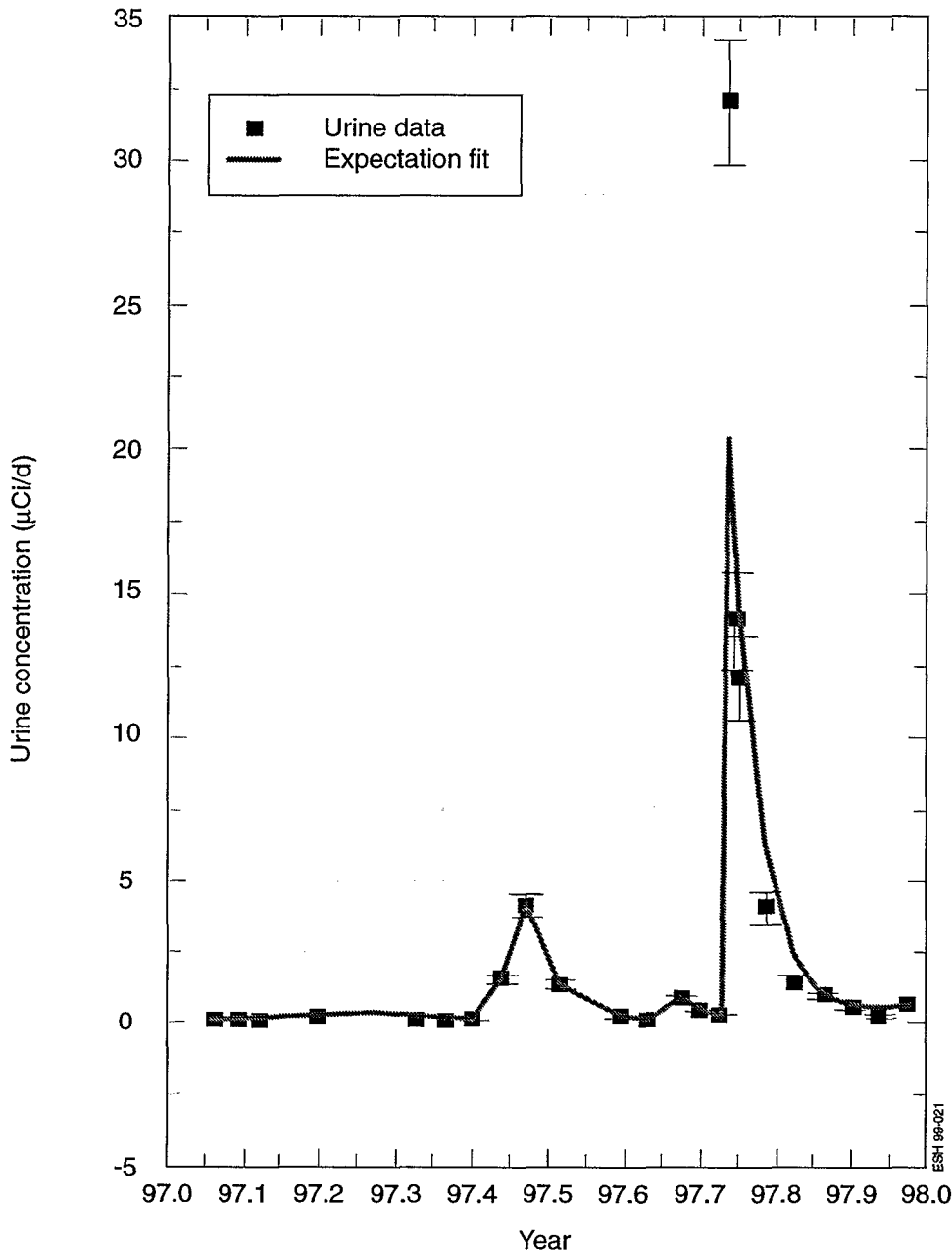
Figure 8. *Bayes expectation fit to tritium urine concentration data using a library of ICRP Publication 30 biokinetic response functions. The biokinetic response function library also contains the response functions for metal tritides.*

HTO. Figure 8 contains an example of a fit to excretion data. The fit is based on minimizing x^2 by varying particle size, time of intake, lung solubility, and systemic retention rates. A library of parameter-specific biokinetic response functions has been generated for HTO and MT.

Discussion

Dissolution measurement results from LRRI indicate that hafnium titride has a significantly lower dissolution rate in lung fluids than rates measured for zirconium tritide and titanium tritide. Results at this time indicate a biological half-time in the pulmonary region on the order of 10^4 to 10^5 days. The dominant biological half time in lung tissue for a

1-μm AMAD particle of titanium tritide is on the order of 30 days (Cheng et al. 1997). Current dose estimates assume all of the decay energy is deposited in the lungs. This assumption is strongly dependent on the particle size. Figure 7 contains an interesting result. As the biological retention time in the pulmonary region increases, the ability to detect a 100-mrem intake decreases at times close to the time of intake. Based on the initial information regarding particle size and solubility, it appears that the ALI and DAC for hafnium tritide will be at least a factor of 100 lower than the corresponding values currently used for tritium oxide.

The project produced a number of useful results including the following:
• contamination action levels have been calculated for hafnium tritide materials,

• a reasonable biokinetic model is complete,

• bioassay response function estimates are complete and may be used as a technical basis for routine and special monitoring frequencies,

• basic biokinetic response functions have been developed and benchmarked, dose coefficients for 1-μm AMAD and 5-μm AMAD hafnium tritide materials have been estimated, and

• associated committed organ dose and committed effective dose models have been developed and benchmarked.

Use of the scanning electron microscope in conjunction with workplace monitoring instrumentation provides the ability to detect hafnium captured on air filters. These results make it possible for LANL to monitor the workplace for releases of hafnium tritide, and monitor workers exposed to metal tritide materials.

References

Brunskill, R. T., "The relationship between surface and airborne contamination," in *Surface Radioactivity*, proceedings of a symposium held at Gatlinburg Tennessee," (Pergamon Press, New York, 1964), pp. 93-105.

Cheng, Y. S., Dahl, A. R., and Jow, H. N., "Dissolution of metal tritides in a simulated lung fluid," *H. Phys.* **73**, 633-638 (1997).

"Limits for intakes of radionuclides by workers," Annals of the International Commission for Radiation Protection, ICRP Publication 30, part 1, (Pergamon Press, New York, 1979).

"Human respiratory tract model for radiological protection," Annals of the International Commission for Radiation Protection, ICRP Publication 66, (Pergamon Press, New York, 1994).

"Internal dosimetry programs for tritium exposure—minimum requirements," ANSI N13-14 (American National Standards Institute, Inc., 1994).

"LUDEP 2.1—Personal Computer Program for Calculating Internal Doses Using the ICRP Publication 66 Respiratory Tract Model," National Radiological Protection Board report NRPB-SR287, England (1997).

Miller, G., W. C. Inkret, and H. F. Martz, "Bayesian Detection Analysis for Radiation Exposure," *Rad. Prot. Dos.* **48**, 251–256 (1993).

Miller, G., W. C. Inkret, and H. F. Martz, "Bayesian Detection Analysis for Radiation Exposure, II," *Rad. Prot. Dos.* **58**, 115–125 (1995).

Miller, G. and W. C. Inkret, "Bayesian maximum posterior probability pethod for interpreting plutonium urinalysis data," *Rad. Prot. Dos.* **63**, 189–196 (1996).

Miller, G. and W. C. Inkret, "Bayesian methods for interpreting plutonium urinalysis data," in *Maximum Entropy and Bayesian Methods*, (Kluwer Academic Publishers, Boston, 1996), pp. 367–373.

Miller, G., W. C. Inkret, and H. F. Martz, "Internal dosimetry intake estimation using Bayesian methods," Los Alamos National Laboratory report LA-UR-96-2178 and *Rad. Prot. Dos.* accepted for publication (1998).

Osborne, R. V., "Absorption of tritiated water vapour by people," *H. Phys.* **16**, 1527–1537 (1966).

Pinson, E. A. and W. H. Langham, "Physiology and toxicology of tritium in Man," *J. Appl. Physio.* **10**, 108–126 (1957).

Strenge, D. L., R. A. Kennedy, M. J. Sula, and J. R. Johnson, "Code for Internal Dosimetry, CINDY Version 1.2, Part I, Conceptual Representation," Pacific Northwest Laboratories report PNL-7493, Pt. 1, Rev. 1, UC-605, (1992).

Proton Recoil Scintillator Los Alamos Neutron Dose Meter (PRESCILA)

Principal investigator: Richard H. Olsher, Health Physics Measurements Group (ESH-4)
Co-Investigators: Shawna L. Eisele, Christopher W. Bjork, David T. Seagraves, William A. Martinez (ESH-4)

Introduction

Neutron meters currently used at Los Alamos National Laboratory (LANL) and elsewhere are based on 1960s technology that relies on a large neutron-moderator assembly surrounding a thermal detector to achieve an accurate dose response. Typically, a BF3 gas-filled detector tube is positioned in the center of a heavy (i.e., 20 pounds) polyethylene moderator. The only commercial exception is the HPI Inc. Model Rem 500, an instrument that weighs five pounds, but is severely limited in sensitivity (only eight counts per minute per mrem/h), offers no thermal response, and is very expensive ($6K).

In general, current dose meters are not only heavy and bulky, but have a poor high-energy response above 10 MeV, which makes them unsuitable for applications at high-energy accelerator facilities (e.g., Los Alamos Neutron Science Center [LANSCE]). Other disadvantages are high cost (as much as $6K) and poor ergonomics for field surveys.

Our goal was to develop a practical proton recoil scintillator (PRESCILA) of low weight (three pounds) with good sensitivity and gamma rejection and enhanced high-energy response. PRESCILA offers the potential of replacing thousands of neutron rem meters in field applications around the world with a lightweight and more accurate design.

Benefits

LANL's Radiation Protection Group (ESH-1) has requested a lightweight alternative to the standard rem meter to facilitate field surveys. The weight of the PRESCILA detector is three pounds versus the 20 pounds of a standard rem meter.

The cost of maintenance of the current inventory is driven by the need to periodically replace the BF3 detector tube ($300 each). Over the life of the inventory (130 rem meters), these costs are estimated to be $60K. Maintenance costs for PRESCILA should be about 50% lower for a savings of $30K.

The poor energy response at high-neutron energies limits the ability of a standard rem meter to accurately measure dose around accelerator facilities such as LANSCE. Standard rem meters with a pure polyethylene moderator seriously underestimate (by up to a factor of 10) neutron dose around accelerator facilities. Two recent designs use lead and tungsten inserts to improve the high-energy response but at a serious weight penalty, pushing the moderator assembly to weigh as high as 60 pounds.

As PRESCILA-type rem meters are accepted throughout the Department of Energy complex, cost savings and improved performance will be realized within every radiation protection program where neutron exposure is present. Patenting this detector will mean the possibility of royalty income to the Laboratory through licensing agreements with instrument vendors.

Methods and objectives

During FY98, the investigators pursued several lines of research with the following objectives:

• Lightweight probe design

• Good neutron sensitivity (minimum of 20 cpm/mrem/h in Cf-252 fields)

• Extended high-energy response

• Gamma rejection in fields up to 100 mR/h

• Use of off-the-shelf components

One line of research evaluated the use of large-area-air-proportional detectors together with ^{10}B-loaded (5% by weight) polyethylene radiators. This research was conducted in collaboration with Ludlum Measurements, Inc. Ludlum fabricated a dual-window large-area detector (180 cm^2 per side) that allowed the addition of a borated radiator over each window. The measured neutron sensitivity for this probe was 11 cpm/mrem/h with good gamma rejection.

The best results, however, were obtained using a probe design incorporating a dual scintillator and a photomultiplier (PM) tube. A conceptual diagram of the latest prototype is shown in Figure 1.
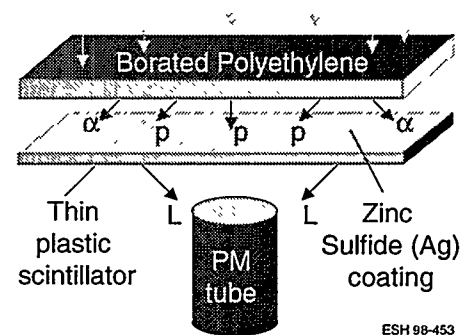

Figure 1. Conceptual diagram of latest prototype.

The physics of the detector are as follows:

• Fast neutrons generate recoil protons in the borated polyethelene and plastic scintillator.

• The recoil protons produce light pulses in the dual-scintillator plate as they pass through the zinc sulfide (ZnS) coating as well as the plastic scintillator material. These plates are available as stock items from several vendors—including Bicron and Eberline—as they are commonly

used in dual alpha-/beta-surface contamination probes. Each plate is sufficiently thick (0.25 mm) to stop the recoil protons.

• The PM tube converts the light pulses to voltage pulses, which are then counted by an external counter.

• Thermal and epithermal neutrons produce alpha particles via the (**n**, α) capture reaction in ^{10}B. The alpha particles interact with the ZnS and produce light pulses.

The elastic-scattering cross section in hydrogen decreases slowly with increasing energy above 2.5 keV, when the n-p scattering cross section in barns is given approximately by $4.5En^{-1/2}$ where En is in MeV. However, the number of radiated protons tends to remain constant with increasing energy due to the following two factors:

• The effective depth from which protons leave the surface of the radiator increases with energy.

• The scattering on protons becomes forward directed above 10 MeV. For example, at 100 MeV, most of the protons are produced at energies between 90 MeV and 100 MeV. In contrast, below 10 MeV, scattering on hydrogen is isotropic in the center of mass system, which means that there is equal probability of producing a proton at any energy up to the neutron energy, En. Figure 2 shows the expected spectrum under these conditions, which is rectangular with an average proton energy of En/2.

Any proton recoil with an energy below about 0.1 MeV cannot be effectively discriminated from gamma pulses. In a mixed neuron/gamma field, many proton pulses will be indistinguishable from those produced by secondary electrons. Therefore, to maximize the neutron to gamma signal ratio, we chose the thinnest possible plastic scintillator plate (Figure 3). Minimum plate thickness obtainable off the shelf is 0.25 mm, as castings cannot reliably be made any thinner. This idea takes advantage of the large difference in range between electrons and protons in plastic scintillator material: 3 mm for a 1-MeV electron versus 0.02 mm for a 1-MeV proton.
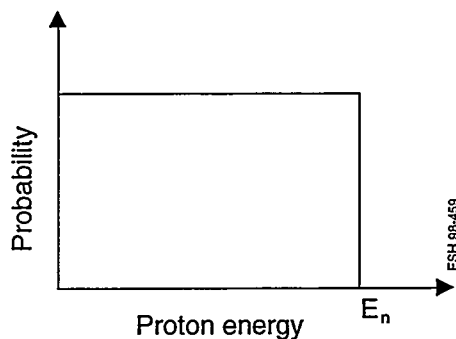

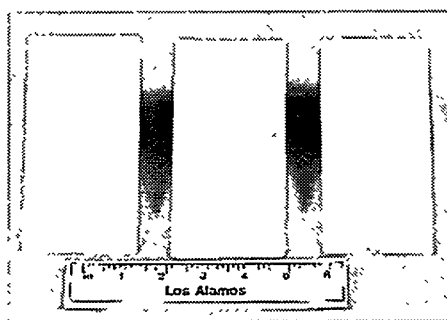**Figure 2.** *Energy distribution of recoil protons produced by monoenergetic nueutons.*

Figure 3. *Plastic scintillator plates chosen for thinness.*

Each plate is coated with a layer of ZnS(Ag) scintillator to a thickness of 6 mg/cm²–8 mg/cm². This is sufficient to stop the radiated alpha particles, but thin enough not to interfere with light transmission. ZnS(Ag) is only available as a polycrystalline powder and is therefore opaque to its own luminescence. It becomes unusable at thicknesses greater than about 25 mg/cm². Any protons radiated from the borated polyethylene layer deposit only a small fraction of their energy in the ZnS(Ag). Most of these protons are stopped in the plastic scintillator.

Progress and results

Initial investigations used a probe design with a single scintillator plate. However, to increase response sensitivity, we found it necessary to use several plates. The final prototype of PRESCILA uses three dual-scintillator/radiator assemblies, each 100 cm² in area. The plates are positioned equidistant from the PM tube. When used in conjunction with the Eberline E-600 hand-held counter

(or an equivalent smart portable), it is possible to define both gamma and neutron channels on the basis of pulse height discrimination. The upper discriminator (30 mV) defines the neutron channel, while the lower discriminator (5 mV) defines a gamma channel in the range of 5 mV to 30 mV. This allows the simultaneous measurement of both gamma and neutron fields—a new capability in portable radiation protection instrumentation.

Sensitivity measurements of PRESCILA operated with the Eberline E-600 were conducted over the Neutron Well at SM-40. The results are shown in Figure 4. As the upper discriminator level (mV) is lowered, neutron sensitivity increases well beyond 25 cpm/mrem/h. However, the cross talk from the gamma channel increases as well and reduces the level of gamma rejection. At a setting of 30 mV, gamma discrimination is effective to 100 mR/hr. The gamma channel response is adjustable from 5,300 cpm/mR/hr to 12,300 cpm/mR/hr (for a Cs-137 field) as the lower discriminator is adjusted from 5 mV to 3 mV.

The results of a linearity study are given in Figure 5. Over the neutron dose rate range from 3 mrem/h to 400 mrem/h the response deviation is within 10%.

A Lucite light guide has been designed for the next generation PRESCILA probe. Figure 6 shows a schematic drawing for the design. The light guide is designed to allow mounting of up to four scintillator plates around a side-view PM tube with a bi-alkali photocathode. Because the index of refraction of Lucite is similar to that of plastic scintillator material, light transfer to the PM tube is greatly increased relative to a plastic-air interface.

Lucite is transparent to light at wavelengths above about 400 nm. The emission from Bicron BC-400 plastic scintillator peaks at a wavelength of 423 nm (see Figure 7). This peak ensures minimal attenuation of the light emission from each scintillator plate. The overall gain in pulse height of proton recoil events will allow better gamma rejection and increased neutron sensitivity.
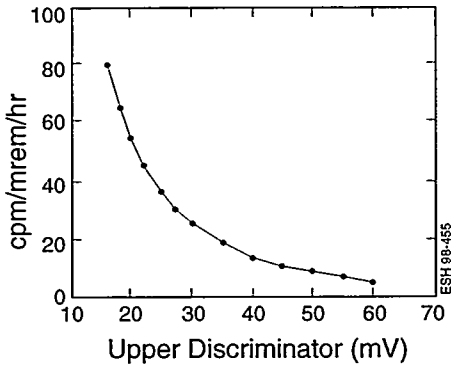
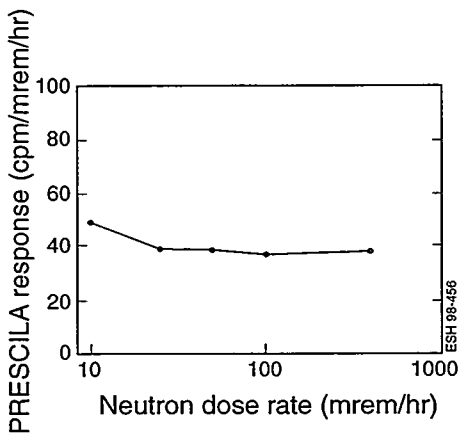**Figure 4.** *Neutron channel response as a function of upper discriminator setting.*
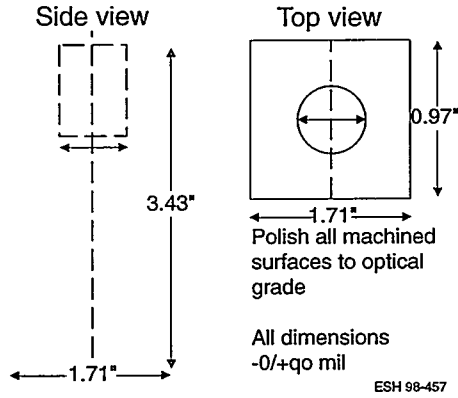

Figure 5. *Linearity study.*

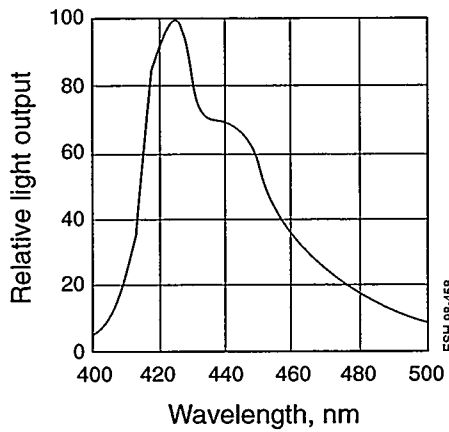**Figure 6.** *Light guide schematic.*

**Figure 7.** *Premium plastic scintillators response to atomic particles.*

Conclusion and deliverables

A final prototype has been constructed and tested (Figure 8).

The performance of the current PRESCILA prototype can be summarized as follows:

• Lightweight probe design (three pounds),

• Capability for both neutron and gamma dose measurements,

• Gamma sensitivity of up to 12,300 cpm/mR/hr (an order of magnitude greater than that of a typical Geiger-Mueller detector) which makes micro R/hr measurements possible, and

• Neutron sensitivity of 25 cpm/mrem/h (about 50% of neutron response of Eberline NRD rem meter) with good gamma rejection to 100 mR/hr.

The performance of this prototype shows the viability of the PRESCILA design as a lightweight neutron dose meter for field applications. The gamma response capability of PRESCILA makes it extremely attractive as a commercial all-in-one dose rate meter. One major radiation protection instrument vendor (Eberline Instruments) has already expressed great interest in commercializing this technology.
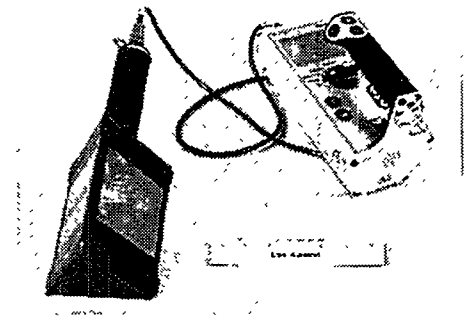
Figures 8. *Photo of the final prototype..*

Determining and Monitoring the Inhalable Fraction of Plutonium Aerosols in an Accident

Principal Investigator: John C. Rodgers, Health Physics Measurements Group (ESH-4)
Co-Investigators: Jeff Whicker, Hongrui Gong, Murray Moore, (ESH-4); Bill Inkret, Radiation Protection Services Group (ESH-12)

Introduction

In Laboratory plutonium facilities where significant quantities of radioactive materials are handled, both retrospective and real-time air monitoring are often required. Real-time monitoring uses continuous air monitors (CAMs) such as the Alpha Sentry CAM, which with internal sample flow measurement are capable of reporting the moment-to-moment air concentration changes of plutonium and background radionuclides. Retrospective monitoring involves collection of continuous air samples from strategic locations with fixed air samplers (FASs), followed later by laboratory analysis to detect and evaluate the average concentration of airborne radioactive particulates. These samples are assumed to be representative of the ambient air at worker locations, although concentrations are only approximate and based on an estimate of the volume of air that would have been sampled during a suspected release episode, and proximity to workers that might have been exposed.

The problem of inclusion of the effects of point-to-point variation in concentration on exposure estimates has been addressed by installing a large number of FASs throughout a workroom. Information on spatial variation can also be helpful in locating the probable release point. Estimates of concentration alone do not, however, tell the dosimetrist how much radioactive material was likely to have been inhaled by a worker exposed in an accident. For this, critical input is needed from bioassay data on that individual. Excretion of the radionuclides of concern may be tracked for a considerable time following an exposure.

However, to apply human metabolism and excretion models to the interpretation of bioassay data, an assumption must be made of the probable particle size of the inhaled radioactive particulate. Until recently, an apparently conservative assumption has been made regarding particle size—one that tends to lead to an overestimation of the dose. The conservative assumption (from ICRP 30, Part I) has been that the activity median aerodynamic diameter (AMAD) of a typical accident aerosol is 1 μm. More recently, in recognition by the nuclear industry that radioactive aerosols are most likely to have AMADs of several micrometers (Strandling et al. 1987), ICRP has adopted a new default AMAD for occupational exposure of 5 μm (ICRP 66, 1994). Moreover, the new respiratory model is intended to be realistic rather than conservative.

A recent survey of the literature on measured particle-size distributions in the nuclear industry (Dorrian and Bailey 1995) indicates median values of somewhat more than 4 μm (σg = 1.4), although relatively little is known about accident aerosol distributions specifically, so the new ICRP default appears to be justified. The implications of a particular assumption of particle-size distribution for estimates of worker uptake are dramatic. Using the new ICRP 66 lung model, for example, if the AMAD is known or assumed to be 0.4 μm, 47% of the uptake is predicted to be deposited in the upper airways (anterior and posterior nose) and about 50% in the bronchial and alveolar regions. But if the AMAD is about 5 mmm, the upper airway deposition would be about 90% of the uptake and 10% in the bronchial and alveolar regions. These outcomes are reflected in predicted committed effective dose equivalent (CEDE) as well—there is twice the CEDE from the smaller of these AMAD distributions for the same exposure (DAC-hr). If the aerosol distribution contains a component of relatively few, very large, but still inspirable particles or large particles of high specific activity, the probability of atypical uptake of such particles during brief pre- and post-alarm worker exposures goes up. The reason for this atypical uptake is that few such particles are likely to be available in each tidal volume. Then, the overestimate of committed dose based on a high-volume FAS sample data set can be very much larger. In such a situation, having data on particle-size distributions at one or more locations in the room would make a significant contribution to dose estimates.

Objectives

The overall objective of the proposed project is to design technologies and methods that will enable particle-size distribution information to be readily and inexpensively obtained in any monitored workroom. Having ready and inexpensive particle-size information will help prepare the Laboratory for the anticipated implementation of regulatory requirements stemming from application of the new lung model and recommendations of ICRP 66. Although many techniques and devices such as cascade impactors are available for particle-size determination, they are costly to install, operate, and maintain, and so are typically applied only to special limited studies.

Approach

The approach to sampler development has been to design a simple, but effective FAS device incorporating a multistage size-fractionating-sampling process that can be readily set up along with ordinary FAS monitors. The FAS monitors operate on house vacuum and are easily disassembled for counting and analysis with existing counting systems and procedures.

The design of the fractionating-filter-pack monitor (FFPM) is based on refinements of the 1970s era concept of sampling with stacked nuclepore filters but incorporates modern improvements. After a sample is collected by an array of sieve-type filters, the radioactivity on each filter would be determined. Then based on the known aerosol penetration response curves for each filter type, the aerosol size distribution can be mathematically reconstructed. The aerosol collection properties of such an array of selected filters are being investigated as a project objective. Using computational fluid dynamics (CFD) modeling and experimental aerosol tests, we have developed relationships between pore sizes, filter separation, and other parameter values that will optimize performance.

Considerable work has already been done to develop a new FAS housing that uses the same Quick Change Filter (QCF) cartridge as the Alpha Sentry CAM, and incorporates a critical-flow venturi to establish a fixed flow through the filter (Parulian et al. 1996). As part of the design, the same FAS housing has been incorporated in the FFPM. The stacked filter pack can be readily mounted in the QCF cartridge. By designing the critical-flow venturi orifice to produce the needed design flow at the pressure drop of the filter pack, we can achieve a highly repeatable design parameter. The new FFPM instrument can then be deployed just as the normal FAS would be, without requiring special setups and in-place calibrations. A photograph of the prototype FFPM housing, together with a QCF cartridge disassembled to illustrate how filters and filter separators would be stacked, is shown in Figure 1.
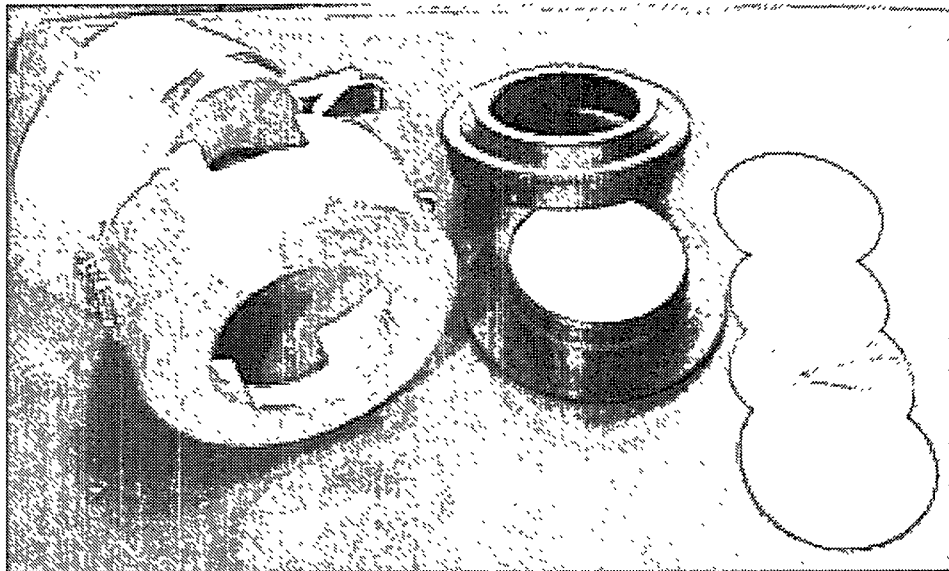
Figure 1. *Fractionating filter-pack monitor prototype: FAS body (left) accepts the Canberra Quick-Change Filter Cartridge (center), shown with the cap removed, and an array of filters and separators (right) that would be mounted in the cartridge as a stacked filter pack. Individual filters in the pack can be gross-alpha counted or analyzed for individual radionuclides by alpha spectroscopy.*

The interpretation of the individual filter activities is carried out by a deconvolution process that proceeds from knowledge of the filtration efficiency for particles of a wide range of sizes (a filtration efficiency response curve) for each of the filters in the filter pack and an analysis procedure called "Expectation Maximization" (Maiher and Laird 1985). The strategy is one of finding the most likely particle-size distribution that would produce the observed distribution of activity on the several filters. What is needed then is good data on filtration efficiency as a function of particle size and statistically significant filter counts.

Studies have been completed of the potential for CFD modeling of aerosol flow through filters and the removal efficiency as a function of particle size. The resultant 2-D and 3-D model predictions of filtration efficiency vs. particle diameter show general agreement with experimental data for flows in a typical single-layer nuclepore filter application (Figure 2), but there have been some discrepancies found in the case of the woven mesh filter type that we will continue to study.

Using these types of efficiency data, we tested of the deconvolution calculation based on published plutonium size distribution data (Elder et al. 1974). First, we estimated the expected total alpha activity on each of three or four filters based on their observed sizes and converted size data to equivalent activity. Then, from the total alpha activity of each filter, we attempted a reconstruction by deconvolution. The result (Figure 3) shows generally good agreement. The procedure is widely used to determine diffusion diameter of the fine particle sizes associated with radon progeny collected on sequences of metal screens and is expected to provide good results in this application.

The characteristic filtration efficiency curves as a function of particle diameter of individual nuclepore membrane filters, and the effects of filter loading and particle bounce need to be documented using monodisperse aerosols in the ESH-4 low-velocity aerosol wind tunnel facility. These will be part of an expanded database for interpreting the results of a size-fractionating filter-pack sample. Then, the performance of a
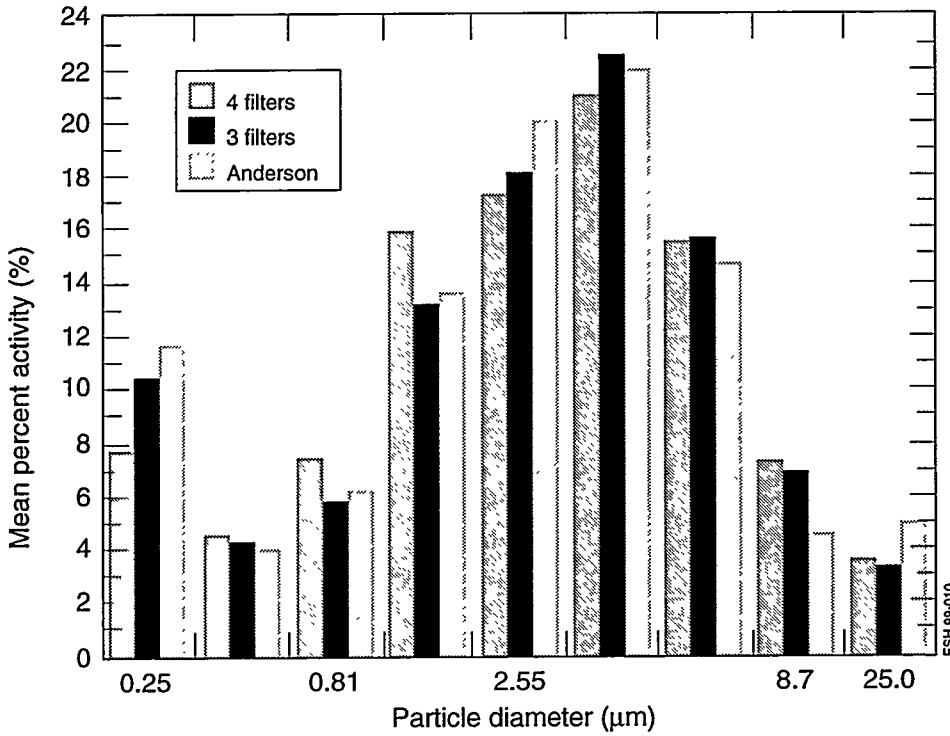
Figure 2. *Predicted filter-removal efficiency as a function of particle size for several types of filters.*
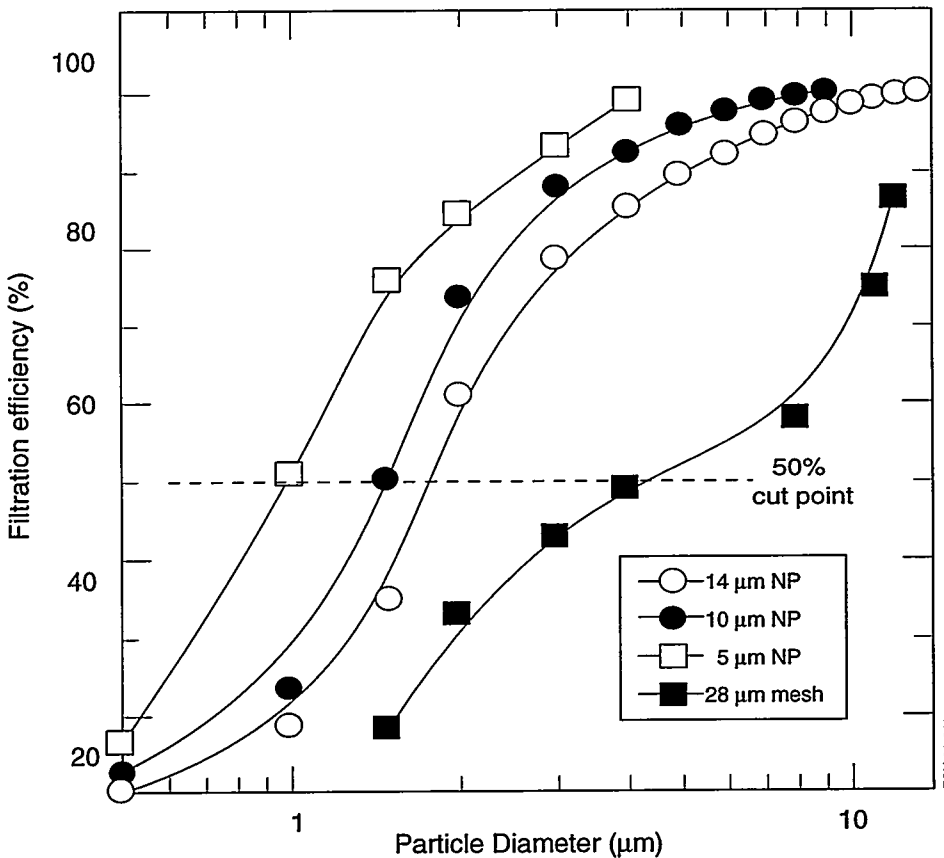

Figure 3. *Particle-size distribution reconstructions using the Expectation Maximization method compared with Anderson impactor data from Elder et al. (1974).*

number of filter-pack designs will be evaluated using a polydisperse particulate aerosol with a size distribution that has been well characterized using a laser aerosol-size spectrometer.

References

Strandling, G. N., Stather, J. W., Gray, S. A., Moody, J. C., Bailey, M. R., Hodgson, A. and Collier, C., *Human Toxicology*, **6**, 365–375 (1987).

ICRP. "Human respiratory tract model for radiological protection," ICRP Publication 66 (Oxford: Pergamon Press, 1994).

Dorian, M. D., and Bailey, M. R., "Particle size distributions of radioactive aerosols measured in workplaces," *Rad. Prot. Dos.* **60**, 119–133 (1995).

Elder, J. C., Gonzales, M., and Ettinger, H. J., "Plutonium aerosol size characteristics," *H. Phys.* **27**, 45–53 (1974).

Maher, E. F., and Laird, N. M., "Algorithm reconstruction of particle size from diffusion battery data," *J. of Aero. Sci.* **16**, 557–570 (1985).

Characterization of Photon Radiation Fields in a Los Alamos National Laboratory (LANL) Plutonium Facility

Principal Investigator: Jeffrey J. Whicker, Health Physics Measurements Group (ESH-4)

Co-investigators: Thomas B. Borak, Department of Radiological Health Sciences, Colorado State University; Fu-Hsing Hsieh, Department of Radiological Health Sciences, Colorado State University; Hsiao-Hua Hsu, Jeffrey M. Hoffman, David L. Wannigman, Richard H. Olsher, Health Physics Measurements Group (ESH-4)

Introduction

Workers at LANL's Plutonium Facilty (PF-4) use personnel dosimeters and workplace exposure rate measurements from ionization chambers for their protection from external radiation hazards. Ionization chambers measure exposure rates from photon fields at work locations, and dosimeters measure a worker's effective dose equivalent (EDE) from external radiation. In combination, these measurements help assure workers that their EDE is below regulatory limits and as low as reasonably achievable (ALARA).

Because of variations in energy and angular response for the dosimeters and ionization chambers, uncertainty in their measurements could increase in areas like PF-4 where multidirectional and low-energy photons (<100 keV) exist. The energy and angular responses of the LANL dosimeter and ionization chambers have been thoroughly measured under ideal laboratory conditions. However, conditions in the workplace are not ideal, but highly complex. Characterization of photon fields includes determination of energy and intensity of the fields and their spatial distributions. Measurements of photon fields and the response of personnel dosimeters and ionization chambers to these fields would increase our understanding of the uncertainty in our measurements and provide a valuable complement to existing laboratory studies.

Measurements of the energy and spatial distribution of photon fields will increase our understanding of dosimeter response under field condi-

tions. Christensen et al. (1994) concluded that large uncertainties in dosimeter response result from angular and energy dependence as compared to other sources of measurement error. The angular and energy dependencies are especially pronounced for photons with low energies (<100 keV), an energy range that includes a significant fraction of the photons emitted from transuranics. The Implementation Guide (IG), External Dosimetry Program, describes acceptable methods for ensuring compliance with 10 CFR Part 835. The guide specifically mentions that the topic of characterizing the photon energies and direction of incidence, especially when the estimated annual EDE approaches established limits, should be included in the technical basis document

Additionally, measurements of the spatial distribution of the photon fields would also provide information about the need for multiple dosimetry. The recent American National Standard for multiple dosimetry (HPS N13.41) recommends supplemental dosimeters when the two conditions are met: the radiation dose to any portion to the body has the potential to exceed 30% of the expected dose equivalent at the reference dosimeter location on the body; and the dose equivalent has the potential to exceed 10% of the limiting value when a significant component of the effective dose equivalent comes from a non-uniform radiation field. Therefore, the need for multiple dosimetry for workers in PF-4 should be assessed because of the potential for nonuniform radiation fields resulting from glove box irregularities (i.e., streaming through glove ports and

other penetrations) and large material concentrations in small locations that could result in dose equivalent (e.g., an organ dose) rates that could exceed 5 rem in a year (10% of annual 50-rem limit).

Finally, the accuracy of workplace measurement made by ionization chambers of differing designs can be better assessed knowing the energy and directional characteristics of the photon fields. The ionization chambers, such as the ones used to measure exposure rates in PF-4 (i.e., Eberline R0-3C and Eberline R0-20), are calibrated using high-energy photons (0.662 MeV, Cs-137 photons) but have been tested at lower energies. These instruments exhibit a relatively flat energy response down to low energies (<10 keV) when taking measurements using an open beta shield and when the radioactive source is directly in front of the instrument. However, both the RO-3C and the R0-20 instruments exhibit a directional response for photons with energies less than about 60 keV. For example, the normalized response for 17-keV photons in the RO-3C is about 70% of the true exposure rate when the source is at 90° to the long axis (Olsher 1995). Comparatively, the normalized responses of the R0-20 ionization chambers were about 20% of the true exposure rates when the source is 90° to the instrument for this photon energy (Seagraves et al. 1997). It is common during operations in PF-4 that workers are positioned at workstations where the radiation is scattered into it from large angles from radioactive sources in neighboring workstations, and possibly even from the glove-box line behind them. Photons entering the

measurement volume at these large angles could affect the measurement accuracy.

The objective of this study was to develop new methods to characterize photon radiation fields in critical workplaces inside the plutonium facility. Characterization of photon fields includes determination of photon-energy distributions, direction of these incident photons, and the spatial distributions of EDE rates.

Methods

Characterization of the photon field requires determining the photon-energy distribution and the directional aspects of the field. Photon-energy-distribution measurements were made using an NaI(Tl) detector, and the energy distributions were then calculated from the measured spectra. A highly collimated field of view was created using copper shielding around the detector. TLDs and ionization chamber measurements were also made to explore the characteristics of the photon fields and their response.

Photon-energy-distribution measurements

Measured spectra from NaI(Tl) detectors provide direct information on the distribution of energies deposited within the active detector volume, but they do not give complete information on the photon-energy distribution that produced the observed spectrum. Determining photon-energy distributions from measured spectra can be especially challenging when the distribution is complex with many photon energies, as expected in PF-4. To determine the photon-energy distributions, spectrometers such as sodium iodide detectors coupled to a multichannel analyzer are used to obtain pulse-height spectra. Such spectra provide direct information on the events of energy deposited within the active volume of the detector, but not for the energies of incident photons responsible for these events, so the photon-energy distribution has to be unfolded from the measured spectra. Spectrum unfolding consists of multiplying the measured spectrum with an inverted response matrix or using spectrum

stripping techniques (Knoll 1979). The unfolded spectrum then can be converted to EDE using dose conversion factors. We used the MICROSPEC-2™ from Bubble Technologies, a NaI(Tl)-based instrument incorporating software that calculates EDE rates from stripped photon-energy distributions under broad-beam geometry conditions.

For the photon-energy-distribution measurements, the MICROSPEC-2™ was used. This instrument is a portable spectroscopic survey system that provides the calculation of dose equivalent and radionuclide identification through spectroscopy. There are three gamma ray (or x-ray) probes offered with the MICROSPEC-2™ for the different measurement purposes: the E-Probe for use in environmental surveys; the G-Probe for use in high-gamma-ray fields; the X-Probe for use in low-energy-gamma or x-ray fields.

The MICROSPEC-2™ uses a spectral stripping technique to convert the acquired spectrum into a pure incident photon-energy spectrum, which is then multiplied with fluence-to-dose conversion factors and integrated to calculated dose-equivalent rates at skin, eye, and deep-dose depths. The fluence-to-dose conversion factors used are found in ICRU report 47(1992). Accounted for are the efficiency of the detector, photo-fraction for different photon energy, and cross-sectional area of probe, which are stored in computer memory. The advantage of this system is that it provides not only dose-equivalent rates in the environmental radiation fields but also information on energies of photons existing in the fields

There were two probes used in this work. First, the G-Probe is designed to detect high-energy gamma rays from 60 keV to above 3 MeV in a high-photon field. It is a 38-mm x 38-mm (1.5-in. x 1.5-in.) NaI detector. The other one is the X-Probe, a 50-mm x 1-mm (2-in. x 0.04-in.) NaI, with a 0.127 (0.005-in.) beryllium window. The X-probe has a range of 5–200keV and is capable of measuring low-energy photons. To estimate the accuracy of MICROSPEC-2™ using the

G-Probe and X-Probe, we measured dose equivalent rates at different distances and compared them with calculated dose equivalent rates. These calculated values were determined from the known radioactivity and fluence-to-dose equivalent conversion factors published in the ICRU report 47.

Determination of directional aspects of the photon fields

We assessed the directional aspects of the photon field using TLDs and a collimated NaI(Tl) detector. To determine fractional contributions to a worker's exposure from all directions of the radiation fields inside PF-4, the collimator was designed to be used with the MICROSPEC-2™ system. Figure 1 illustrates the design of the collimator used throughout the tests. To minimize x-rays generated by interaction of photon with the attenuator, we used copper to attenuate low-energy photons. The X-probe was placed in the copper box.
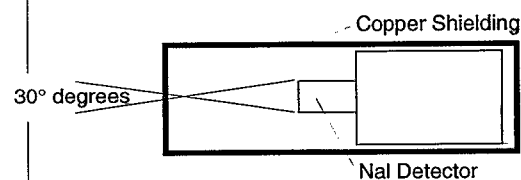

Figure 1. *Schematic representation of the collimator.*

The photon beam was collimated through a small hole just large enough to cover the dimension of the sodium iodide crystal. This shielding arrangement provided only an approximate, not exact, broad-beam parallel geometry. The LANL TLD dosimeters were mounted on cylinder water phantoms to simulate placement on a worker. The dimensions of the cylindrical water phantoms, which were filled with water, are 11-in. diameter and 18-in. high. One phantom containing 12 LANL personnel dosimeters was placed at each work location for about 16 hours. Four sets of three dosimeters were positioned on the phantom, and each set was positioned at 90° to each other. The three dosimeters in each set were positioned at different heights on the phantom and separated by

about 4 inches. The distance from the closest dosimeters to the glove-box face was about 3 in., and the height from the floor to the top dosimeters was about 50 in.

LANL personnel dosimeter

At present, the Model 8823 TLD dosimeter is used to measure personnel exposure to external source of radiation at LANL. The dosimeter contains two Harshaw/Bicron TLD cards each of which contains four TLD chips of varying thickness and of different composition. One TLD card is a Harshaw/Bicron-NE Model 7774 TLD card containing three TLD-700 (LiF:Mg,Ti enriched in ^{7}Li) chips in position 1, 2, and 3, and one TLD-400 (CaF:Mn) chip in position 4. This card is used for estimating beta and photon dosimetry at deep, shallow and lens-of-the-eye depths. The other card is a Harshaw/Bicron-NE Model 6776 TLD card containing two paired TLD-700 and TLD-600 (LiF:Mg,Ti enriched in ^{6}Li) chips. This card placed in the Model 8823 TLD cardholder within a cadmium box is used for evaluating neutron doses. The Model 8823 dosimeter has been developed to separate the responses due to photon, beta, and neutron radiation. As to the angular dependence for low-energy photons, Mallett (1997) demonstrated that the normalized angular response at 90° for ^{241}Am in the LANL Model 8823 dosimeters is about 60% of the deep dose equivalent at 0° with vertical axis.

Ionization Chambers

The ionization chambers, such as the ones used to measure exposure rates in the plutonium facility (i.e., Eberline RO-3C and RO-20), are calibrated using high-energy photon field (0.662 MeV ^{137}Cs photons). These instruments exhibit a relatively flat energy response down to low energy (<10 keV) when taking a measurement with open beta shields and when the window of the instrument directly faces toward the radioactive source. However, both the Eberline RO-20 and RO-3C exhibit a noticeable directional response for photons with energies less than 60 keV (Olsher 1995, Seagraves et al. 1997).

Experimental setup

The selected site for measurements was a glove box located in PF-4 (shown in Figure 2). This site was selected because workers assigned to work at this glove-box line received some of the highest photon doses in the facility due to the high ^{241}Am content in the material in the glove box. There are four work locations encircling the glove-box. Near this glove box there are several other process glove boxes that contain transuranic material as well.
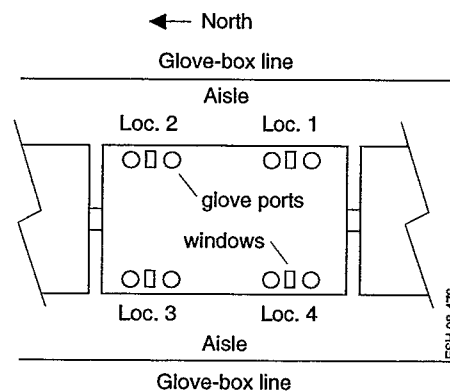

Figure 2. *Schematic of the glove-box around which photon fields were measured.*

The measurement distance from the face of the glove box to the center of the detector was about 5 in. When working in and around the workstation, the actual distance to a worker's torso from the glove box varies considerably. The measurement distance of 5 in. was as close as we could get the instrument to the glove-box face and still maneuver it to make the measurements at the various orientations. The response to these radiation fields was estimated using both instruments and dosimeters as mentioned above.

Two types of ionization chambers, i.e., RO-3C and RO-20, with open shield were used to measure radiation exposure rates at each work location. The three positions at which measurements were made included the window, left glove port, and right glove port. When measurements were made at the glove ports, the gloves were pushed into the glove ports.

The MICROSPEC-2™, equipped with the X-probe and the copper collimator, measured photon-energy distributions at each specific work location in various source-detector geometries. The MICROSPEC-2™ coupled with the G-probe, but not with the collimator, also measured photons at multiple locations. These measurements then were unfolded and provided estimates for the EDE rates.

Data analysis

First, we tested the accuracy of the MICROSPEC-2™ instrument by measuring at different distances from ^{137}Cs and ^{241}Am sources and comparing the measured values to the calculated values. Additionally, we categorized data into front, nonfront, and glove-port categories for both the TLD and the MICROSPEC-2™ measurements. We then made comparisons between these two categories. Because of the lack of normality in the measurements or in log transformed values, the nonparametric Mann-Whitney test was used to evaluate for differences. We made additional paired comparisons between measurements from the two types of ion chambers using the nonparametric sign test.

Results

Using the instruments and measurement techniques described above, we were able to characterize photon radiation fields in a plutonium facility. Overall, the results at this glove box suggest that dosimeters worn on the upper chest according to procedure will probably record a reasonable estimate of workers' average EDE values for photons. Although the results are preliminary and confined to one high-exposure box, we have found no evidence of the need for multiple dosimetry for photon EDE measurements. Also, we found that deposits of transuranic dust on the inside of the glove-box gloves are a significant contributor to a workers dose when the gloves are hanging out the glove ports. Finally, a paired comparison of measurements made with ionization chambers at different orientations suggested some directional dependence. Further investigations would be required to fully test the

accuracy of the ionization chambers under field conditions.

MICROSPEC-2™ accuracy

The measurement results from the MICROSPEC-2™, equipped with the G-probe, were compared to the calculated EDE rates using a ^{137}Cs source. The percent differences were less than 3%. However, the response from the same system for [241]Am had relatively larger differences from the calculated values. In comparison, the measurement results obtained using the X-probe and the calculated dose equivalent rates for low-energy photons generated by [241]Am, showed percent differences that ranged from ~1.4% to 20%. Figure 3 shows the result of the measurements of dose equivalent rates at different distances from an [241]Am source. Generally, the measured values match closely (within a few percent) to the calculated values except at the longer distances where the counting statistics become poorer and effects of photon buildup might be more pronounced.

Spatial distribution of DE

At individual locations, photons are incident to workers omnidirectionally but are not completely uniform, unless averaged over all locations. Both the TLD and Microspec-2 data showed that when averaged over all four workstations, no significant differences were found in photon EDE rates between front and nonfront measurements (Figures 4 and 5). However, when TLD measurements were analyzed by individual locations, the highest measurements were always those at 90° facing the center of the glove box. But, as we witnessed, workers moved from one workstation to the next and so the dose distribution would be determined from a combination of work performed at all the workstations. It would be helpful to know the work patterns around this glove box to better assess the spatial dose distribution to the workers. Additionally, the EDE rates at a workstation were significantly reduced when the nearby gloves were inserted into the glove ports.
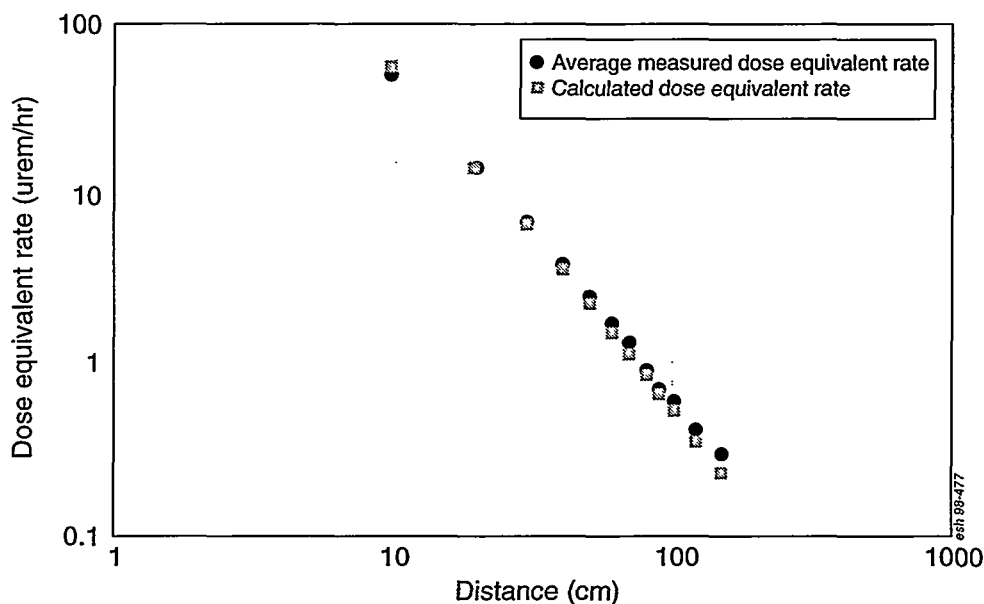

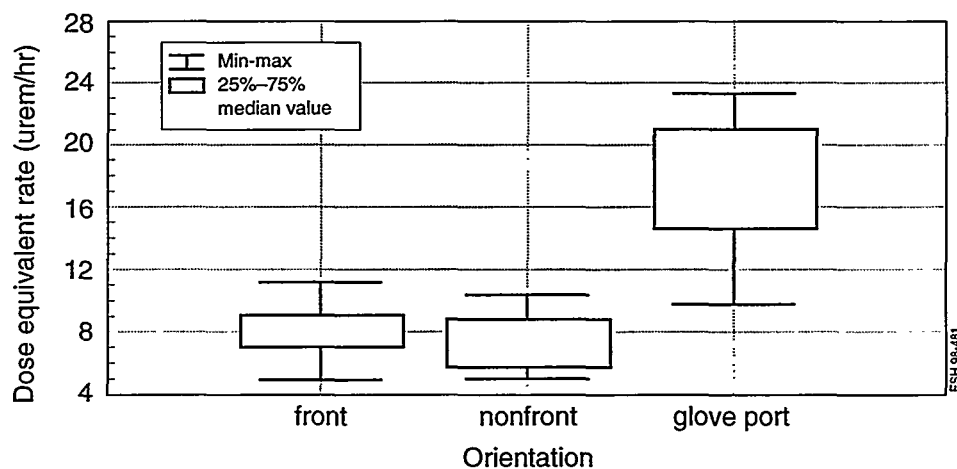**Figure 3.** Total dose equivalent rate varying with distance from a [241]Am source.

Figure 4. Dose equivalent rates measured by the collimated MICROSPEC-2 at different orientations.
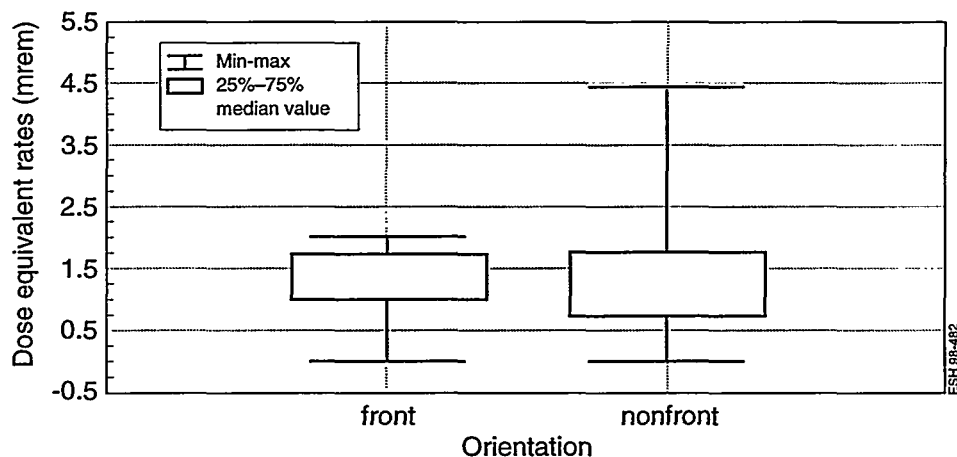

Figure 5. Dose equivalent rates measured by TLDs at different orientations.

Measurements at the glove ports (more correlated to extremity dose) were significantly higher than those at the window (more correlated to whole-body dose). This finding suggests that some streaming of photons out through the port occurs and also supports the use of extremity dosimeters when hands are inserted into the glove ports.

Dosimeters placed at the upper chest level measured significantly higher doses than those at a waist level. Figure 6 shows the results from this analysis. These results were averaged over all locations.

Assessment of need for multiple dosimetry

The implications of all our findings with regard to multiple dosimetry is that whole-body dosimeters worn according to LANL procedures (chest level in front of body) should provide a reasonable estimate of the average whole-body dose, especially considering the work patterns of the workers at this particular high gamma field glove box. In addition, use of extremity dosimetry is recommended when inserting hands into the glove boxes due to the much higher exposure rates, as is the current policy. The possibility of the need for multiple dosimetry at other locations, or for other processes can be assessed using the same techniques described in this paper.

Energy spectra measured at different orientations

In most cases, when the collimated Microspec system was pointed at 90° or 180° to the workstation, 60-keV photons were measured. These photons were not measured when the system was pointed directly at the glove box. At 0°, we speculate that the metal plate covering the middle window effectively shielded out the 60-keV photons, but it was not thick enough to completely shield out the more energetic plutonium x-rays above 100 keV. That is, the window shielding effectively "hardened" the photon-energy distribution. Figures 7 and 8 show the measured and unfolded energy distributions for the orientations of 0° and 90° for work location 2, respectively.
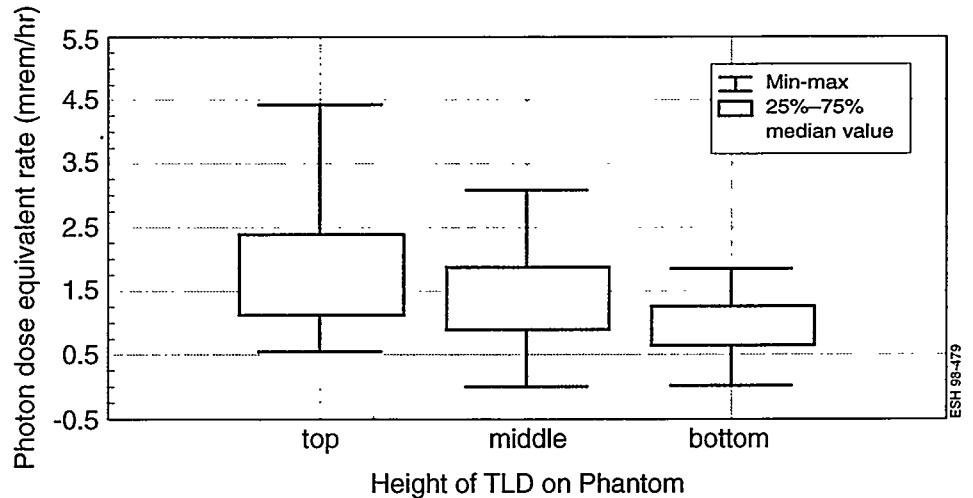

Figure 6. Dose equivalent rates at all work locations measured by TLDs on phantoms at three heights.
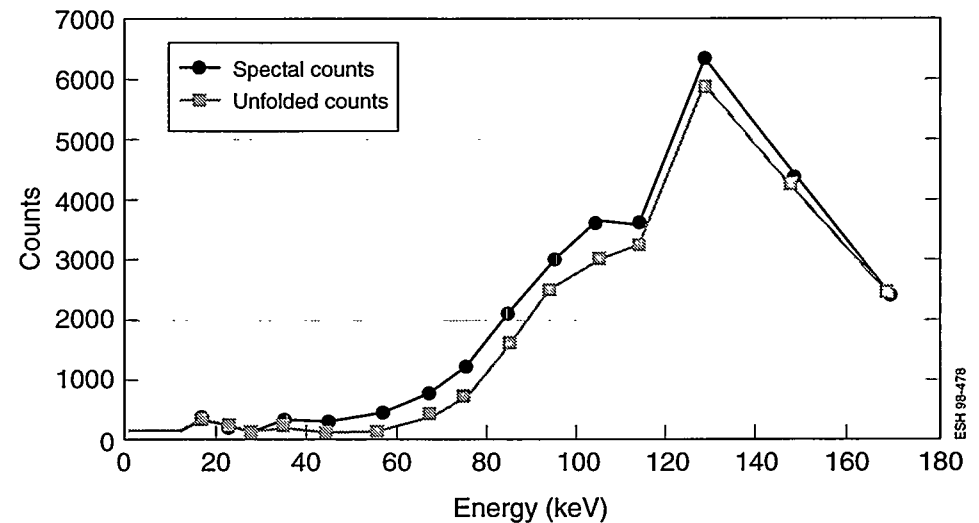

Figure 7. Measured and unfolded spectra obtained with a X-probe at location #2 with a 0 degree orientation.
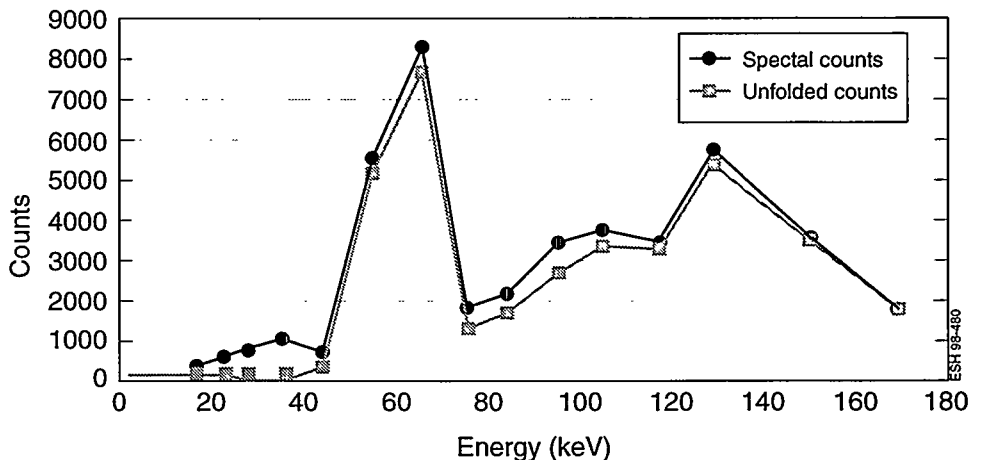

Figure 8. Measured and unfolded spectra obtained with a X-probe at location #2 using a 90° orientation toward the North.

The source of the 60 keV photons measured at 90° was the gloves hanging out of the boxes, and this was confirmed by direct measurement of the gloves. It is believed that the inside of these gloves have a layer of transuranic "dust," including ^{241}Am, and the thickness of Pb layer in the gloves was not sufficient to completely eliminate the 60-keV photons. The 60-keV photons measured at 180° probably originated from gloves and glove ports on the opposite side of the aisle.

Ion Chamber Results

Overall, the energy spectra measured showed that most of the photons were of energies ≥60 keV, and therefore the ionization chambers should give reasonably accurate measurements. But, some directional dependence would be expected. In fact, we found limited evidence that this was the case. For example, the highest measurements were recorded when the instrument was at 0° to the glove box for both the Eberline RO20 and the RO3C models when compared to measurements made at 90°. The percent differences in median exposure rates measured at 0° and 90° at the window locations were about 20% for both instruments. However, to fully test the effects of orientation, more measurements are needed and the confounding effects of the photons from nearby hanging gloves and partial shielding of photons from the person making the measurements should be addressed. On the other hand, the ion chamber measurements were made under normal operating conditions (i.e., gloves outside the boxes, person holding the instrument, and at the same distance defined in ESH-1 procedures). The ESH-1 procedure of pointing the "open" beta window of the ion chamber at 0° generally provided the most conservative (highest) measurement. The absolute accuracy of the field measurement with the ionization chambers still needs to be assessed.

Deliverables

Techniques were developed to help measure the spatial and energy characteristics of photon radiation fields. These techniques were then tested for accuracy and used to characterize the photon radiation field at a process line in PF-4 where assigned workers had some of the highest photon exposures relative to other workers in PF-4. The results of this investigation showed that the torsos of workers are exposed to photons from all directions. The intensities of the fields at individual locations of the process line studied were unevenly distributed. However, when averaged over all the work locations in the line, we found no differences between photon field intensities directed to the front of the torso (to be measured by the dosimeter without shielding by the body) and those to the side and the back. Averaging over all work locations is a more appropriate estimate of a worker's actual dose because workers move quickly and frequently from one workstation to the next. The worker's dose then reflects the time-weighted average of the exposures received at each location. Based on these preliminary findings, we have found no evidence of the need for multiple dosimetry. The energy distribution measurements showed the significant contribution to a worker's dose from the nearby gloves that are typically left hanging out of the glove ports. Inserting the gloves into the ports reduced significantly the dose rates at the neighboring workstations.

References

"Criteria for performing multiple dosimetry," American National Standards Institute# HPS N13.4 (1997).

Bubble Technology Industries, *Spectroscopic survey system, MICROSPEC-2^{TM}, for high-sensitivity radiation surveying with isotopic identification,"* (Chalk River, Ontario, Canada: Bubble Technology Industries Inc., 1995).

Department of Energy, "External dosimetry program," Implementation Guide G-10 CFR 835/C2-Rev.1., (1994).

Hoffman, J. M., Mallett, M. W.,"The LANL model 8823 whole-body dosimeter and associated dose algorithm," draft Los Alamos National Laboratory internal report ESH4-PDO-TD-01, RO (1998).

"Measurement of dose equivalents from external photon and electron radiations," (International Commission on Radiation Units and Measurements, 1992) ICRU Report 47.

Knoll, G. F., *Radiation detection and measurement*, (John Wiley and Sons, New York, 1979).

Mallett, M. W., "Model 8823 personnel dosimeter: lower limit of detectability and angular dependence studies," Los Alamos National Laboratory internal report ESH-4-MTS-97:047 (1997).

Olsher, R., "Technical basis document, Eberline RO-3C survey meter, portable air ionization chamber exposure rate meter," Los Alamos National Laboratory internal report ESH4-RIC-TBD-008 (1995).

Seagraves, D. T., Bates, R. L., Olsher, R. H., "Photon energy response of exposure rate meters in use at the Los Alamos National Laboratory, presented at the 42nd Annual Health Physics Society Meeting," Abstract: *H. Phys.*, supplement Vol. 72(6):S7 (1997).

Implications of Room Ventilation and Containment Design to Minimize Worker Exposure to Plutonium Aerosols

Principle investigator: Jeff Whicker, Health Physics Measurements (ESH-4)

Co-investigators: John Rodgers, Murray Moore (ESH-4); Hongrui Gong, consultant; Ricky Lopez, Industrial Hygiene (ESH-5); Piotr Wasiolek, long-term visiting scientist from New Mexico Institute of Mining and Technology

Introduction

When there are accidental plutonium aerosol releases at chemical and nuclear facilities, the level of protection achieved for nuclear workers depends upon two factors: the concentration of plutonium aerosol to which the workers are exposed and how quickly workers are alerted to the release and evacuate the area. Both concentration levels attained and the rapidity of continuous air monitor (CAM) response depend on dispersion patterns of the aerosol into worker breathing zones and into areas occupied by CAMs. The time course of mixing and transporting an aerosol into a worker's breathing zone determines in part the potential internal exposure to the worker. The pattern of transport from the point of release to CAM locations determines whether and how quickly the CAM alarms and the potential, therefore, for limiting worker exposure.

Aerosol transport throughout workrooms is largely controlled by complex, poorly understood interactions between the ventilation configuration, worker presence, release dynamics, and room furnishings. At Los Alamos National Laboratory (LANL) and many chemical and nuclear facilities, little is known about the details of the airflow patterns in workrooms. Even less is known about the effects of variations in critical variables, i.e., containment structure geometry, ventilation rate and inlet and exhaust configurations, worker presence, etc., on aerosol dispersion and subsequent worker risk. Consequently, health and safety professionals make important decisions regarding the application of CAMs and other air-sampling instruments to minimize inhalation risk by using qualitative engineering judgments and limited airflow pattern data, such as are obtained with smoke tubes. Detailed knowledge of aerosol dispersion dynamics can significantly improve worker protection in LANL plutonium facilities (Crites 1994, Whicker et al. 1997). Seeking improved ways to reduce inhalation exposure to accidentally released plutonium aerosols at LANL is very important considering that significant, unplanned LANL plutonium inhalation exposures to workers have occurred within the past five years.

Measurements by ESH-4 in the Plutonium Facility (PF-4) have revealed that at most workstations, the velocity direction of the airflow is upward into breathing zones. Because most accidental plutonium releases occur at a height below the breathing zone (Wannigman 1998), the concentrated plutonium aerosol at the point of release is most often lifted into the breathing zone before its being dispersed into the rest of the room, possibily triggering a CAM alarm later.

Strategies for enhanced worker protection could be realized through a better understanding and prediction of aerosol dispersion as affected by ventilation-induced airflow patterns, geometry of containment structures (glove box, slot box, chemical hood, etc.), and interactions with a worker positioned in front of a containment structure. That is, it is possible to collect a detailed database on airflow patterns and aerosol transport and mixing under a variety of conditions. This database can serve as a solid technical base for providing inexpensive recommendations for ventilation designs that could enhance the probability of rapid movement of plutonium aerosol away from worker breathing zones and provide for optimal use and placement of CAM instruments.

Method

Field Studies

One of the critical requirements for understanding particle dispersion in workrooms is the characterization of airflow patterns. Such characterization can be accomplished with computational fluid dynamic (CFD) computer simulations or with experimental techniques, such as measurements with smoke, neutrally buoyant markers, trace gases, or aerosol particles. Each of these techniques has advantages and disadvantages.

Last year we explored the use of a sonic anemometer (Figure 1), another tool that assists in characterizing airflow. The sonic anemometer could provide accurate, highly frequent (up to 60 Hz), and three-dimensional measurements of air-velocity vectors with a sensitivity of less than 1 cm s^{-1}. A general description of the principle of operation of sonic anemometers is contained in Stull (1988). No other experimental technique provides measurements with all these qualities. Our effort demonstrates the utility of using sonic anemometers for measurements at velocities typical of the indoor environment (often around a few cm s^{-1}). Highly frequent measurements allowed analysis of the turbulent structure of the airflow, which drives aerosol mixing through turbulent eddy diffusion. We tested the benefits of using sonic

anemometry by making measurements in the ultra-high temperature reactor experiment (UHTREX) test room and in a PF-4 laboratory. This portion of the work was summarized and submitted for publication (Wasiolek et al. 1998). The air-velocity vector measurements are very useful for CFD flow-field-prediction verification and can provide a fundamental understanding of the effects of people and containment structures on local airflows.

Computational modeling

Before proceeding with experimental measurements, we conducted CFD modeling to test the effects of alterations in ventilation or room configurations on airflow patterns in the UHTREX test room. We also calculated airflow patterns resulting from several different configurations using CFD modeling and then compared these calculations to the baseline ventilation configuration, a horizontal flat-plate supply diffuser with four corner exhausts at the floor level, which is similar to that installed in PF-4 rooms. The tested configurations included

• a conically shaped supply diffuser with four corner exhausts,

• ceiling deflector plates with four corner exhausts,

• a downward-directed air curtain from the entire ceiling with four corner exhausts,

• a modified air curtain with a ceiling air supply placed only above worker locations with under-glove-box exhausts, and

• supply ventilation from wall panels on the sides with under-glove-box exhausts.

We evaluated airflow directions and velocities in the vertical plane for numerous locations to help us determine which of the alternative configurations resulted in the most favorable airflow patterns. For credible computer-aided design, establishing confidence in the predictions of selected CFD-modeling approaches and boundary conditions is crucial; therefore, much work was done to verify a range of CFD model predictions. We used the CFD code CFX to

obtain computational model predictions for turbulence intensity, air velocities, and particle concentrations. We then compared the predictions to experimental data collected in PF-4, room 420.

Progress and results

An example of a time series for measurements of air velocity in a single direction and at a point in the UHTREX test room is shown in figure 2. This figure shows the average vertical velocity and the turbulent structure is seen in the fluctuations in the velocities. Using the mean velocity and the variations of the fluctuations about the mean, we calculated turbulence intensity (TI) as the

standard deviation of the velocities divided by the mean velocity.

Figure 3 shows measurements of air velocity in the x, y plane made at locations in room 420 in PF-4 and the TI at the same locations, respectively. One of the aspects shown by these data is the relative contribution to aerosol transport from forced convective flow verses turbulent eddy diffusion. Additionally, analysis of these turbulent fluctuations using Fast Fourier Transform (FFT) techniques can give us some insight to the size of eddies that have formed within the inherent limitations of the sonic anemometer. Combined, these measurements help provide a fundamental
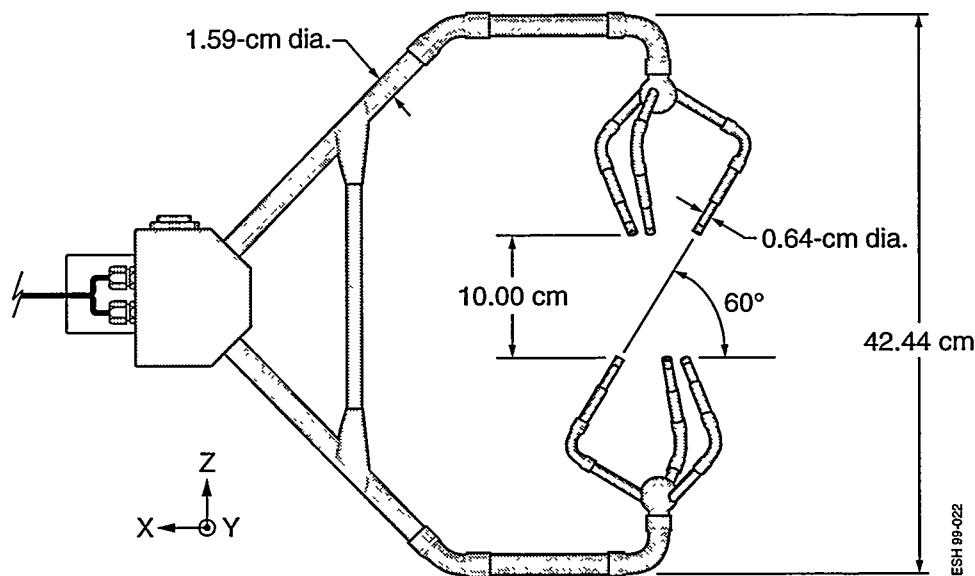

Figure 1. Sonic anemometer head geometry with approximate dimensions.
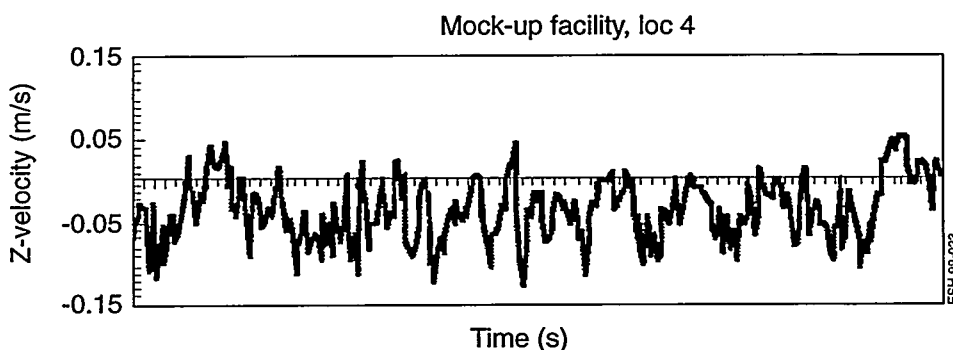
Figure 2. Vertical air velocity over time—measurements made in the UHTREX test room.

understanding of aerosol dispersion through rooms, which provides a powerful basis for confirming aspects of physical models of aerosol dispersion in indoor environments that have not been previously available.

The use of sonic anemometry allows for additional verification of airflow patterns generated from a variety of room conditions. Verification of model predictions using both UHTREX and PF-4 measurement data continues to show acceptable accuracy. Figure 4 shows a comparison of measured and CFD-predicted time profiles for aerosol concentrations.

Figure 3. Turbulence intensity (right) and air velocity (left) measurements in room 420.

Figure 4. Concentration profiles for a release in room 420 simulated by CFD modeling and compared to the experimental data.

Note the similarity in the shapes of the concentration time profiles and the similar time-to-peak concentrations. These results are very encouraging given the complexity of the room geometry and conditions. A more thorough and systema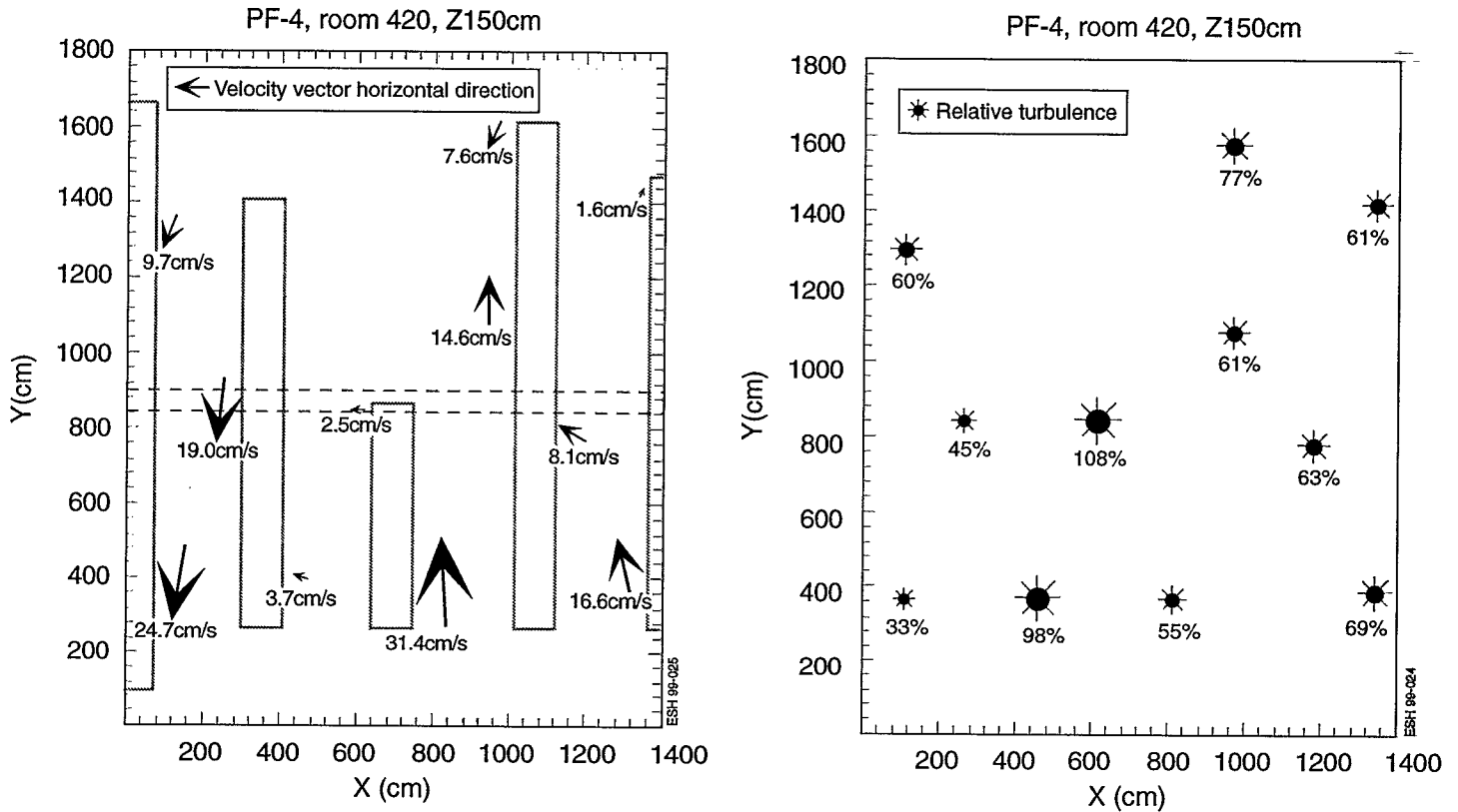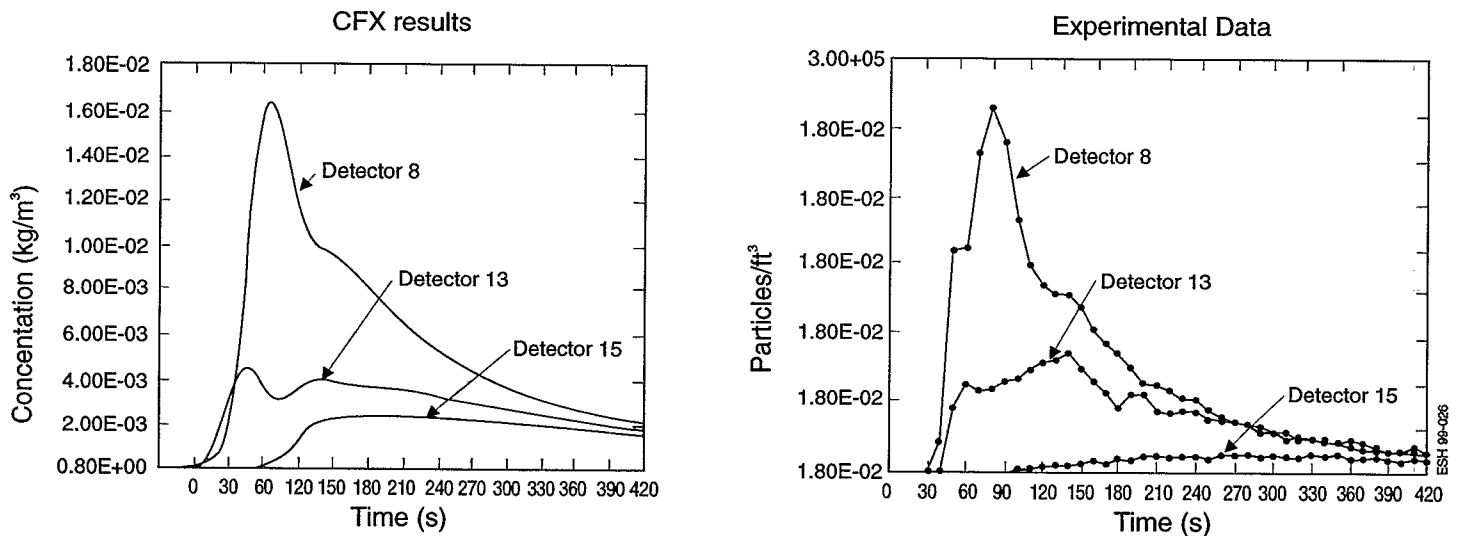tic intercomparison of predicted behavior of convective flows and released particles remains as necessary in the more controlled environment of the test room at UHTREX. For this intercomparison, a large database of sonic anemometer measurements and spatial and temporal tracer-particle concentrations from tracer releases were gathered from the UHTREX test room. Our comparisons of these data to CFD predictions are not yet complete.

During the past fiscal year, we made significant progress that addresses the question of whether changes in the design of room heating, ventilation, and air-conditioning inlet and exhaust systems could reduce the potential for worker exposure because aerosols are being carried up into the breathing zone. For this evaluation, we tested computer-aided CFD of the effects of alternative ventilation designs on room airflow patterns. With combined input from ESH-1, NMT-8, and ESA-DE, we identified seven alternative designs to be tested against the baseline design (similar to that in PF-4). These alternatives were designed to try directing airflow in a downward direction at the faces of the mock glove boxes (simulated workstations).

All alternative designs showed a marked improvement in creating downward air movement; however, in several cases, we found large-scale eddies could develop and create upward flow at some locations. Variations on air-curtain designs were also compared and showed good downward airflow movement. Air-curtain designs appear to be very promising ventilation designs for creating more protective airflow patterns (Rodgers et al. 1998), but first we must further test a variety of worker and containment structure configurations and perform a cost analysis for PF-4 use.

Conclusions and Deliverables

Substantial reductions in worker risk could derive from better understanding of airflow that leads to its accurate prediction—including turbulent structure—and the subsequent dispersion of radioactive or toxic aerosols or gases under a variety of ventilation and containment structure geometries and release conditions. The result would enable proactive design of ventilation systems and CAM use. Reduction in worker risk would also result in cost savings (perhaps >$10K per event) because of fewer and lower accidental plutonium intakes that require fewer whole-body counts, medical assessments, internal and external agency accident investigations, numbers of CAMs and fixed-air samplers, and lost work days. Overall, the benefits of this project are

- better worker protection,
- doses to as low as reasonably achievable,
- much lower probability of exceeding dose limits,
- regulatory compliance, and
- contribution to meeting the University of California contract performance measures.

Finally, similar benefits may be extended beyond the narrow scope of LANL plutonium facilities to other facilities working with toxic or radioactive aerosols and/or gases.

Deliverables

Deliverables include evaluations of a number of possible ventilation and containment configurations designed to create favorable airflow patterns and upon which recommendations will be based. Also, valuable information on CFD model validation will be obtained along with a sensitivity analysis to help determine the important variables influencing the capture efficiency of slot boxes and local airflow patterns.

As part of our deliverables, we will inform the larger audience of safety professionals and facility owners of our findings through technical presentations and peer-reviewed journal articles.

References

Crites, T. R., "Alpha air monitor alarm sensitivity: operational experience," *Rad. Prot. Dos*, **53**, 65–68 (1994).

Rodgers, J. C., Whicker, J. J., Voss, J. T., "Comparison of continuous air monitor utilization: A case study," *Rad.Prot. Man.*, May/June: 56–64 (1998).

Stull, R. B., *An introduction to boundary layer meteorology* (Kluwer Academic Publishers, Dordrecht, The Netherlands, 1988).

Wasiolek, P. T. Whicker, J. J., Gong, H., Rodgers, J. C., "Room airflow studies using sonic anemometry," Los Alamos National Laboratory report LAUR-98-3497. (Also submitted to *Indoor Air J.*, 1998.)

Wannigman, D., personal communication to the authors (1998).

Whicker, J. J., Rodgers, J. C., Fairchild, C. I., Scripsick, R. C., Lopez, R. C., "Evaluation of continuous air monitor placement in a plutonium facility," *H. Phys.*, **72**(5), 734–743 (1997).
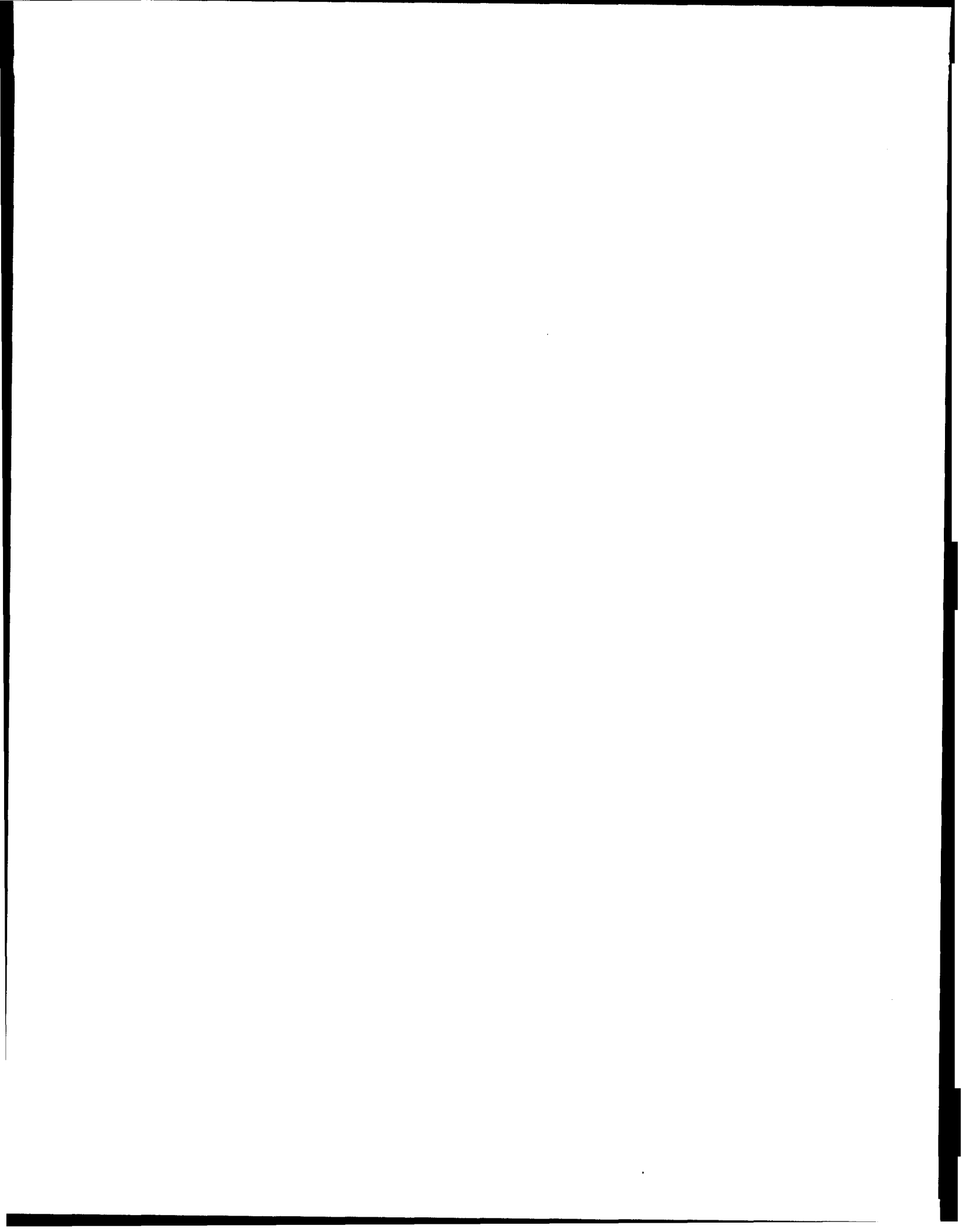
Industrial Hygiene and Safety

Pressure-Deformation Correlation in Waste Containers (PDCWC)
Reusability of organic vapor air-purifying respirator cartridges

Since ESH Division initiated the TDEA program in 1995, it has supported six industrial hygiene and safety projects.

Studies to date

FY95

Pilot Program for the Risk-Based Surveillance of Lung Cancer

A Polymeric Barrier Monitor to Protect Workers

Evaluation of a Real-Time Beryllium Detection Instrument

FY96

A Polymeric Barrier Monitor to Protect Workers

Evaluation of Commercial Air-Purifying Respirator Cartridges for Protection against Vapors of Nitric Acid

FY97

Reusability of Organic Vapor Air-Purifying Respirator Cartridges

FRHAM-TEX II Cool Suit Material Testing for Water (and Therefore, Tritium) Protection

A Polymeric Barrier Monitor to Protect Workers

Summary of progress

Industrial hygiene and safety projects have produced 14 professional papers and presentations since the TDEA program was started in FY95. The primary focus of projects has been evaluations of commercial products for purposes other than the original design specifications. The implementation of the recommendations of these studies have the potential to generate significant cost savings.

The project that studied pressure deformation in waste has received praise from industrial safety and hazardous material response communities from throughout the country. The project produced information that can be used immediately by any organization dealing with the potentially deadly hazard of pressurized drums and produced a device that will allow workers to determine the severity of a hazard.

Pressure-Deformation Correlation in Waste Containers (PDCWC)

Principal Investigators: Michael D. Larrañaga, Industrial Hygiene and Safety Group (ESH-5), David L. Volz, Hazardous Materials Response Group (ESH-10), Fred N. Bolton, Training and Support Group (NMT-10)

Introduction

Since 1992, there have been 123 occurrences within the Department of Energy involving incompatible chemical mixing and pressurization of drums where drums became pressurized to unknown levels. Failure of a pressurized metal drum can cause a rapid release of pressure, possibly ejecting the drum top or bottom and resulting in flying debris and release of internal drum contents, which could result in personnel injury and environmental contamination.

Pressurized drums present several personnel hazards including (1) possible injury from expelled debris, a pressure release, or burst drum; (2) exposure to radioactive or hazardous contents of the drum; and (3) exposure to pyrophoric, flammable, or combustible materials, which can ignite and burn.

Hazardous materials (HazMat) teams have little or no training on how to respond or approach bulging drum incidents, and there are many unknowns when working with pressurized drums. Pressurized drum incidents occur frequently across the United States in the public, private, and government sectors. Currently, there is no quick, inexpensive, and reliable method for determining pressures inside drums. In an attempt to develop training criteria and a device for determining internal pressures in 55-gallon drums, research conducted at Los Alamos National Laboratory explores the effect of pressure on new closed- and open-head 55-gallon metal and plastic drums, 30-gallon metal and plastic drums, 20-gallon plastic drums, and 85-gallon metal overpacks.

The objectives of this research are (1) to determine at what pressures 20-, 30-, and 55-gallon drums (metal and plastic), and 85-gallon metal overpacks experience failure; (2) to quantify the amount of deformation 55-gallon metal drums experience at various pressures under separate treatments; (3) to determine if the data for the 55-gallon metal drums supports developing an instrument for determining internal pressures; and (4) to conduct a statistical analysis on the mean failure pressures of the collected data for 55-gallon drums.

The information gained will provide critical information to emergency responders, including tools to assess a bulging drum situation. The most noteworthy is the development of a "safe working envelope," which will help responders determine how to safely deal with and approach pressurized drums.

Methods

Drums of different types were pressurized from zero pounds per square inch gauge (psig) to failure at 5.0 psig intervals. Linear deformation along the center line of metal drums was measured and recorded with corresponding pressures. A test apparatus was built to complete measurements and allow for pressurization. A containment cage was built around the apparatus to contain flying debris ejected during drum failure. Figure 1 illustrates the test apparatus.

Pressure was increased for each test interval then allowed to stabilize (<30 sec) until both gauges were equal. When measuring deformation, measurements were taken using two devices placed in the center of the top and bottom ends of each drum. Both devices consisted of a rod that traveled up with increasing deformation and indicated a graduated measurement in a 1:1 ratio. Both the top and bottom devices were zeroed before each test.

Observations were made through a 30x60 magnification spotting scope approximately 75 feet from the test apparatus. Measurements were clearly visible and zeroing of the gauges was completed by adjusting the gauges and linear measuring devices and confirming zero through the spotting scope. The reason for collecting data remotely was the danger of flying debris and the rapid pressure release during the failure of the pressurized drums.

55-gallon metal drum tests

Two separate drum types were used in this experiment: UN/1A1 55-gallon metal drum, and UN/1A2 55-gallon metal drum. The UN/1A1 closed-head drums were pressurized and observed under three separate treatments: (1) one-half full of water; (2) three-quarters full of water; and (3) empty. The UN/1A2 open-head drums were pressurized and observed under three separate treatments: (1) one-half full of water; (2) three-quarters full of water; and (3) cement spun (partially filled with cement and spun in a machine similar to a centrifuge to simulate radioactive waste packaging techniques at Los Alamos National Laboratory). The rings of the empty and water-fill open-head drums were tightened using an impact wrench and sledge hammer to within one centimeter of the ring ends meeting. The rings of the cement-fill open-head drums were tightened to 40 foot pounds of torque using an impact wrench.

Each drum type and respective treatment was pressurized from psig to a failure pressure at 5.0 psig intervals. Linear deformation along the center line of metal drums was measured and recorded with corresponding pressures. The purpose of the treatments was to determine if differences in deformation
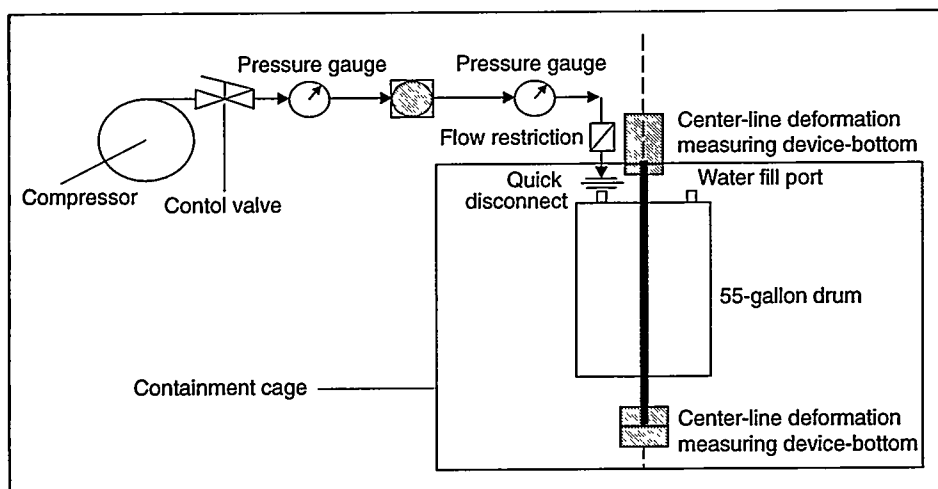
Figure 1. *Drum test apparatus flow diagram.*

exist between drums of each treatment, between drum types, and if mean failure pressures were significantly different.

55-gallon plastic drum tests

Five 55-gallon seamless high-density polyethylene (HDPE) drums were tested to determine their failure pressures. Deformation of these drums was not measured because both radial and axial deformation was observed. Four of the 55-gallon HDPE drums were tested empty and one was tested one-half full of water. These drums were steadily pressurized until failure.

Two 55-gallon open-head HDPE drums were tested to determine their fail pressures. One 55-gallon plastic-lined metal drum was pressurized and deformation measurements recorded up to failure.

85-gallon metal overpack tests

Six 85-gallon metal overpack drums were tested empty to determine a mean failure pressure for the drums, and top deformations were measured as described in the *Test Procedures* section.

30-gallon metal drum tests

Four 30-gallon metal drums were tested to determine their failure pressures. Deformation was not measured because the measuring devices were not designed to measure deformation of 30-gallon drums. Two of the 30-gallon metal drums were of the closed-head type, and the other two were of the open-head type. The drums were slowly pressurized until

failure occurred or the pressurization was discontinued due to dangerously high pressures.

20- and 30-gallon plastic drum tests

Two 20-gallon seam construction and four 30-gallon seamless HDPE drums were pressurized to determine their failure pressures and characteristics.

Drum information

Table 1 lists each drum type tested and includes the UN/DOT/HM181 specifications, capacity, number of drums tested, and tests conducted. All drums tested were new and unused because of the possible bias associated in drawing conclusions from old or used drums.

Progress and results

55-gallon metal drums

The following observations are noted with respect to new closed- and open-head 55-gallon metal drums. There were notable differences in the failure characteristics among drum types:

• 55-gallon metal open-head drums

– Drums appear to vent immediately adjacent to the nut and bolt fastener on the ring. See Figure 2.

– 100% of drums tested vented at pressures at or below 32 psig.

– Pinging was noticeable between 15 and 20 psig.

– The 55-gallon metal open-head drums

appear to bulge at only the top and bottom ends.

– Body seams (top to bottom) experienced no visible distortion or apparent weakening.

• 55-gallon metal closed-head drums

– 95% of the drums tested failed explosively.

– Of the catastrophic failures, 68% failed at the bottom end, making the entire drum a projectile.

– 100% of the drums tested failed at the top or bottom ends.

– When filled with liquid (1/2 or 3/4 full), bottom failures appear to be increasingly violent with increasing water levels up to 3/4 full.

– Approximately 5.0 psig before failure, a significant amount of distortion of the drum chime is apparent. See Figure 3.

–Appear to bulge at only the top and bottom ends.

– Body seams (top to bottom) experienced no visible distortion or apparent weakening.

– Pinging was noticeable between 15 and 20 psig, and increased dramatically immediately before drum failure.

– T-test indicates a probability that 99% of the failures will occur above 48.7 psig.

These observations show that bulging drums, especially the closed-head type, are extremely dangerous. Noticeable differences exist between closed- and open-head drums under pressure. However, both types of drums are inherently dangerous when pressurized and present many hazards. The t-test provides a reasonable certainty that new closed-head 55-gallon drums will fail above 48.7 psig and helps in determining a "safe working envelope" for working with these drums.

The averages of the top deformation of the closed- and open-head drum treatments were plotted against pressure. See Figure 4.0. The open- and closed-head top deformation averages are sufficient to use the data in developing a

53

Table 1. Drum capacities, specifications, and tests conducted

Capacity and description	UN/DOT/HM 181 specifications	Drums tested	Tests conducted
20 gallon HDPE-seam construction	1H1/Y1.9/150	2	Failure pressure-characteristics
30 gallon HDPE-seamless	1H1/Y1.8/100	4	Failure pressure-characteristics
30-gallon metal closed-head	1A1/Y1.8/300	2	Failure pressure-characteristics
30-gallon metal open-head	1A2/Y1.5/150	2	Failure pressure-characteristics
55-gallon HDPE open-head	1H2/Y150/S	2	Failure pressure-characteristics
55-gallon HDPE closed-head-seamless	1H1/Y1.9/150	5	Failure pressure-characteristics
55-gallon metal open-head	1A2/Y1.5/150	12	Failure pressure-characteristics, deformation
55-gallon metal open-head-cement fill	1A2/Y1.5/140	6	Failure pressure-characteristics, deformation
55-gallon metal closed-head	1A1/X1.8/300	14	Failure pressure-characteristics, deformation
55-gallon metal-plastic lined	6HA1/Y1.8/100	1	Failure pressure-characteristics
85-gallon metal open-head overpacks	1A2/X440/S	6	Failure pressure-characteristics, deformation

device to correlate pressure versus deformation for estimating the internal pressures of visibly bulging 55-gallon metal drums.

• 55-gallon plastic drums

  – The five 55-gallon HDPE-seamless drums tested failed explosively at pressures of 48, 48, 50, 30, and 58 psig.

  – Four of five failures occurred through the sides of the drums at no particular or identifying location. One failed at 30 psig out of the top end of the drum.

These are significant observations because they show the potential for seamless HDPE drums to fail out of the sides. Deformation was observed at the tops, bottoms and sides of the drum.

• 55-gallon open-head HDPE drums

  – The two 55-gallon open-head HDPE drums failed explosively at 23 and 24 psig, ejecting the entire top off the drum.

  – One 55-gallon plastic-lined metal drum self vented at 50 psig with a top bulge characteristic of the curve for the closed-head top deformation.

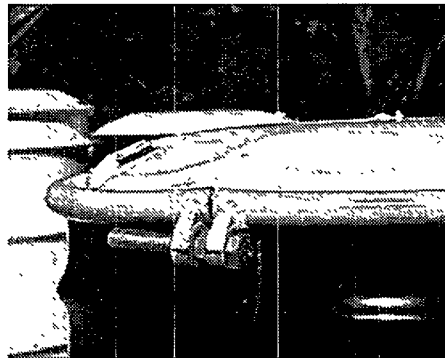 – A device for estimating internal pressures in 55-gallon drums will not

Figure 2. 55- (left) and 85-gallon (right) open-head drums leak immediately adjacent to the nut and bolt fastener on the ring (note the crease in the metal at that location).
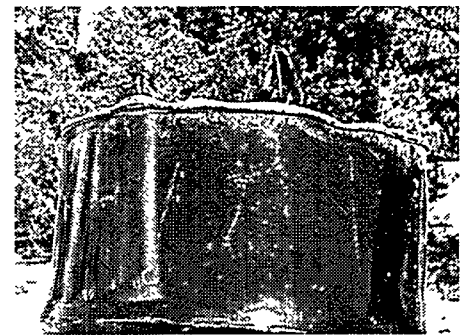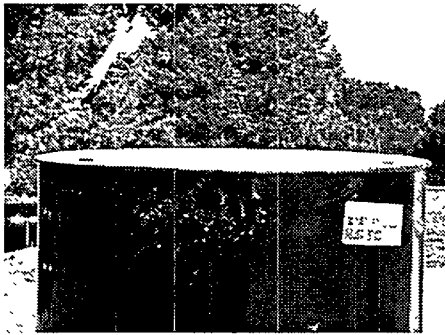

Figure 3. The chime of 55-gallon closed-head metal drums becomes severely distorted immediately before catastrophic failure (right).
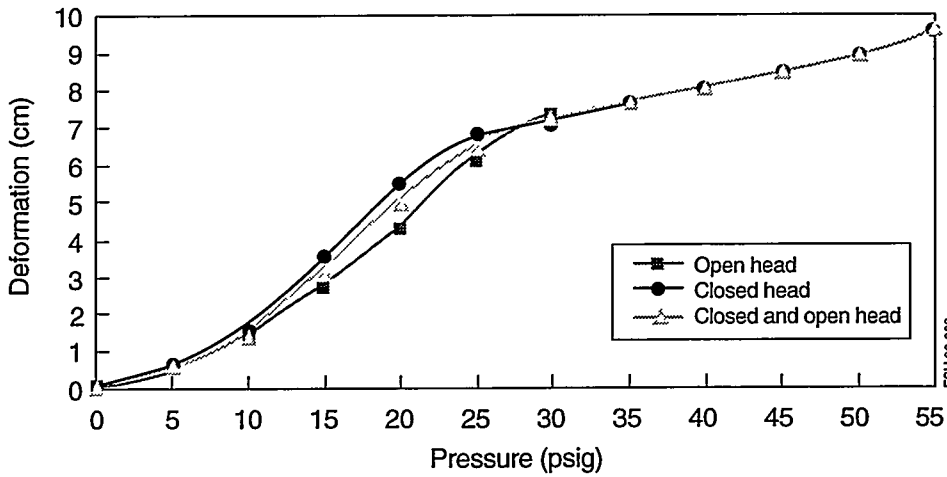
Figure 4. Closed- and open-head drum top deformation averages.

be useful on plastic or plastic-lined drums because deformation was not measured or differences exist in construction between these drums.

85-Gallon Overpacks

– The six 85-gallon metal overpacks tested failed at or below 16 psig and appeared to self-vent immediately adjacent to the placement of the nut and bolt fastener on the ring.

–The overpacks appeared to bulge only at the top and bottom ends.

30-gallon metal drums

The four 30-gallon metal drums (2 open-head, 2 closed-head) tested show that significant hazards exist when a 30-gallon metal container is pressurized. The high pressures associated with these containers present many hazards:

• 30-gallon metal closed-head drums

– Extremely high pressures (>120 psig) were possible in 30-gallon metal closed-head drums.

– These drums maintained extremely high pressures without venting.

– The failure of these drums under these conditions can be anticipated as catastrophic and extremely violent.

– Other than bulge, no apparent failure indicators, such as pinging, were noted.

– The 30-gallon metal closed-head drums appear to bulge at only the top and bottom ends.

• 30-gallon metal open-head drums

– Of the two 30-gallon metal open-head drums tested, one failed explosively, and one self-vented.

– Both 30-gallon metal open-head drums tested maintained pressures greater than 50 psig.

– Other than bulge, no apparent indicators, such as pinging, were noted.

–The 30-gallon metal open-head drums appear to bulge at only the top and bottom ends.

• 20- and 30-gallon HDPE plastic drums

– The seam and seamless construction 20- and 30-gallon HDPE drums failed at pressures above 45 psig.

– Both the seam and seamless construction 20- and 30-gallon HDPE drums can maintain high pressures for extended periods of time.

– Two of four seamless construction 30-gallon HDPE drums failed explosively from the side at no particular location on the drum, making the entire drum a projectile.

– The seam construction 20-gallon HDPE drums failed explosively along the bottom seam of the drum, making the drum a projectile.

– The 20- and 30-gallon HDPE drums appear to bulge from the top, bottom, and sides of the drum.

Conclusions and recommendations

Deformation of a drum indicates the drum has been subjected to internal pressure, not that it is under pressure at the time of inspection. The design of these containers makes them capable of violent rupture, and caution should be taken in approaching deformed drums. It was assumed that the experimental method of pressurization at increasing 5.0 psig intervals was representative of "real" pressurized drums in the field, although the speed and method of pressurization may be different. Also, it was assumed that the deformation observations correspond to "real-world" pressurized drum deformations in the field.

The results of this study indicate that significant differences exist among the failure characteristics of drum types and materials; The 55-gallon drum data was sufficient to support the development of a device for estimating internal pressures in 55-gallon metal drums because of the similarity between pressure vs. deformation curves. The safe discovery and mitigation of a pressurized drum can make the difference between a minor incident with limited and controlled consequences and a major one with the potential loss of life and significant property damage. With the information contained in this report, Department of Energy personnel, private and municipal fire departments, HazMat teams, hazardous device teams, and other emergency responders can make educated decisions during bulging drum incidents.

Many observations were noted and should be used as indicators of danger when approaching bulging drums. The following indicators and observations are considered to be of extreme importance for emergency responders and waste workers:

• The distortion of the chime on 55-gallon metal closed-head drums at approximately 5 psig before failure.

• Intermittent pinging of 55-gallon open- and closed-head metal drums at 15-25 psig.

• Rapid and intense pinging of 55-gallon metal closed-head drums immediately before drum failure.

- A strong potential exists for closed-head 55-gallon and closed- and open-head 30-gallon metal drums to fail explosively.
- All the 85-gallon and 55-gallon open-head drums tested self-vented.
- 30-gallon metal closed-head drums can hold and maintain in excess of 120 psig.
- One of two open-head 30-gallon metal drums tested failed explosively.
- Four of five seamless 55-gallon closed-head HDPE drums failed explosively out of the side of the drum.
- Two of four 30-gallon HDPE drums failed explosively out of the side of the drum, and two self-vented.
- The seam construction 20-gallon drums tested failed explosively on the bottom seam.
- Sealed containers of all types have the potential to become pressurized.
- Based on the conclusions of this study, we recommend the development of training criteria using the data contained in this report. The training criteria should include the following information:
  - Indicators of drum pressurization.
  - Inherent hazards associated with drum incidents and chemical properties such as flammability, corrosiveness, and reactivity.
  - Failure characteristics and differences between types of drums.
  - Pressurized drum mitigation techniques such as remote venting, direct cooling (ice bath), or shooting with a projectile (water cannon or disrupter).
  - Inappropriate mitigation techniques.

Deliverables

- A method for determining pressures inside bulging 55-gallon metal drums.
- A method for recognizing hazardous conditions of pressurized waste containers.
- Information for safer responses to pressurized drums.
- Training video and papers requested by and distributed to over 130 organizations.
- Community outreach to a national and international audience.

- Six-hour training course.
- Contacts with emergency response and hazardous waste personnel.

References

29 CFR 1910.120, Hazardous Waste Operations and Emergency Response, July 1, 1995, Department of Labor, Washington DC.

Graziano, R. M., *R.M. Graziano's Tariff No. 29, Hazardous Materials of the Department of Transportation,* December 15, 1974, effective January 14, 1975.

Ott, R. L., *An Introduction to Statistical Methods and Data Analysis,* 1993, Duxbury Press, Belmont, CA.

Feedback

"Truly Outstanding...an excellent application of science and technology to solve a problem." —1998 ESH Division Review Committee, Los Alamos National Laboratory

"I commend you on your promptness in getting this useful information to the public."—Joseph M. Harrisson, MPH, CIH, Russell Corporation

"We have never seen such a video. This is information emergency responders can use." —Garland Hanson, CSP, Arizona Safety Center

"This is an area that not too many of us are familiar with, and your work fills a big gap. Let your bosses know that people are benefiting from your work." —Jeff DeBell, Kansas Consolidated Fire District #2

"Our emergency response teams will benefit greatly from this information." —Floyd Cobb, Intel Corporation

"This is much needed information for the emergency response and hazmat community." —Bobby Clark, Commonwealth of Virginia, Department of Emergency Services

"We can really use this for training and education courses." —Dr. Ron K. Bhada, New Mexico State University

"We are going to use this information as the core for one of our training sessions."—Chuck Rives, Cedar Rapids Fire Department

"The paper and video are very informative and good tools for our hazardous waste team." —Marty Sosby, CIH, Huntsman Corporation

"Excellent project and pertinent information." —Larry Borgelt, PE, CSP, Oklahoma State University

Reusability of Organic Vapor Air-Purifying Respirator Cartridges

Introduction

The purpose of this study has been to develop data to define the conditions, if any, under which an organic vapor air-purifying respirator cartridge can be reused. Two types of organic vapor (OV) air-purifying respirator cartridges, MSA GMC-H and GME-H, are currently being used at Los Alamos National Laboratory (LANL). In the absence of information on their reusability, the best practice has been to use such cartridges only once before disposing of them. However, does this mean only for one work shift? Or, does it mean between breaks during one work shift? Or, can they be used for a full work week? Are there storage conditions that could extend the number of times a cartridge can be used?

Improved worker protection, cost savings, and compliance with Occupational Safety and Health Act (OSHA) regulations are the potential benefits to the LANL from understanding the effects of first use, usage breaks, and storage conditions on the remaining OV cartridge service life. There is a tendency to reuse OV cartridges as a matter of convenience and cost savings. In industrial operations, especially paint shops, excessive reuse of cartridges may be a serious problem. As we generate appropriate data and disseminate it at LANL and to the industrial hygiene community, whatever the conclusion, it will help in training and supervision and could reduce worker exposures to solvents and other organic vapors and gases. An obvious, though secondary, benefit of demonstrating the reusability of OV cartridges is cost savings. Fewer cartridges may need to be purchased, stored, distributed, and disposed of as waste.

In October 1998, the Occupational Safety and Health Administration implemented new respirator-use regulations, which require organizations to set cartridge change-out schedules based on "objective information," rather than sensory perceptions (e.g., odor) of breakthrough. With two years of this study already completed, LANL is in an excellent position to complete models that will provide some of this required "objective information."

The objectives of this work have been

• to develop experimental data on vapor migration within OV cartridges used at LANL after single or multiple uses and storage at various conditions; and

• to prepare a mathematical model and computer program that will provide guidance to industrial hygienists on the reusability of OV cartridges at actual use and storage conditions, e.g., vapor, concentration, humidity, temperature, times, etc. We will disseminate the data, models, and programs to the international industrial hygiene community and the military, as well as to LANL industrial hygienists.

The US Army Edgewood Research, Development, and Engineering Center (Aberdeen Proving Ground) continues to provide funding for related experimental and modeling studies, specifically for the C2A1 military gas mask canister.

Methods

Details of the experiments done to measure effects of storage on reuse have been published previously (Wood and Kissane May 1998, July 1998). The procedure starts with exposing cartridges to selected organic vapors at selected first-use conditions, e.g., concentration, flow rate, etc., for less than their break-through times, i.e., service lives. The cartridges are set aside for varying periods of simulated storage. Finally they are rechallenged at what are usually close to the same conditions to simulate reuse. Reuse breakthrough curves—concentration vs. time—especially breakthrough concentrations immediately following reuse, provide information on what happened, i.e., migration of adsorbed vapor, during storage.

Experimental measurements of micropore volumes and adsorption isotherms were added to the experimental plan to provide input to theoretical models. Duplicate samples of four carbons, including two taken from GMC-H and GME-H cartridges, were weighed, dried, and placed in closed containers also containing a volatile liquid, i.e., ethyl acetate or hexane. These samples were periodically weighed to determine vapor uptake. When constant weights were reached, the total weight increases were converted to micropore volumes. Adsorption isotherms were measured by placing incompletely saturated carbon samples in plastic bags and allowing equilibrium to be reached. The vapor phase was analyzed using a photoacoustic infrared spectrometer. Weighings gave the corresponding adsorbed phase loadings.

Mathematical models and computer programs have been developed to describe experimental breakthrough curves and to understand migration mechanisms during storage. First, well-established adsorption/desorption mechanisms were converted into simulations of vapor breakthrough of a granulated carbon bed as a function of time. Microsoft QuickBasic, a DOS-based software was used initially, but then replaced with the more versatile and user-friendly Windows 95-based

Microsoft Visual Basic 5. Figure 1 shows an output screen for the program BREAKTHROUGH, describing a full breakthrough curve of 2040 ppm methylene chloride. It was an easy step to the simulation of a breakthrough curve after storage of a partially loaded bed. The storage simulation was more difficult because the mechanism was unknown. Several rate-limiting steps, e.g., desorption, adsorption, gas-phase diffusion, and carbon-granule diffusion and combinations of them have been tried. The goal has been to describe no-flow migration by one parameter related to an easily obtained property of the vapor.

Results

In previous work (Wood and Kissane May 1998), we demonstrated that there really is a problem with reusability of organic vapor respirator cartridges after a period of storage. An often-significant increase in breathed vapor may occur after storage. This vapor was not penetrating the cartridge before storage. Ethyl acetate, hexane, and methylene chloride vapor increases upon storage were measured with GMC-H cartridges at a variety of conditions. We also studied the effects of water vapor preloading and concurrent loading in humid air situations. Water vapor coadsorption (hexane vapor in humid-air exposure) resulted in higher storage effects for three days storage. Water vapor preadsorption—humid air exposure before and during hexane vapor challenge—resulted in even higher effects.

Figure 2 shows data obtained with GME-H cartridges and ethyl acetate. Vapor increases upon reuse are shown to be a function of the amount of loading during the first use, a function of storage time, and a function of storage temperature. In one experiment, a cartridge was stored at 3°C in a refrigerator for two weeks before being warmed up and rechallenged at room temperature. The increase in vapor after storage was halved by the storage under refrigeration.

In related work, military C2A1 gas mask canisters were challenged with ethyl acetate, hexane, or heptane and
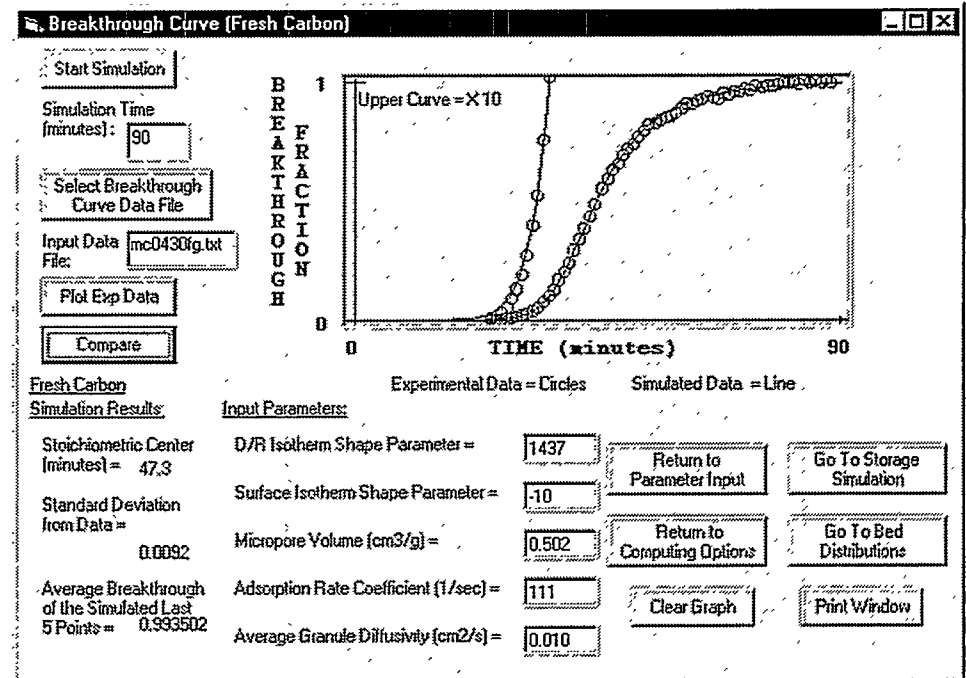
Figure 1. *Results window for the computer program BREAKTHROUGH for experimental data (circles) and simulation (line) of a methylene chloride breakthrough curve for a fresh GMC-H cartridge.*
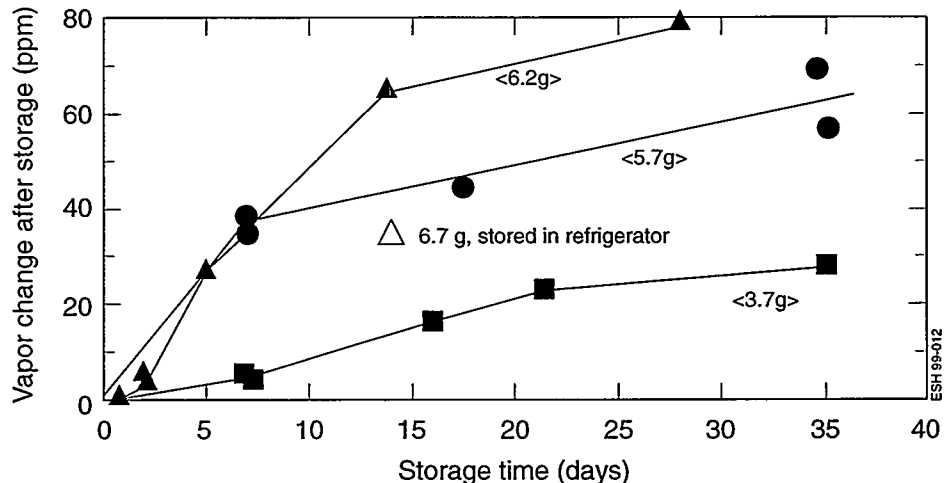
Figure 2. *Effects of storage time, first-use loading, and refrigeration on effluent vapor changes for GME-H cartridges challenged with ethyl acetate.*

studied for effects of storage on reusability. As expected, heptane, the least volatile of the compounds we have studied, showed the slowest migration rate.

Micropore volumes obtained by the method described above are listed in Table 1. The experimental adsorption isotherm plots for four carbons and hexane are shown in Figure 3, normalized

by the micropore volumes. Similar results were obtained for ethyl acetate.

The computer simulations of mathematical models were tested against and calibrated with experimental breakthrough curves. Inputs included experimental conditions and measured micropore volumes. In simulating first-use breakthrough curves, an asymmetry

parameter was required. Breakthrough curves that we and others have measured are often not symmetrical, as would be predicted by simple kinetic and isotherm equations. Several (unsatisfactory) means have been used to explain this asymmetry. We developed a Dubinin/ Radushkevich-Langmuir isotherm model that gives a single parameter that describes breakthrough curve asymmetry of both kinds. This work was discussed at the University of Neuchatel, Switzerland, and presented at the EUROCARBON Conference in Strasbourg, Switzerland, in July 1998 (Wood July 1998).

Parameters obtained by fitting full first-use breakthrough curves were then applied to simulations of experimental reuse breakthrough curves. Figure 4 shows a GMC-H/methylene chloride reuse breakthrough curve simulation (line) and measured data (circles). Migration rate during 12,780 minutes (8.9 days) of storage was selected to match the observed initial vapor concentration upon reuse.

Efforts to find a no-flow migration mechanism that explains the reuse breakthrough results have been less rewarding. None of rate limiting steps, e.g., desorption, adsorption, gas phase diffusion, and carbon granule diffusion and combinations tried so far have been able to describe no-flow migration by one parameter related to an easily obtained property of the vapor. One problem is that experimentally, migration seems to slow down more with storage time than the models seem to predict. But, progress has been and is being made and success is expected.

Conclusions

Reuse of OV respirator cartridges after storage can result in substantially increased exposures to vapors, depending on

• conditions and loading of first use,

• type (volatility) of vapor,

• storage time and temperature, and

• reuse conditions.

This result has been shown experimentally with three chemical vapors and the two cartridges used at LANL. We

Table 1. *Micropore Volumes Measured by Saturation with Two Vapors*

Activated Carbon Source	Carbon per Cartridges or Canister (g)[a]	Micropore Volume (cm^3/ g)[a]	
		Measured with Hexane	Measured with Ethyl Acetate
GMC-H	91.7 [b]	0.509	0.478
GME-H	136.7 [b]	0.441	0.421
C2A1	113.7	0.391	0.392
BPL (Calgon)	N/A	0.616	0.605

[a] Based on original, not dried, carbon weight

[b] For two cartridges
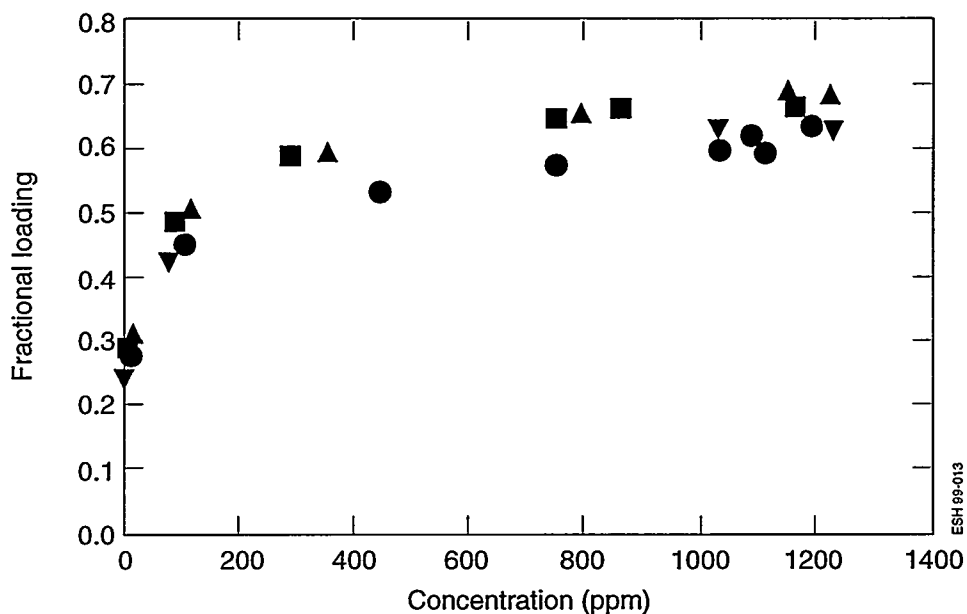
Figure 3. *Hexane isotherms normalized by measure saturation capacities (micropore volumes). p=GMC-H carbon; ¢=GME-H carbon; ó=C2A1 carbon; q= Unimpregnated BPL activated carbon.*

have also shown that there are some situations in which reuse is acceptable. Modeling is proposed as the means of determining these cases.

Simple methods of measuring micropore volume and adsorption isotherms were successful in providing data for breakthrough simulation models. Micropore volume and capacities were smaller for GME-H carbon than for GMC-H carbon (Table 1), but the larger bed volume for the former compensates for the difference. Impregnants on the GME-H carbon account for its reduced capacity. Likewise, the impregnated C2A1 military canister carbon has a

lower micropore volume than an unimpregnated BPL carbon. There was good agreement among the isotherms of the four carbons when capacities were normalized using micropore volumes (figure 3).

Computer programs for use on desktop or laptop computers by industrial hygienists are closer to reality. Such programs provide a means for incorporating all the cartridge and use parameters. Breakthrough simulation programs have been developed and used in a correlative mode, e.g., the fitting of experimental data in this project but they also can be developed into predictive tools to provide
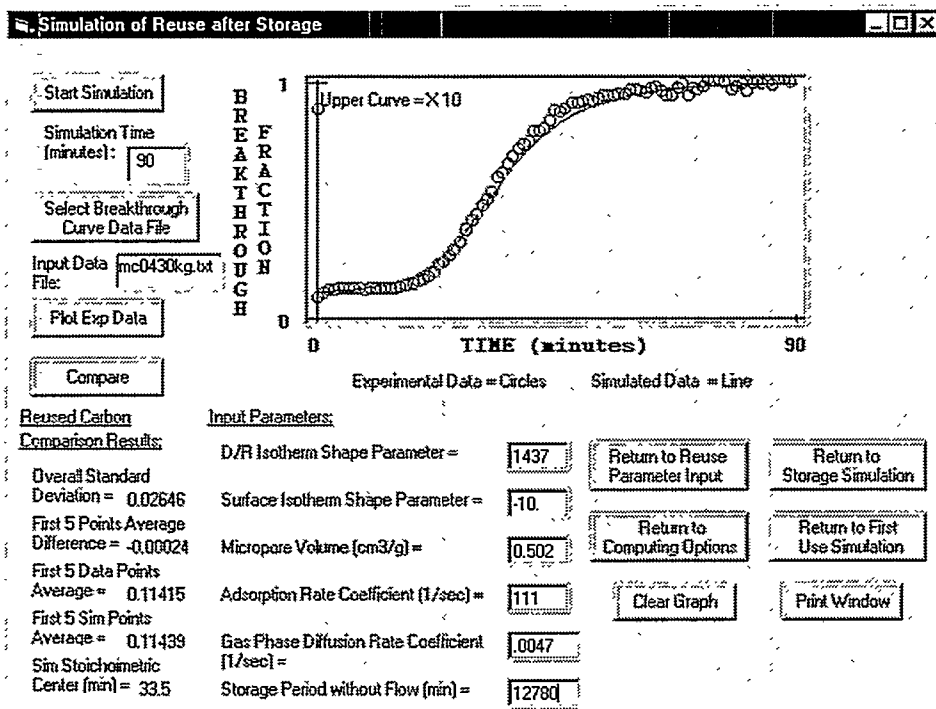
Simulation of Reuse after Storage

Start Simulation

Simulation Time [minutes]: 90

Select Breakthrough Curve Data File

Input Data File: mc0430kg.txt

Plot Exp Data

Compare

BREAKTHROUGH CURVE

Upper Curve = X 10

TIME (minutes)   90

Experimental Data = Circles   Simulated Data = Line

Reused Carbon Comparison Results:

Overall Standard Deviation = 0.02646

First 5 Points Average Difference = -0.00024

First 5 Data Points Average = 0.11415

First 5 Sim Points Average = 0.11439

Sim Stoichometric Center [min] = 33.5

Input Parameters:

D/R Isotherm Shape Parameter = 1437

Surface Isotherm Shape Parameter = -10.

Micropore Volume [cm3/g] = 0.502

Adsorption Rate Coefficient [1/sec] = 111

Gas Phase Diffusion Rate Coefficient [1/sec] = .0047

Storage Period without Flow [min] = 12780

Return to Reuse Parameter Input

Return to Storage Simulation

Return to Computing Options

Return to First Use Simulation

Clear Graph

Print Window

Figure 4. *Reuse results window for the computer program BREAKTHROUGH for experimental data (circles) and simulation (line) of a methylene chloride breakthrough curve for reuse of a GMC-H cartridge after 8.9 days of storage.*

the "objective information" that OSHA requires of LANL and others. Such further development is planned for FY99.

Identifying the no-flow storage migration mechanism and rate was only partially successful. We have found many things that do not work. However, it is only a matter of effort and time to come up with something useful. Then, the goal of providing the industrial hygienist with a tool for predicting storage effects can be reached.

References

Wood, G., and R. Kissane, "Reusability of organic vapor air-purifying respirator cartridges," in Technology Development, Evaluation, and Application (TDEA) FY 1997 Progress Report, Los Alamos National Laboratory report, LA-13438-PR, pp. 36–38 (May 1998).

Wood, G., and R. Kissane, "Reusability Study with Organic Vapor Air-Purifying Respirator Cartridges," published in the Proceedings of the 1997 ERDEC Scientific Conference on Chemical and Biological Defense Research, ERDEC-SP-063, pp. 873–877, Aberdeen Proving Ground, Md. (July 1998).

Wood, G. O., and R. J. Kissane, "Migration of organic vapors in activated carbon beds between periods of airflow," in Extended Abstracts and Programme of the EUROCARBON '98 Conference on the Science and Technology of Carbon, Strasbourg, France, July 5–9, 1998, vol.1, pp. 271–272.

Wood, G. O., "Adsorption isotherms and their influence on breakthrough curve shapes," presented at the EUROCARBON '98 Conference on the Science and Technology of Carbon, Strasbourg, France, July 5–9, 1998.

Publications and Presentations

The publications and presentations listed below have received full or partial funding from the TDEA program. In some instances, a project has been ongoing and TDEA contributed toward supporting progress.

Biggs et al.

Publications

Bennett, K., J. Biggs, and P. R. Fresquez, "Development and application of a movement predictive model for elk," Los Alamos National Laboratory report LA-UR97-4796 (1997). To be submitted to peer-review journal.

Biggs, J., K. Bennett, and P. R. Fresquez, "Estimation of observation rates of global positioning collars deployed on elk," Los Alamos National Laboratory report LA-UR-98-1080 (1998). Submitted to *Great Basin Naturalist*.

Biggs, J., K. Bennett, and P. R. Fresquez, "Resource use, activity patterns, and disease analysis of rocky mountain elk (*Cervus elaphus nelsoni*) at the Los Alamos National Laboratory," Los Alamos National Laboratory report LA-13536-MS.

Fresquez, P. R., J. Biggs, K. Bennett, D. Kraig, M. Mullens, and J. Ferenbaugh, "Radionuclide concentrations in deer and elk at Los Alamos National Laboratory: 1991–1998," Los Alamos National Laboratory report LA-13553-MS.

Fresquez, P. R., J. Biggs, K. Bennett, D. Kraig, M. Mullens, and J. Ferenbaugh, "Radionuclides in deer and elk from Los Alamos National Laboratory and the doses to humans from the ingestion of muscle and bone." In press *J. Enviro Sci. and Hlth*,

Presentations

J. Biggs, K. Bennett, and P. R Fresquez, "Movement and activity patterns of elk at Los Alamos National Laboratory," a symposium of Biological Research in the Jemez Mountains, Santa Fe, NM, November 6, 1998, Los Alamos National Laboratory report LA-UR-98-4535 (1998).

J. Biggs, K. Bennett, and P. R. Fresquez, " Estimating observation rate biases of GPS collars deployed on elk," The Wildlife Society 5th Annual Conference, Buffalo, NY, September 22–26, 1998, Los Alamos National Laboratory report LA-UR-98-1080 (1998).

K. Bennett and J. Biggs, "Demonstration of applications of the Geographic Information System (GIS) to applied ecology problems," WERC Seminar Series: New Mexico State University, Las Cruces, NM, March 1998.

J. Biggs and K. Bennett, "Development of management strategies for large mammals through multiple agency interaction and the application of innovative research tools," WERC Seminar Series: New Mexico State University, Las Cruces NM, May 1998.

J. Biggs and K. Bennett, "Application of GPS radio collars to Rocky Mountain Elk studies in the southwest US," Guest Scientist Seminar Series: University of Kentucky School of Forestry, Lexington, KY, March 1998.

J. Biggs, K. Bennett, and P. R. Fresquez, "Estimation of home ranges and water use of elk at Los Alamos National Laboratory," Los Alamos National Laboratory report LA-UR-97-3977, a symposium of Biological Research in the Jemez Mountains, Santa Fe, NM, October 18, 1997.

Hansen et al.

Presentations

Fourth Wildlife Society Conference, September 21–27, 1997, Snowmass, CO.

Second Symposium of Biological Research in the Jemez Mountains, November 7, 1997, Santa Fe, NM.

Thirty-first Joint Annual Meeting, Arizona and New Mexico Chapters of the Wildlife Society and the Arizona, New Mexico Chapter of the American Fisheries Society, February 5–7, 1998, Sierra Vista, AZ.

WERC Seminar Series, New Mexico State University, February 1998, Las Cruces, NM.

Inkret et al.

Publications

Inkret, W. C., D. W. Efurd, M. J. Hameedi, G. Miller and M. E. Schillaci, "Age-dependent dose estimates from ingestion of marine and terrestrial biota in the Beaufort Sea and Northwestern Alaska," Los Alamos National Laboratory report LA-UR-98-1817 (1998).

Inkret, W. C., M. E. Schillaci, Y. S. Cheng, D. W. Efurd, G. Miller, J. A. Musgrave and J. R. Wermer, "Internal dosimetry for inhalation of hafnium tritide," Los Alamos National Laboratory report LA-UR-98-4814 (1998). Accepted for publication in the *J. Envir. Rad.*

Inkret, W. C., D. W. Efurd, G. Miller, D. J. Rokop, T. M. Benjamin, "Applications of thermal ionization mass spectrometry to the detection of ^{239}Pu and ^{240}Pu Intakes," *Int. J. Mass Spectro. Ion Processes*, **178**, 113–120 (1998).

Presentations

Presented results at DOE headquarters in April 1998.

Presented results at DOE headquarters in April 1999.

Presented results at DOD in April 1998.

Presented results at DOD DIA in April 1999.

Presented results to DOE Internal Dosimetry Workshop, May 1998.

Results presented at Annual Meeting of the Health Physics Society, June 1999.

Larranga et al.

Publications

Larrañaga, M.D. and D. L. Volz, "Pressurized drum mitigation Los Alamos National Laboratory," Los Alamos National Laboratory report LA-UR-98-2542 (1998).

Larrañaga, M. D., D. L. Volz, and F. Baker, "Bulging drums—what every responder should know," Los Alamos National Laboratory report LA-UR-98-2543 (1998).

Larrañaga, M. D., D. L. Volz., and F. N. Bolton, "Pressure effects and deformation of waste containers," Los Alamos National Laboratory report LA-UR-98-2541 (1998). To be published in the July issue of *Fire Engineering*.

Presentations

Larrañaga, M.D., D. L. Volz, "Associated Hazards and Mitigation of Pressurized Drum Incidents," Los Alamos National Laboratory, 1999. Submitted for presentation to the 1999 American Nuclear Society 7th Topical Meeting on Emergency Response.

Larrañaga, M. D., D. L. Volz, F. N. Bolton, and D. M. Casserly, "Pressure effects and deformation of waste containers," 1998 American Industrial Hygiene Association Conference, Atlanta, GA, May 1998.

Larrañaga, M. D., "Pressurized drum emergency response," presented at The University of Houston, Clear Lake, TX, to satisfy the requirements for the degree of master of science, Los Alamos National Laboratory reports LA-UR-98-2543 and –2541 (1998).

Community outreach

Combinations of the papers and video were distributed to the following requesting organizations:

Federal

Centers for Disease Control and Prevention, National Institute for Occupational Safety and Health, US Army, Department of Bio-environmental Engineering, Air National Guard, Kalama Services—Johnston Atoll, Bettis Atomic Power Laboratory, Bureau of Indian Affairs—Navajo Nation, NASA Lewis Research Center

State

California Environmental Protection Agency—Department of Toxic Substances Control, State of California, Wisconsin Department of Transportation, Commission on Fire Prevention and Control—Connecticut Fire Academy, Commonwealth of Virginia-Emergency Services Unit, Oklahoma Fire Service Training, Florida Department of Environmental Protection, Florida Department of Emergency Services, California Department of Industrial Relations, University of Nevada—Reno Fire Protection Training Academy, Utah Fire and Rescue Academy, California Specialized Training Institute, South Florida Regional Planning Council

Municipal, City, and County

Elmira City School District—New York; City and County of San Francisco—California; Cedar Rapids Fire Department—Iowa; Dallas Fire Department—Texas; El Paso Fire Department—Texas; Lowell Fire Department—Arkansas; Winter Park Volunteer Fire Department—Colorado; Bradford Fire Department—New Hampshire; Austin Fire Department-Hazardous Materials Section—Texas; Reykjavik City Fire Department—Iceland; Phoenix Fire Department—Arizona; Chillicothe Fire Department—Illinois; East Charles Parish Fire Department—Louisiana, Jacksonville Fire Department—North Carolina; Central Jackson County Fire Protection District—Missouri; Aurora Public Schools—Colorado; Cordelia Fire Protection District —California; Mason Deerfield Joint Fire District—Ohio; Aiken County HazMat Team—South Carolina; Rio Rancho Department of Public Safety—New Mexico; Santa Fe Fire Department—New Mexico; Exeter Fire Department—New Hampshire; Palatine Fire Department —Illinois; Poudre Fire Authority—Colorado; Consolidated Fire District #2—Kansas; Devils Lake Fire Department—North Dakota; Broward-Miami Dade-Monroe Local Emergency Planning Committee—Florida

Department of Energy

Hanford Site Fire Department, Oak Ridge National Laboratory Fire Department, Los Alamos National Laboratory; Department of Energy—Albuquerque; Idaho National Engineering and Environmental Laboratory, Kaiser-Hill Rocky Flats Facility

Academic

New Mexico State University; Waste-management Education and Research Consortium; Fire Protection Publications; Oklahoma State University; International Fire Service Training Academy; University of Pennsylvania; North Carolina Education and Research Consortium; University of North Carolina at Chapel Hill; Midwest Center for Occupational Health and Safety; University of Arizona; University of Alabama—Birmingham; University of California—San Diego; University of Nebraska—Lincoln, Harvard University; University of California—Los Angeles; University of New Haven; Mesa Community College—Arizona; J. Sargeant Reynolds Community College—Virginia; Stanford University Fire Marshalls Office; Utah Valley State College; Mississippi State University; University of California—Berkeley; University of Houston—Clear Lake

Industrial—Consulting

Akzo Nobel Chemicals; RAMFAN; Marathon Oil Company; Refinery Terminal Fire Company—Texas; Hygienetics Environmental; Roche Bioscience; Allied Signal Aerospace; QST Environmental; Ground Engineering Consultants; Westinghouse Electric Corporation; Phoenix OHC Corporation; URS Operating Services Corporation; Rohm and Haas Company; Elvin Safety Supply; Eastman Kodak; Motorola; Mayo Clinic; Environmental Investigations; DuPont Imaging Systems; pH2 Environmental Corporation; MedImmune Corporation; Nexstar Pharmaceuticals Corporation; Occupational Health and Safety; Morton International Corporation; Huntsman Corporation; Clean Harbors

Services; Abbot Laboratories; ManTech Environmental Technology Corporation; Electric Boat Corporation; General Dynamics; Metcalf and Eddy; ERP; Elf Atochem; Bay West Engineering; Conoco; Merck and Company;Arizona Safety Center; Aon Risk Services; Celanese; Occidental of Oman;Texaco E andP; Texas Instruments; Duke Engineering; SJO Consulting Engineers; Caltex Petroleum; Zurich-American Insurance; HPR Engineering; Wassau Insurance; ARCO Prudhoe Bay Fire Department—Alaska; Lockheed Martin Engineering; Intel Corporation; Russell Corporation; Huntsman Corporation; Mobil Oil; Shell Oil, ARCO—China; Hewlett Packard; Science Applications International Corporation; Johnson Controls Northern New Mexico; International Union of Operating Engineers—International Environmental Technology and Training Center; Chemical Manufacturers Association—Lending Library

Awards

The Hazardous Materials Response Group (ESH-10) has won three 1998 Aegis awards and two 1999 Telly Awards for the video production, "Bulging drums—what every responder should know."

Whicker et al. (a)

Publication

Whicker, J. J., F. H. Hsieh, H. H. Hsu, and T. B. Borak, "A method for characterizing photon radiation fields," Los Alamos National Laboratory report LA-UR-99-662 (1999).

Presentations

Hsieh, F. H., T. B. Borak, and J. J. Whicker, "Measurements of equivalent dose using a photon spectrometer," Technical Meeting of the Rocky Mountain Chapter of the Health Physics Society (1998).

Whicker et al. (b)

Publications

Rodgers, J. C., J. J. Whicker, and J. T. Voss, "Comparison of continuous air monitor utilization: A case study," *Rad. Prot. Man.*, May/June: 56–64 (1998).

Wasiolek, P. T., J. J. Whicker, H. Gong, and J. C. Rodgers, "Room airflow studies using sonic anemometry," Los Alamos National Laboratory report LA-UR-98-3497, *Indoor Air J.*, In press (1998).

Whicker, J. J., J. C. Rodgers, and R. C. Lopez, "Assessment of need for transport tubes when continuously monitoring for radioactive aerosols," *Health Phys.*, In press (1998).

Presentations

Whicker, J. J., H. Gong, J. C. Rodgers, P. T. Wasiolek, and R. Morgan, R., "Room airflow studies using sonic anemometry," Los Alamos National Laboratory report LA-UR-98-337, Annual Health Physics Society Meeting, Minneapolis, MN (1998).

Whicker, J. J., J. C. Rodgers, H. Gong, and P. T. Wasiolek "Some issues in workplace air monitoring," Spring Technical Meeting for the Rio Grande Chapter of the Health Physics Society, Albuquerque, NM (1998).

Whicker, J. J., J. C. Rodgers, and R. C. Lopez, "Assessment of need for transport tubes when continuously monitoring for radioactive aerosols," Los Alamos National Laboratory report LA-UR-98-1490 (1998). Submitted to *H. Phys.*

Wood et al.

Publications

Wood, G., and R. Kissane, "Reusability of organic vapor air-purifying respirator cartridges," in Technology Development, Evaluation, and Application (TDEA) FY 1997 Progress Report, Los Alamos National Laboratory report, LA-13438-PR, pp. 36–38 (May 1998).

Wood, G., and R. Kissane, "Reusability Study with Organic Vapor Air-Purifying Respirator Cartridges," published in the Proceedings of the 1997 ERDEC Scientific Conference on Chemical and Biological Defense Research, ERDEC-SP-063, pp. 873–877, Aberdeen Proving Ground, MD (July 1998).

Wood, G. O., and R. J. Kissane, "Migration of organic vapors in activated carbon beds between periods of airflow," in Extended Abstracts and Programme of the EUROCARBON '98 Conference on the Science and Technology of Carbon, Strasbourg, France, July 5–9, 1998, vol.1, pp. 271–272.

Presentations

Wood, G. O., "Adsorption isotherms and their influence on breakthrough curve shapes," presented at the EUROCARBON '98 Conference on the Science and Technology of Carbon, Strasbourg, France, July 5–9, 1998.